9-15-2016

Time Domain Analysis of Electromagnetic Scattering From Multiple Cavities Embedded in a Ground Plane

Richard P. Uber

TIME DOMAIN ANALYSIS OF ELECTROMAGNETIC SCATTERING FROM MULTIPLE CAVITIES EMBEDDED IN A GROUND PLANE

DISSERTATION

Richard P. Uber, Captain, USAF

AFIT-ENC-DS-16-S-004

DEPARTMENT OF THE AIR FORCE
AIR UNIVERSITY

AIR FORCE INSTITUTE OF TECHNOLOGY

Wright-Patterson Air Force Base, Ohio

The views expressed in this dissertation are those of the author and do not reflect the official policy or position of the United States Air Force, the Department of Defense, or the United States Government.

AFIT-ENC-DS-16-S-004

TIME DOMAIN ANALYSIS OF ELECTROMAGNETIC SCATTERING FROM MULTIPLE CAVITIES EMBEDDED IN A GROUND PLANE

DISSERTATION

Presented to the Faculty

Graduate School of Engineering and Management

Air Force Institute of Technology

Air University

Air Education and Training Command

in Partial Fulfillment of the Requirements for the

Degree of Doctoral of Philosophy in Applied Mathematics

Richard P. Uber, B.G.S., M.S.

Captain, USAF

September 2016

AFIT-ENC-DS-16-S-004

TIME DOMAIN ANALYSIS OF ELECTROMAGNETIC SCATTERING FROM MULTIPLE CAVITIES EMBEDDED IN A GROUND PLANE

Richard P. Uber, B.G.S., M.S.
Captain, USAF

Committee Membership:

Dr. Aihua W. Wood
Chair

Dr. Alan V. Lair
Member

Dr. Michael J. Havrilla
Member

ADEDEJI B. BADIRU, Ph.D.
Dean, Graduate School of Engineering
and Management

Abstract

This work examines the scattered fields produced when a transient wave is reflected from an infinite perfect electric conductor (PEC) ground plane with multiple embedded cavities. Incident and reflected waves will be decomposed into transverse magnetic to the z direction (TM^z) and transverse electric to the z direction (TE^z) polarizations, with primary focus given to the TM^z. Cavities may be unfilled, partially filled, or fully filled with non-magnetic dielectric material and no assumptions are made regarding similarity, regularity, or periodicity. The Newmark method is used to discretize time and a variational formulation is presented for each time step. The principle outcome is to show that the variational formulation of the scalar problem is well posed.

Additionally, the variational formulation is applied in a stable numerical model using the finite element-boundary integral (FE-BI) method. Interior fields are approximated using the finite element method (FEM) for each time step, then the boundary integral is applied using the appropriate Green's function to approximate exterior scattered fields. The exterior fields for one time step provide the boundary conditions for the interior problem at the next time step. In this way, the numerical model marches through time.

Various numerical experiments are run to examine the effect of coupling on aperture and external fields. Of particular interest are the differences between single-cavity and multiple-cavity solutions.

This dissertation is dedicated to my family, whose faith and encouragement kept me focused over the years.

Acknowledgments

I would like to sincerely thank my advisor, Dr. Aihua Wood, for providing guidance and direction throughout this journey. I would also like to express my gratitude to my committee members, Dr. Alan Lair, and Dr. Michael Havrilla. Their counsel and perspective were pivotal in crafting this final product. Additionally, I would like to thank Dr. Pete Collins, Dr. Jonah Reeger, Dr. Mike Gilbert, Dr. Tri Van, Mr. Hirsch Chizever, and Mr. Alex Knisely for thought-provoking discussions and instruction which have helped shape my understanding of computational electromagnetics.

Richard P. Uber

Table of Contents

Page

List of Figures

Figure Page

List of Tables

List of Acronyms

Acronym	Definition
CEM	computational electromagnetics
DtN	Dirichlet-to-Neumann
EM	electromagnetic
FDTD	finite difference time domain
FE-BI	finite element-boundary integral
FEM	finite element method
HPC	high-powered computing
MoM	method of moments
PEC	perfect electric conductor
RCS	radar cross section
TM^z	transverse magnetic to the z direction
TE^z	transverse electric to the z direction
USAF	United States Air Force

TIME DOMAIN ANALYSIS OF ELECTROMAGNETIC SCATTERING FROM MULTIPLE CAVITIES EMBEDDED IN A GROUND PLANE

I. Background

In today's digital world, electromagnetic (EM) waves are omnipresent, surrounding us every day in every place on earth. Analysis of the patterns present in these waves holds the promise of a vast quantity of potential information about position, size, shape, composition, and motion of objects in our environment. The challenge presented by this ocean of data is in how to filter, collect, process, and exploit the knowledge available to us in these waves. As a military organization, the United States Air Force (USAF) is in the business of leveraging advantages in knowledge and technology to the ends of securing our nation's domestic and foreign interests. While we attempt to know increasingly more about our adversaries actions, we face the challenge of preventing others from gaining insight into our military operations. Thus, in order to gain and maintain the upper hand, the U.S. must continue to improve both detection and anti-detection technologies. Applications for EM wave scattering models support this goal by providing relatively cost-effective ways to test proposed designs prior to prototype production for expected scattering profiles and radar cross section (RCS).

1.1 A Brief History

The study of electromagnetic phenomena dates back over many centuries to the discovery and description of the compass over two millenia ago. The earliest documented description of magnetism as such may have been by Pierre de Maricourt in 1269 [11]. Static electricity and attractive forces had also been observed long before the term *electric*

was coined by William Gilbert in the 17th century [11]. Properties of electric and magnetic forces and fields were researched extensively in the 18th and 19th centuries by heavyweights like Henry, Poisson, Coulomb, Gauss, Ampère, Faraday, and Maxwell, leading to the mathematical understanding of electromagnetics still employed today. More recently, in World War II, air forces found applications in radar (originally an acronym for RAdio Detection And Ranging) for air defense purposes. Proliferation of radar technologies sparked an electronic arms race where better sensors led to more reliable air defense systems, prompting development of electronic countermeasures like avoidance methods, jammers, anti-radiation missiles, and stealth - or low observable - technologies. In order to stay one step ahead of competitors, continued research into the strengths and weaknesses of low-observable technology as well as properties of EM radiation and scattering is required.

Presently, RCS analysis is common when considering new aircraft acquisitions and possible modifications. Unfortunately, full scattering analysis of large, complex structures continues to be computationally challenging. Most real-world applications require high-powered computing (HPC) with parallel processing to produce accurate models. To this end, much recent research into computational electromagnetics (CEM) has focused on reducing the computational complexity of scattering problems.

The study of scattering from cavities is very useful in this context because engine inlets and other cavity-like structures on aircraft "have a very significant impact on the overall signature of the airplane structure" [3]. Major scattering sources can be separated into the following categories: reentrant structures, specular scattering, traveling wave echoes, edge and vertex diffraction, creeping waves, interations, and surface discontinuties [24], of which the greatest contributors are reentrant structures and specular scattering. As RCS reduction methods are growing in sophistication, understanding lesser scattering sources, such as edge diffraction, interactions, and discontinuities, becomes of greater

importance. A few examples of necessary aircraft features that create gaps or cavities are control surfaces, access panels, ordnance bay doors, engine inlets, exhaust nozzles, etc. [34]. Additionally, the electromagnetic environment has become more complex, and engineers must now consider a wider range of frequencies than in the past. A structure which may respond like a gap or crack at one frequency [33], may function like a reentrent structure at a much higher frequency. Transient analysis of scattering is useful in this case because it generates a wide-band solution and may capture potential non-linear behavior and interactions not visible in time-harmonic solutions.

A survey of recent work, specifically related to the cavity scattering problem is given in Chapter 2.

1.2 General Problem Statement

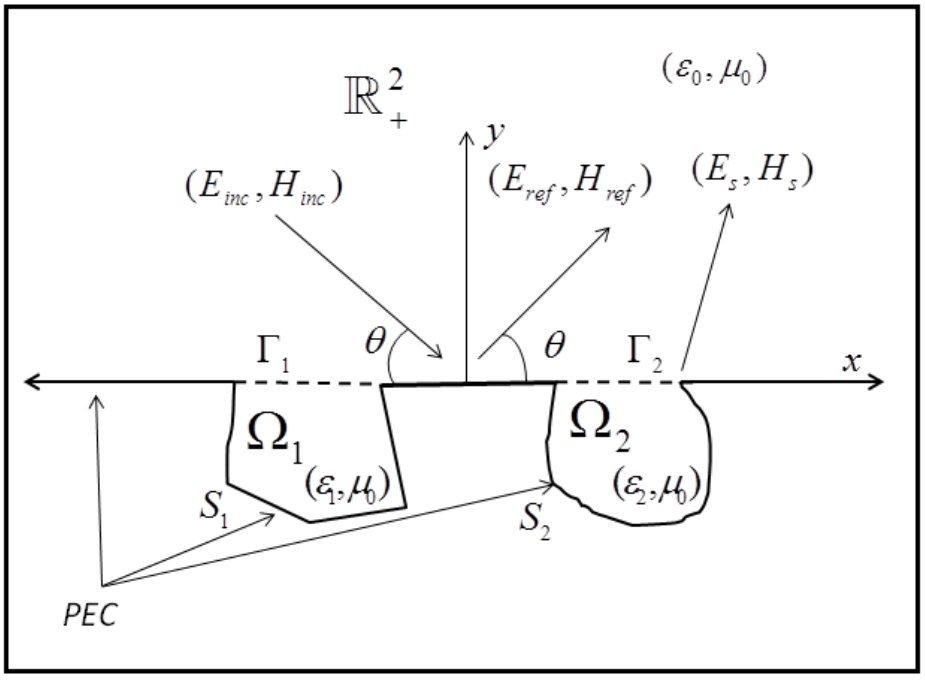

Figure 1.1: Two cavity environment

This work examines the scattered fields produced when a transient wave is reflected from an infinite PEC ground plane with multiple embedded cavities. For ease of orientation, the planar surface is refered to as the ground plane, and the axes will be oriented such that the PEC lies in the xz-plane. Incident and reflected waves are decomposed into TM^z and TE^z polarizations, with primary consideration given to the TM^z case for numerical implementation. Cavities may be unfilled, partially filled, or fully filled with non-magnetic dielectric material. Additionally, no symmetry or similarity among cavity geometries is assumed.

Consider an infinite PEC ground plane with n embedded two-dimensional cavities. In three dimensions, these cavities are z-invariant infinite grooves, or channels. Orientation of the fields is TM^z, indicating that wave propagation and the magnetic field are fully described in the xy-plane, and the electric field is fully z-directed, but described as a function of (x, y). The region above the ground plane is considered free space $\mathbb{R}^2_+ = \{x, y \in \mathbb{R}^2 : y \geq 0\}$ with constant material parameters ε_0, μ_0 describing the permittivity and permeability of free space.

The cavities themselves are denoted by Ω_j, $j = 1, 2, ..., k$. Within each cavity, there may be a non-magnetic, homogeneous, dielectric filler, with parameters μ_0, ε_j with $\varepsilon_j \in \mathbb{C}, \text{Re}\{\varepsilon_j\} \geq \delta > 0, \text{Im}\{\varepsilon_j\} \geq 0$. Finally, the walls of the cavity are considered PEC as well. Figure 1.1 illustrates an example domain for $k = 2$.

Through the development and analysis of the multiple cavity scattering problem, the primary aim of this research is to establish a variational formulation for the weak solution and prove that said variational formulation is well-posed. The secondary aim of this work is to demonstrate that the proposed solution method may be numerically implemented in a stable manner using FEM. The final goal is to establish methods for quantifying the influence of coupling between additional cavity scatterers on a solution.

This research contributes to the growing body of work in the field by providing a framework for numerically modeling the total transient scattered field produced by multiple cavities using a coupled boundary condition at the aperture of each cavity and proving that a unique solution to this problem exists for each discrete step in time.

This document is laid out as follows. Chapter two is a summary of related work. Chapter three contains the analysis of the discretized multiple cavity problem, including Green's function derivation, variational formulation, and proof that the variational formulation is well-posed. Chapter four describes the numerical methods for implementing the FE-BI. Chapter five demonstrates results from computational experiments with two and three cavities. Finally, chapter six discusses conclusions and directions for future research.

1.3 Electromagnetics Fundamentals

In this section, we present for reference Maxwell's equations, requirements for electromagnetic fields at boundaries, as well as common function spaces and theorems that are background information for problem development.

1.3.1 Maxwell's Equations.

The building blocks of modern EM research regarding transmission and scattering are the differential (curl) equations formalized by James Clerk Maxwell and based on the works of Gauss, Ampere, and Faraday [4].

$$\nabla \times \vec{E} = -\frac{\partial \vec{B}}{\partial t} \tag{1.1}$$

$$\nabla \times \vec{H} = \vec{J} + \frac{\partial \vec{D}}{\partial t} \tag{1.2}$$

In source-free linear, homogeneous, isotropic media, these equations simplify to

$$\nabla \times \vec{E} = -\mu \frac{\partial \vec{H}}{\partial t}, \qquad \text{and} \qquad \nabla \times \vec{H} = \varepsilon \frac{\partial \vec{E}}{\partial t}. \tag{1.3}$$

Table 1.1: Definition of Symbols from Maxwell's Equations

Symbol	Description
$\nabla\times$	Curl operator
$\vec{E}$	Electric field intensity (volts/meter)
$\vec{B}$	Magnetic flux density (webers/meter)
$\vec{H}$	Magnetic field intensity (amperes/meter)
$\vec{J}$	Electric current density (amperes/square meter)
$\vec{D}$	Electric flux density (coulombs/square meter)
μ	Magnetic permeability (henries/meter)
ε	Electric permittivity (farads/meter)
t	Time

The electric and magnetic fields, $\vec{E}$ and $\vec{H}$ may be represented by their scalar components, E_x, E_y, E_z, H_x, H_y, and H_z such that

$$\vec{E} = \hat{x}E_x + \hat{y}E_y + \hat{z}E_z, \qquad \vec{H} = \hat{x}H_x + \hat{y}H_y + \hat{z}H_z. \tag{1.4}$$

Let E_x, E_y, E_z, H_x, H_y, and H_z all be twice differentiable continuous functions that map from $\mathbb{R}^3 \times \mathbb{R}^+$ into $[0, \infty)$. Substituting (1.4) into (1.3) gives

$$\begin{aligned}
\nabla \times (\nabla \times \vec{E}) &= \nabla \times \left(-\mu \frac{\partial \vec{H}}{\partial t} \right) \\
&= -\mu \frac{\partial (\nabla \times \vec{H})}{\partial t} \\
&= -\mu \frac{\partial (\varepsilon \frac{\partial \vec{E}}{\partial t})}{\partial t} \\
&= -\mu\varepsilon \frac{\partial^2 \vec{E}}{\partial t^2}.
\end{aligned}$$

For the magnetic field equations, applying the same analysis produces the equation

$$\nabla \times (\nabla \times \vec{H}) = -\varepsilon\mu \frac{\partial^2 \vec{H}}{\partial t^2}.$$

In the case of TM^z polarization, the electric field is wholly described in its E_z component as a function of x and y. Setting $E_x = E_y = 0$, and any partial derivatives with respect to z equal to zero, the equations above simplify to

$$\nabla \times (\nabla \times \vec{E}) = -\frac{\partial^2 E_z}{\partial x^2} - \frac{\partial^2 E_z}{\partial y^2} = -\mu\varepsilon \frac{\partial^2 E_z}{\partial t^2}. \tag{1.5}$$

In the case of TE^z polarization, the magnetic field is wholly described in its H_z component as a function of x and y. Letting $H_x = H_y = 0$, and any partial derivatives with respect to z equal zero, the equations for the magnetic field simplify to

$$\nabla \times (\nabla \times \vec{H}) = -\frac{\partial^2 H_z}{\partial x^2} - \frac{\partial^2 H_z}{\partial y^2} = -\varepsilon\mu \frac{\partial^2 H_z}{\partial t^2}. \tag{1.6}$$

1.3.2 Boundary Conditions.

In the absence of external electric or magnetic sources, fields must satisfy the following four conditions [23] along an interface:

$$\hat{n} \times (\vec{E}_1 - \vec{E}_2) = 0 \tag{1.7}$$

$$\hat{n} \times (\vec{H}_1 - \vec{H}_2) = 0 \tag{1.8}$$

$$\hat{n} \cdot (\vec{D}_1 - \vec{D}_2) = 0 \tag{1.9}$$

$$\hat{n} \cdot (\vec{B}_1 - \vec{B}_2) = 0 \tag{1.10}$$

$\hat{n}$ is the normal vector to the interface pointing into region 1. In simple media, $\vec{D} = \varepsilon\vec{E}$ and $\vec{B} = \mu\vec{H}$, which allows equations (1.9, 1.10) to be restated as

$$\hat{n} \cdot (\varepsilon_1\vec{E}_1 - \varepsilon_2\vec{E}_2) = 0$$

$$\hat{n} \cdot (\mu_1\vec{H}_1 - \mu_2\vec{H}_2) = 0.$$

PEC surfaces are idealized materials which contain no internal fields. Consequently, equation (1.7) reduces to

$$\hat{n} \times (\vec{E}) = 0.$$

This is to say that tangential electric fields are zero on the surface of a PEC.

1.3.3 Function Spaces.

Maxwell's equations in differential form, as introduced in section 1.3, are only valid when "the field vectors are single-valued, bounded, continuous functions of position and time and exhibit continuous derivatives." [4] However, at interfaces with discrete changes in material parameters, discontinuities may exist. Relaxing the requirements on continuity of the derivatives in order to find a weak solution, the function space for our solutions will be constrained to those which are square integrable and which have square integrable derivatives. Due to the non-zero boundary condition and potential discontinuities at interfaces, the Sobolev space $W^{1,2}$, or H^1, will be used.

$$\mathrm{H}^1(\Omega) = \{u \in L^2(\Omega) : \|\nabla u\|_{L^2}^2 + \|u\|_{L^2}^2 < \infty\}.$$

The following definition will be used for norms of Sobolev spaces adapted from [35]: For functions in $\mathrm{H}^1(\Omega)$ when $\Omega \subset \mathbb{R}^2$,

$$\|u\|_{\mathrm{H}^1(\Omega)} = \left(\int_\Omega u^2\, dr + \int_\Omega \nabla u \cdot \nabla u\, dr\right)^{1/2}.$$

For functions in $\mathrm{H}^{1/2}(\Gamma)$ where $\Gamma \subseteq \partial\Omega$,

$$\|g\|_{\mathrm{H}^{1/2}(\Gamma)} = \left(\int_\Gamma g(x)^2\, dx + |g|_{1/2}^2\right)^{1/2},$$

$$|g|_{1/2}^2 = \int_\Gamma \int_\Gamma \frac{|g(x) - g(y)|^2}{|x - y|^2}\, dxdy.$$

As a result, $g \in \mathrm{H}^{1/2}$ implies piecewise differentiability of g on the contour Γ.

Additionally, we define $\mathrm{H}^{-1/2}(\Gamma)$ as the dual space to $\mathrm{H}^{1/2}(\Gamma)$ such that for $f \in \mathrm{H}^{1/2}(\Gamma)$ and $g \in \mathrm{H}^{-1/2}(\Gamma)$, the inner product $\langle f, g\rangle_\Gamma$ is a bounded linear functional. In other words,

$$\int_\Gamma f(r)g(r)dr \in \mathbb{R} < \infty.$$

We define the space $\mathbb{H}^m(\Omega)$ required for the multiple cavity problem, which allows for a coupled interior function defined over a finite number disjoint domains. Let Ω be a finite

collection of disjoint domains $\Omega_i,\ i = 1, 2, ...k$ defined by

$$\Omega = \bigcup_{i=1}^{k} \Omega_i, \quad \Omega_i \cap \Omega_j = \begin{cases} \emptyset & i \neq j \\ \Omega_i & i = j \end{cases} \quad i = 1, 2, ..., k,\ j = 1, 2, ..., k.$$

Then the multiple-cavity function space is defined as

$$\mathbb{H}^m(\Omega) = \mathrm{H}^m(\Omega_1) + \mathrm{H}^m(\Omega_2) + ... + \mathrm{H}^m(\Omega_k),$$

by which we mean given , $\Omega = \bigcup_{i=1}^{k} \Omega_i$, for any $f \in \mathbb{H}^m(\Omega)$, there exist k unique functions $f_i,\ i = 1, 2, ..., k$, such that

$$f(\vec{r}) = f_i(\vec{r}), \text{ for all } \vec{r} \in \Omega_i,$$

and each component function, f_i, there exists a function $h \in \mathrm{H}^m(\Omega_i)$ such that f_i can be written as

$$f_i = \begin{cases} h & \text{in } \Omega_i, \\ 0 & \text{in } \Omega \backslash \Omega_i. \end{cases}$$

Thus, we write for $f \in \mathbb{H}^m(\Omega)$,

$$f = \sum_{i=1}^{k} f_i.$$

Additionally, we define some useful notation for functions in these spaces. We define integration over Ω by

$$\int_\Omega f(\vec{r})\, d\vec{r} = \sum_{i=1}^{k} \int_{\Omega_i} f_i(\vec{r})\, d\vec{r},\ i = 1, 2, ..., k, \tag{1.11}$$

and multiplication of two functions in $\mathbb{H}^m(\Omega)$ by

$$fg = \sum_{i=1}^{k} f_i g_i. \tag{1.12}$$

The norm of functions in these spaces is defined as

$$\| \cdot \|^2_{\mathbb{H}^m(\Omega)} = \sum_{i=1}^{k} \| \cdot \|^2_{\mathrm{H}^m(\Omega_i)}.$$

The spaces presented in this section are necessary for the analysis conducted in Section 3.7 and are introduced now as a background for the problem statement.

1.3.4 Useful Theorems.

In this section, some common theorems are presented to provide background for the problem statement and development. In section 3.7, these important results will be used to prove the well-posedness of the multiple-cavity variational formulation.

The **Trace theorem**, as presented in [35] states that for $u \in W^{s,p}(\Omega)$, with $1 < p < \infty$, $g : \Gamma \to \mathbb{R}$ is the *trace* of u on boundary set Γ defined by $\Gamma \subseteq \partial\Omega$ *if and only if* $g \in W^{s-1/p,p}(\Gamma)$. And there exists a bounded linear operator L_{tr}, such that $g = L_{tr}u = u|_{\partial\Omega}$, and

$$||u||_{1-1/p,p,\Gamma} \leq ||u||_{1-1/p,p,\partial\Omega} \leq C||u||_{1,p,\Omega}.$$

The **Poincaré inequality** is useful in demonstrating an operator is coercive. For $u \in \mathrm{H}_0^k(\Omega)$ and differential operator, D^α of order α, Poincaré's inequality, as presented in [32], states:
there exists a constant $c \in (0, \infty)$ such that

$$||u||_2^2 \leq c \sum_{|\alpha|=k} ||D^\alpha u||_2^2, \quad \forall u \in \mathrm{H}_0^k(\Omega).$$

When working with inner products and norms, one will commonly refer to the **Cauchy-Schwarz inequality**, which is defined in [18] as

$$||\alpha + \beta|| \leq ||\alpha|| + ||\beta||$$

The proof that a variational formulation is well posed often relies on the **Lax-Milgram theorem**, which, as presented in [32], states that if B is a bilinear mapping of two elements x and y each members of a Hilbert space, H, *i.e.* $B : \mathrm{H} \times \mathrm{H} \to \mathbb{R}$, then as long as $\exists\, c_1,\, c_2 \in \mathbb{R},\, c_1,\, c_2 < \infty$ such that

$$|B(x, y)| \leq c_1 ||x||_{\mathrm{H}} ||y||_{\mathrm{H}} \quad \forall x, y \in \mathrm{H},$$

$$B(x, x) \geq c_2 ||x||_{\mathrm{H}}^2 \quad \forall x \in \mathrm{H},$$

then for every f, a functional of x in the conjugate space H^*, there exists a unique $y \in H$ such that

$$B(x, y) = f(x) \quad \forall x \in H.$$

II. Related Work

Recent work on cavities and cavity-backed apertures have focused on the FE-BI method [23] as an efficient way to couple the interior cavity region, solved numerically with the finite element method, and the exterior region which is solved analytically with the half-space Green's function. Transient scattering from a single cavity in three dimensions was analyzed in [27], and numerical modeling of the two-dimensional problem was described in [36], utilizing the Newmark method for time-stepping. The Newmark method discretizes the time-dependent equations into forced time-independent Helmholtz equations solved at each time step. Numerical handling of the multiple-cavity time-harmonic problem was well explained in [25] along with proof of well-posedness of the problem. The finite element method is utilized due to its flexibility in conforming to different geometries as well as the ease of imposing the boundary conditions.

2.1 Cavity Scatterers

In most cases, cavity problems are set into an infinite ground plane, where cavity edges are flush to the ground. Thus, half-plane Green's functions and image theory are applied to simplify the exterior problem. The two-dimensional half space analysis of electromagnetic problems is well established in various texts, including [4, 23], and Green's functions for PEC planar surfaces are relatively straightforward to derive, as will be shown in section 3.3.1. A thorough development of a time-harmonic Green's function including impedence conditions at the ground plane is given in [29], and [7] demonstrates how to derive the time-variant Green's function for a similar problem. The time-harmonic scattering of a cavity embedded in the ground plane is well described in [25] and [23]. For high frequencies or large cavities, [39, 42] present highly accurate computational methods, while bounds and stability are addressed in [5, 6, 9]. For overfilled cavities, such that the material filling

protrudes somewhat from the cavity opening, or cavities with non-flush edge conditions, the FE-BI method is still appropriate as in [19–21]. For cavities which are completely flush with the ground plane, the transparent boundary can be drawn at the aperture itself using the half-space Green's function for the exterior solution. However, for overfilled cavities, as with other general surface discontinuities, a semi-circular boundary is drawn surrounding the cavity and protruding material and the known Green's function for the semi-circle used for the exterior solution. In the same manner, scattering from a cavity covered by a dielectric layer is examined in [31]. A straightforward proof of existence and uniqueness of a solution to the general single-cavity time-harmonic problem is presented in [2] utilizing the Fredholm Alternative theorem.

Integral methods are also used for certain cavity scattering problems, as in [29, 30], and are calculated specifically according to the shape of the cavity or protrusion. Far field patterns are computed using Green's functions build from Sommerfeld integrals.

2.2 Time-Variant Single Cavity

Van and Wood [36], present a thorough analysis of the one-cavity problem in the time domain. The key result being that the variational formulation of the TM^z problem has a unique weak solution for each discretized time step. Callihan [7], extended this result to transient scattering from a single overfilled cavity in an impedence ground plane. Alternatively, Huang *et al.* [21] used a Laplace transform method to represent the scattered fields and define boundary conditions on a semi-circular region enclosing the cavity. The interior problem was discretized using a central difference scheme and solved using FEM at each time step.

The multiple cavity problem discussed in this work has many parallels with the single-cavity problem. The primary difference that is faced in the multiple cavity problem is the coupling between cavities.

2.3 Multiple Scatterers

A multiple-body scattering problem in free space is examined in [16]. This analysis provides a backbone for similar analysis of coupled scatterers in the half-plane as was conducted in [25] for the time-harmonic problem. Additionally, a thorough treatment of a general 2-D multiple scattering problem for time-harmonic waves in free space is found in [38], where the treatment of various boundary conditions and interfaces as well as their numerical handling is discussed in depth. Furthermore, a general solution for multiple rectangular cavities is presented in [12] using Fourier transform methods. In two papers, Li and Wood [25, 26] present thorough analysis of the n-cavity problem in the frequency domain. The key result is that the variational formulation of the TM^z problem has a unique weak solution. This result is extended in this work to the multiple-cavity transient problem.

2.4 Computational Methods

Computing numerical models for complex or wideband problems is a challenging task. Operationally, CEM is currently one of the largest consumers of HPC processing time. Computational methods for reducing complexity of the standard matrix operations and domain decomposition for use with parallel processing are active areas of mathematical research. Generally speaking, three principle techniques are commonly employed for CEM problems: FEM, method of moments (MoM), and finite difference time domain (FDTD). As the name might imply, FDTD is designed around application to transient field problems. However, FDTD models are cumbersome to adapt to variable geometries and irregular boundaries. Furthermore, in scattering problems, the infinity of free space must be truncated with an artificial boundary condition which introduces additional error to the solution.

The MoM utilizes integral methods to compute total fields based on known principles, incident fields and other imposed conditions. One drawback of this method for ground plane scattering problems is that truncation must be applied to the infinite ground plane

which introduces unnecessary error into the system. A popular application for MoM is to model scattering patterns from closed, mostly-convex shapes.

Following dramatic increases in computing power and numerical methods for inverting matrices, FEM has become the favored method for many of today's complex CEM problems. The theory of finite elements is general enough to be applied to a variety of problems. The basis functions provide an efficient vehicle for imposing boundary conditions and continuity constraints. Additionally, the elements themselves are units of a decomposed domain, which allow for convenient parallel processing. The largest limitation of FEM in computational handling of electromagnetic scattering problems is inverting the $N \times N$ model matrix, for which in some problems, N may be several millions or more.

Stability of solutions is a critical piece of numerical simulations in the time domain. Time-domain FEM relies on time-discretization to step through time. Explicit methods will generally be subject to constraints on the size of time steps in order to guarantee stability. Implicit solvers, like the Newmark method, are numerically stable for larger time steps but lose accuracy as the step size increases [22]. Recently, an unconditionally stable explicit method for three-dimensional problems has been developed in [17] by building upon the mode-matching methods and removing unstable modes.

III. Multiple Cavity Formulation

Consider k cavities embedded in a PEC ground plane as illustrated for $k = 2$ in Figure 1.1. The three-dimensional equivalent is k infinite trenches or grooves in a PEC ground plane. The axes are oriented such that the ground plane is at $y = 0$, the geometry is invariant with respect to the z-axis, so a two-dimensional analysis is sufficient to characterize the fields. For consistency, cavity interiors will be denoted with Ω_i, $i = 1, 2, ..., k$. PEC cavity walls are denoted S_i, $i = 1, 2, ..., k$, and cavity apertures are denoted Γ_i, $i = 1, 2, ..., k$, respectively for cavities 1 through k. Throughout this chapter, examples for $k = 2$ will be given to clarify to arguments. We stipulate that $\partial\Omega_i = \Gamma_i \cup S_i$, is a continuous Lipschitz boundary and that for $i \neq j$, $\partial\Omega_i \cap \partial\Omega_j = \emptyset$. Define regions

$$\Omega,\ \Gamma,\ S$$

as the union of k disjoint subdomains.

$$\Omega = \bigcup_{i=1}^{k} \Omega_i, \quad \Gamma = \bigcup_{i=1}^{k} \Gamma_i, \quad S = \bigcup_{i=1}^{k} S_i.$$

With the following properties:

$$\begin{aligned} \exists C_x,\ C_y,\ \text{with } 0 < C_x,\ C_y < \infty,\ \text{such that } \forall (x,y) \in \Omega,\ |x| < C_x,\ \text{and } -C_y < y < 0, \\ \forall (x,y) \in S,\ |x| \leq C_x,\ \text{and } -C_y \leq y < 0, \\ \forall (x,y) \in \Gamma,\ |x| \leq C_x,\ \text{and } y = 0. \end{aligned}$$

Define the upper half plane

$$\mathbb{R}^2_+ := \{(x,y) \in \mathbb{R}^2, y > 0\}.$$

Finally, define the PEC ground plane

$$\Gamma^C := \left\{(x,y) \in \mathbb{R}^2, y = 0, (x,y) \notin \Gamma\right\}.$$

For this problem, assume that the upper half plane $\mathbb{R}^2_+$ consists of free space with electric permittivity and magnetic permeability ε_0, μ_0 respectively. Assume that Γ^C, and S are PEC and therefore tangential electric fields are zero along those surfaces. The cavities may be filled with non-magnetic, non-dispersive, simple dielectric materials, with relative permittivity, ε_r satisfying

$$\varepsilon_r \in L^\infty(\Omega),\ \mathrm{Re}\{\varepsilon_r(x,y)\} \geq \delta > 0,\ \mathrm{Im}\{\varepsilon_r(x,y)\} \geq 0, \qquad \text{for all } (x,y) \in \Omega.$$

3.1 TM^z Field Problem Statement

This work assumes that all media are linear and isotropic, with homogeneous free space above the ground plane and homogeneous, non-dissapative, dielectric material inside the cavities. Making use of linear superposition, the electric field may be split into its TM^z and TE^z components, and each field can be analyzed independent of the other. The TM^z field can be described as in equation (1.5). Letting $u = E_z$ and scaling time to free space light meters (LM) gives the following scalar wave equations for $u \in \mathrm{H}^1(\mathbb{R}^2_+ \cup \Omega)$:

$$\begin{cases} \Delta u - u_{tt} = 0 & \text{in } \mathbb{R}^2_+, \\ \Delta u - \varepsilon_r u_{tt} = 0 & \text{in } \Omega. \end{cases} \tag{3.1}$$

Applying PEC boundary conditions and field continuity properties gives

$$\begin{cases} u = 0 & \text{on } \Gamma^C \cup S, \\ \lim\limits_{y\to 0+} \frac{\partial}{\partial y} u(x,y) = \lim\limits_{y\to 0-} \frac{\partial}{\partial y} u(x,y) & (x,0) \in \Gamma. \end{cases} \tag{3.2}$$

It is known that the total field can be decomposed into the sum of its parts. Given an incident TM^z field with $E_z^{inc} = u^{inc}$, where $u^{inc} \in \mathrm{H}^1(\mathbb{R}^2)$, the total field u can be written

$$u = \begin{cases} u^{inc} + u^{ref} + u^s & \text{in } \mathbb{R}^2_+ \cup \Gamma, \\ u_i & \text{in } \Omega_i, \end{cases} \tag{3.3}$$

where $i = 1, 2, ..., k$ and u^{ref} is defined as the reference field, equivalent to a full reflection from a PEC planar surface, and u^s is the outward-directed scattered field from the cavities.

$$u^{ref}(x, y) = \begin{cases} -u^{inc}(x, -y) & \text{in } \mathbb{R}^2_+, \\ 0 & \text{in } \Omega. \end{cases} \tag{3.4}$$

Note that, by definition, $\forall x \in \mathbb{R},\ u^{ref}(x, 0) + u^{inc}(x, 0) = 0$.

$$u^s = \begin{cases} u - u^{inc} - u^{ref} & \text{in } \mathbb{R}^2_+, \\ u_\Gamma & \text{on } \Gamma, \\ 0 & \text{in } \Omega \backslash \Gamma. \end{cases} \tag{3.5}$$

It is assumed that the outgoing scattered field satisfies the radiation condition as in [36]

$$\lim_{r\to\infty} \sqrt{r}\left(\frac{\partial}{\partial r} + \frac{\partial}{\partial t}\right) u^s = 0 \quad \text{in } \mathbb{R}^2_+,$$

with $r = |\vec{r}| = \sqrt{x^2 + y^2}$.

Interior fields are similarly defined as

$$u_i = \begin{cases} 0 & \text{in } \mathbb{R}^2_+ \bigcup_{j\neq i} \Omega_j \bigcup_{j\neq i} \Gamma_j, \\ u_\Gamma & \text{on } \Gamma_i, \\ u & \text{in } \Omega_i, \end{cases} \tag{3.6}$$

Finally, the fields along the ground plane are subject to continuity requirements and are represented as

$$u_\Gamma = \begin{cases} 0 & \text{in } \mathbb{R}^2_+ \cup \Gamma^C, \\ u = u^s = u_i & \text{on } \Gamma_i,\ i = 1, 2, ..., k, \\ 0 & \text{in } \Omega. \end{cases} \tag{3.7}$$

With functions thus defined, it can be seen that $u \in \mathrm{H}^1(\mathbb{R}^2_+ \cup \Omega \cup \Gamma)$ can be summarized by

$$u = u^{inc} + u^{ref} + u^s - u_\Gamma + \sum_{i=i}^{k} u_i.$$

Therefore, the problem is stated as follows: Given an incident TM^z field, u^{inc}, we are seeking the full-field solution u at time $t = T > 0$ satisfying:

$$\begin{cases} -\Delta u + \varepsilon_r \dfrac{\partial^2}{\partial t^2} u = 0 & \text{in } \mathbb{R}^2_+ \cup \Omega \cup \Gamma, \\ u = 0 & \text{on } \Gamma^c \cup S, \\ \lim\limits_{y \to 0+} \dfrac{\partial}{\partial y} u(x,y) = \lim\limits_{y \to 0-} \dfrac{\partial}{\partial y} u(x,y) & \text{for all } x : (x,0) \in \Gamma, \\ \sqrt{r}\left(\dfrac{\partial}{\partial r} + \dfrac{\partial}{\partial t}\right) u^s \to 0 & \text{as } r \to \infty. \end{cases} \tag{3.8}$$

3.2 Newmark Method

In order to address the time-varying nature of the transient scattering problem, we apply Newmark's method as the computational time-stepping scheme. The Newmark method was initially proposed for solving problems in structural dynamics in 1959 [28] and is preferred to central difference discretization routines due to its unconditional stability [23]. The Newmark method, as used in [7, 36], has the beneficial properties of being unconditionally stable with correctable linear growth in error [8, 14], as well computationally lean compared to Kirchhoff-type methods which require storage of solutions at all previous time steps. Using a fixed time step length h, the total number of time steps needed to approximate the fields at final time T is $N = T/h$. Assuming that initial data are provided either in the form of an incident plane wave or some other functional form for the upper half-plane, we apply the Newmark method to make temporal approximations for these functions at each discrete time $t_n = nh$ for $n = 1, 2, ..., N$. The notation, $u^n(x, y)$ and $\dot{u}^n(x, y)$ are used to denote the approximations of $u(x, y, t_n)$ and $u_t(x, y, t_n)$, respectively. The generating equations for the Newmark method are:

$$u(t+h) = u(t) + h u_t(t) + \left(\frac{1}{2} - \beta\right) h^2 u_{tt}(t) + \beta h^2 u_{tt}(t+h) \tag{3.9}$$

$$u_t(t+h) = u_t(t) + (1-\gamma) h u_{tt}(t) + \gamma h u_{tt}(t+h), \tag{3.10}$$

with β and γ being free parameters for controlling stability and accuracy. For the TM^z case, including the discretized wave equation from equation (3.8), this can be written as

$$\begin{cases} u^{n+1} = u^n + h\dot{u}^n + \left(\frac{1}{2} - \beta\right) h^2 \ddot{u}^n + \beta h^2 \ddot{u}^{n+1} & 0 \le n < N, \\ \dot{u}^{n+1} = \dot{u}^n + (1-\gamma) h\ddot{u}^n + \gamma h \ddot{u}^{n+1} & 0 \le n < N, \\ \Delta u^{n+1} - \varepsilon_r \ddot{u}^{n+1} = 0 & 0 \le n < N. \end{cases} \tag{3.11}$$

This method generally requires that $0 \le \gamma \le 1$ and $0 \le \beta \le 1/2$, however to gain unconditional stability, the following conditions must hold [37]:

$$\gamma \ge \frac{1}{2}, \quad \text{and} \quad \beta \ge \frac{1}{4}\left(\frac{1}{2} + \gamma\right)^2.$$

When $\gamma = 0.5$, this is known as the Newmark-β method [23]. Assuming that $\beta > 0$, the Newmark method is implicit. In order to implement this implicit method, a prediction-correction scheme is used.

Let $\tilde{u}$ be the prediction based on current time, t_n, data

$$\tilde{u}^{n+1} = u^n + h\dot{u}^n + \left(\frac{1}{2} - \beta\right) h^2 \ddot{u}^n, \tag{3.12}$$

then from (3.11),

$$u^{n+1} - \beta h^2 \ddot{u}^{n+1} = \tilde{u}^{n+1}. \tag{3.13}$$

Substituting $\Delta u = \varepsilon_r \ddot{u}$ and $\alpha^2 = (\beta h^2)^{-1}$, into equation (3.13) gives

$$-\Delta u^{n+1} + \alpha^2 \varepsilon_r u^{n+1} = \alpha^2 \varepsilon_r \tilde{u}^{n+1}, \tag{3.14}$$

which is of similar form to the time-harmonic wave equation with a source term. Solving equation (3.14) for u^{n+1} is possible using numerical methods. Once a solution is obtained, the Newmark correction will be applied as

$$\begin{aligned} \ddot{u}^{n+1} &= \alpha^2 (u^{n+1} - \tilde{u}^{n+1}), \\ \dot{u}^{n+1} &= \dot{u}^n + (1-\gamma) h\ddot{u}^n + \gamma h \ddot{u}^{n+1}. \end{aligned} \tag{3.15}$$

In practice, the computational domain for the FEM will be restricted to the interior of each cavity. The intereior fields will be solved for as a series of coupled equations using FEM with a Dirichlet-to-Neumann (DtN) boundary condition at the apertures. The exterior fields will then be determined analytically from the solution for the interior fields.

3.3 Exterior Solution

Given that u^{inc} is known for all time, then by applying image theory, u^{ref} is also known. That leaves u^s as the only unknown in the total exterior field u in $\mathbb{R}^2_+$. Following the method of [36], we seek to solve for the scattered field which satisfies (3.14), (3.2), and (3.5):

$$\begin{cases} -\Delta u^{s,n+1} + \alpha^2 \varepsilon_r u^{s,n+1} = \alpha^2 \varepsilon_r \tilde{u}^{s,n+1} & \text{in } \mathbb{R}^2_+, \\ u^{s,n+1} = g & \text{on } \Gamma, \\ u^{s,n+1} = 0 & \text{on } \Gamma^C. \end{cases} \tag{3.16}$$

Let g_0 be the zero extension of g, defined as

$$g_0 = \begin{cases} g & \text{on } \Gamma, \\ 0 & \text{on } \Gamma^C, \end{cases} \tag{3.17}$$

so that $u^{n+1}|_{y=0} = u^{s,n+1}|_{y=0} = g_0$ is defined for the entire ground plane. If $u^{inc} \in \mathrm{H}^1(\mathbb{R}^2_+)$ and $g_0 \in \mathrm{H}^{1/2}(\mathbb{R})$ are known, then the exterior problem (3.16) can be solved analytically using the half-space Green's function, $G^e_\alpha(\vec{r}, \vec{r'})$, as in [23, 36]. Note that $G^e_\alpha(\vec{r}, \vec{r'})$ is required to satisfy the homogeneous differential equation everywhere except $\vec{r} = \vec{r'}$, where it operates as a Dirac delta.

$$\begin{cases} -\Delta G^e_\alpha(\vec{r}, \vec{r'}) + \alpha^2 G^e_\alpha(\vec{r}, \vec{r'}) = \delta(\vec{r}, \vec{r'}) & \text{in } \mathbb{R}^2_+ \\ G^e_\alpha(\vec{r}, \vec{r'}) = 0 & \text{on } \Gamma_1 \cup \Gamma_2 \cup \Gamma^C \\ \sqrt{|\vec{r}|}\left(\dfrac{\partial}{\partial \vec{r}} + \dfrac{\partial}{\partial t}\right) G^e_\alpha(\vec{r}, \vec{r'}) \to 0 & \text{as } |\vec{r}| \to \infty. \end{cases} \tag{3.18}$$

Multiplying (3.16) by G^e_α and integrating, also substituting $\varepsilon_r = 1$ because the upper half plane is free space, gives

$$\int_{\mathbb{R}^2_+} G^e_\alpha(-\Delta u^{s,n+1} + \alpha^2 u^{s,n+1})\, d\vec{r'} = \int_{\mathbb{R}^2_+} G^e_\alpha \alpha^2 \tilde{u}^{s,n+1}\, d\vec{r'}. \tag{3.19}$$

Green's second scalar theorem, as presented in [35], gives

$$\int_{\mathbb{R}^2_+} G^e_\alpha \Delta u^{s,n+1}\, d\vec{r'} = \int_{\mathbb{R}^2_+} u^{s,n+1} \Delta G^e_\alpha\, d\vec{r'} + \int_{\partial\mathbb{R}^2_+} \hat{n} \cdot (G^e_\alpha \nabla u^{s,n+1} - u^{s,n+1} \nabla G^e_\alpha)\, dS. \quad (3.20)$$

Substituting (3.20) into (3.19) and rearranging yields

$$\int_{\mathbb{R}^2_+} u^{s,n+1}(-\Delta G^e_\alpha + \alpha^2 G^e_\alpha)\, d\vec{r'} = \int_{\partial\mathbb{R}^2_+} \hat{n} \cdot (G^e_\alpha \nabla u^{s,n+1} - u^{s,n+1} \nabla G^e_\alpha)\, dS + \int_{\mathbb{R}^2_+} G^e_\alpha \alpha^2 \tilde{u}^{s,n+1}\, d\vec{r'}. \quad (3.21)$$

Applying the delta function property in (3.18) to the left hand side of (3.21) gives

$$u^{s,n+1}(\vec{r}) = \int_{\partial\mathbb{R}^2_+} \hat{n} \cdot (G^e_\alpha \nabla u^{s,n+1} - u^{s,n+1} \nabla G^e_\alpha)\, dS + \int_{\mathbb{R}^2_+} G^e_\alpha \alpha^2 \tilde{u}^{s,n+1}\, d\vec{r'}. \quad (3.22)$$

Examining the contour integral in (3.22) and defining $\hat{n} \cdot \nabla f = \frac{\partial}{\partial n} f$ allows the following simplifications:

$$\begin{aligned}
\int_{\partial\mathbb{R}^2_+} \hat{n} \cdot (G^e_\alpha \nabla u^{s,n+1} - u^{s,n+1} \nabla G^e_\alpha)\, dS &= \int_{\partial\mathbb{R}^2_+} \hat{n} \cdot G^e_\alpha \nabla u^{s,n+1} - \hat{n} \cdot u^{s,n+1} \nabla G^e_\alpha\, dS \\
&= \int_{\partial\mathbb{R}^2_+} G^e_\alpha \hat{n} \cdot \nabla u^{s,n+1} - u^{s,n+1} \hat{n} \cdot \nabla G^e_\alpha\, dS \\
&= \int_{\partial\mathbb{R}^2_+} G^e_\alpha \frac{\partial}{\partial n} u^{s,n+1} - u^{s,n+1} \frac{\partial}{\partial n} G^e_\alpha\, dS.
\end{aligned}$$

$$u^{s,n+1}(\vec{r}) = \int_{\partial\mathbb{R}^2_+} G^e_\alpha \frac{\partial}{\partial n} u^{s,n+1} - u^{s,n+1} \frac{\partial}{\partial n} G^e_\alpha\, dS + \int_{\mathbb{R}^2_+} G^e_\alpha \alpha^2 \tilde{u}^{s,n+1}\, d\vec{r'}. \quad (3.23)$$

By definition, $G^e_\alpha(\vec{r}, \vec{r'}) = 0$ on $\partial\mathbb{R}^2_+$, so (3.23) becomes,

$$u^{s,n+1}(\vec{r}) = -\int_{\partial\mathbb{R}^2_+} u^{s,n+1} \frac{\partial}{\partial n} G^e_\alpha\, dS + \int_{\mathbb{R}^2_+} G^e_\alpha \alpha^2 \tilde{u}^{s,n+1}\, d\vec{r'}. \quad (3.24)$$

The radiation condition, $\lim_{r\to\infty} u^s = 0$, and the boundary condition, $u^s = 0$ on Γ^C, are appied to reduce the countour integral to

$$\int_{\partial\mathbb{R}^2_+} u^{s,n+1} \frac{\partial}{\partial n} G^e_\alpha\, dS = \int_\Gamma u^{s,n+1} \frac{\partial}{\partial n} G^e_\alpha\, dx'.$$

Thus (3.24) is simplified to the following result for the scattered field which is very similar to the form in [36].

$$u^{s,n+1}(\vec{r}) = \int_{\mathbb{R}^2_+} G^e_\alpha \alpha^2 \tilde{u}^{s,n+1}\, d\vec{r'} - \int_\Gamma u^{s,n+1} \frac{\partial}{\partial n} G^e_\alpha\, dx', \quad (3.25)$$

where Γ represents the multiple disjoint apertures. Then, the total exterior field, discretized from (3.3) with $t = h(n+1)$ can be expressed as

$$u^{tot}(\vec{r},t) \approx u^{inc}(\vec{r},t) + u^{ref}(\vec{r},t) + u^{s,n+1}(\vec{r}), \quad \vec{r} \in \mathbb{R}^2_+$$

or, using the image of $\vec{r} = (x,y)$, $\vec{r}_i = (x,-y)$,

$$u^{tot}(\vec{r},t) \approx u^{inc}(\vec{r},t) - u^{inc}(\vec{r}_i,t) + \int_{\mathbb{R}^2_+} G^e_\alpha \alpha^2 \tilde{u}^{s,n+1}\, d\vec{r'} - \int_\Gamma g \frac{\partial}{\partial n} G^e_\alpha \, dx'. \tag{3.26}$$

Therefore, in summary, the exterior solution for $u^{s,n+1}$ can be written in terms of the precalculated estimate $\tilde{u}^{s,n+1}$ and the aperture fields given by $g_1 = u^{s,n+1}|_\Gamma$. Because it is problematic to solve for u^s in terms of g defined by u^s, we note that g can also be described by the interior function $u^{n+1} \in \mathbb{H}^1(\mathbf{\Omega})$, as $g = u^{n+1}|_\Gamma$. This relationship lays the basic foundation for how the numerical method will is developed.

3.3.1 Green's Function.

The Green's function is a crucial peice of the FE-BI method. With the appropriately defined Green's function, the exterior fields may be expressed as a sum of known values and integrals as in (3.26). In development of the Green's function, the following Fourier transform convention is used:

$$F[g(x)] = \hat{g}(\xi) = \frac{1}{\sqrt{2\pi}} \int_{-\infty}^{\infty} g(x) \mathrm{e}^{-\mathrm{i}x\xi} dx$$
$$F^{-1}[\hat{g}(\xi)] = g(x) = \frac{1}{\sqrt{2\pi}} \int_{-\infty}^{\infty} \hat{g}(\xi) \mathrm{e}^{\mathrm{i}x\xi} d\xi.$$

Following the method used in [7], the Fourier transform is applied to construct the Green's function which satisfies the requirements of (3.18). Taking the Fourier transform with respect to the x direction gives,

$$F[G] = \hat{G}(\xi, y) = \frac{1}{\sqrt{2\pi}} \int_{-\infty}^{\infty} G(\vec{r}, \vec{r'}) \mathrm{e}^{-\mathrm{i}\xi x} dx.$$

Note that the Green's function satisfies the radiation condition at infinity, so the second derivative may be "transferred" onto the transform operator.

$$\begin{aligned} F\left[\frac{\partial^2}{\partial x^2}G\right] = \frac{\partial^2}{\partial x^2}\hat{G}(\xi, y) &= \frac{1}{\sqrt{2\pi}}\int_{-\infty}^{\infty}\left(\frac{\partial^2}{\partial x^2}G(\vec{r}, \vec{r'})\right)\mathrm{e}^{-\mathrm{i}\xi x}dx \\ &= \frac{1}{\sqrt{2\pi}}\left[\mathrm{e}^{-\mathrm{i}\xi x}\frac{\partial}{\partial x}G(\vec{r}, \vec{r'})\Big|_{-\infty}^{\infty} - \int_{-\infty}^{\infty}\frac{\partial}{\partial x}G(\vec{r}, \vec{r'})\frac{\partial}{\partial x}\mathrm{e}^{-\mathrm{i}\xi x}dx\right] \\ &= \frac{1}{\sqrt{2\pi}}\left[-G(\vec{r}, \vec{r'})\frac{\partial}{\partial x}\mathrm{e}^{-\mathrm{i}\xi x}\Big|_{-\infty}^{\infty} + \int_{-\infty}^{\infty}G(\vec{r}, \vec{r'})\frac{\partial^2}{\partial x^2}\mathrm{e}^{-\mathrm{i}\xi x}dx\right] \\ &= -\xi^2\frac{1}{\sqrt{2\pi}}\int_{-\infty}^{\infty}G(\vec{r}, \vec{r'})\mathrm{e}^{-\mathrm{i}\xi x}dx = -\xi^2\hat{G}(\xi, y). \end{aligned}$$

Considering that the homogeneous solution is independent of the fixed horizontal source point, without loss of generality let $x' = 0$. Taking the Fourier transform of the delta function gives

$$\begin{aligned} F[\delta(\vec{r}, \vec{r'})] = F[\delta(x-0)\delta(y-y')] &= \frac{1}{\sqrt{2\pi}}\int_{-\infty}^{\infty}\delta(x-0)\delta(y-y')\mathrm{e}^{-\mathrm{i}\xi x}dx \\ &= \delta(y-y')\frac{1}{\sqrt{2\pi}}\int_{-\infty}^{\infty}\delta(x-0)\mathrm{e}^{-\mathrm{i}\xi x}dx \\ &= \delta(y-y')\frac{1}{\sqrt{2\pi}}. \end{aligned}$$

Thus, the Fourier transform of the differential equation (3.18) can be written as

$$\begin{cases} -\dfrac{\partial^2}{\partial y^2}\hat{G}^e_\alpha(\xi, y) + (\xi^2 + \alpha^2)\hat{G}^e_\alpha(\xi, y) = \delta(y-y')\dfrac{1}{\sqrt{2\pi}} & \text{in } \mathbb{R}^2_+ \\ \hat{G}^e_\alpha(\xi, y) = 0 & \text{on } \Gamma \cup \Gamma^C. \end{cases} \tag{3.27}$$

Additionally, the half-space Green's function must satisfy (3.27) at values for y other than y' and satisfy the continuity and jump conditions at $y = y'$. Observing that radiation conditions must still be satisfied, this differential equation has solutions of the form

$$\Phi(\xi, y) = \begin{cases} C_1\mathrm{e}^{-\sqrt{\xi^2+\alpha^2}y} & \text{for } y > y' \\ C_2\mathrm{e}^{\sqrt{\xi^2+\alpha^2}y} & \text{for } y < y' \end{cases} \tag{3.28}$$

Matching constants for continuity at $y = y'$ gives

$$\begin{aligned} C_1\mathrm{e}^{-\sqrt{\xi^2+\alpha^2}y'} &= C_2\mathrm{e}^{\sqrt{\xi^2+\alpha^2}y'} \\ C_1\mathrm{e}^{-2\sqrt{\xi^2+\alpha^2}y'} &= C_2. \end{aligned}$$

Examining the first derivative in y to ensure jump condition at $y = y'$ as stated in [35] gives

$$\begin{aligned}
\lim_{y\to y'+}\frac{\partial}{\partial y}\Phi(\xi,y) - \lim_{y\to y'-}\frac{\partial}{\partial y}\Phi(\xi,y) &= -1\\
-C_1\sqrt{\xi^2+\alpha^2}\mathrm{e}^{-\sqrt{\xi^2+\alpha^2}y'} - C_2\sqrt{\xi^2+\alpha^2}\mathrm{e}^{\sqrt{\xi^2+\alpha^2}y'} &= -1\\
-C_1\sqrt{\xi^2+\alpha^2}\mathrm{e}^{-\sqrt{\xi^2+\alpha^2}y'} - C_1\sqrt{\xi^2+\alpha^2}\mathrm{e}^{-2\sqrt{\xi^2+\alpha^2}y'}\mathrm{e}^{\sqrt{\xi^2+\alpha^2}y'} &= -1\\
-C_1\sqrt{\xi^2+\alpha^2}\mathrm{e}^{-\sqrt{\xi^2+\alpha^2}y'} - C_1\sqrt{\xi^2+\alpha^2}\mathrm{e}^{-\sqrt{\xi^2+\alpha^2}y'} &= -1\\
-2C_1\sqrt{\xi^2+\alpha^2}\mathrm{e}^{-\sqrt{\xi^2+\alpha^2}y'} &= -1.
\end{aligned}$$

Thus solving for the constant coefficients,

$$C_1 = \frac{\mathrm{e}^{\sqrt{\xi^2+\alpha^2}y'}}{2\sqrt{\xi^2+\alpha^2}} \tag{3.29}$$

$$C_2 = \frac{\mathrm{e}^{\sqrt{\xi^2+\alpha^2}y'}}{2\sqrt{\xi^2+\alpha^2}}\mathrm{e}^{-2\sqrt{\xi^2+\alpha^2}y'} = \frac{\mathrm{e}^{-\sqrt{\xi^2+\alpha^2}y'}}{2\sqrt{\xi^2+\alpha^2}}. \tag{3.30}$$

Inserting these constants into equation (3.28) gives

$$\Phi(\xi,y) = \begin{cases} \dfrac{\mathrm{e}^{-\sqrt{\xi^2+\alpha^2}(y-y')}}{2\sqrt{\xi^2+\alpha^2}} & \text{for } y > y' \\ \dfrac{\mathrm{e}^{-\sqrt{\xi^2+\alpha^2}(y'-y)}}{2\sqrt{\xi^2+\alpha^2}} & \text{for } y < y', \end{cases} \tag{3.31}$$

which can be simplified as

$$\Phi(\xi,y) = \frac{\mathrm{e}^{-\sqrt{\xi^2+\alpha^2}|y-y'|}}{2\sqrt{\xi^2+\alpha^2}}. \tag{3.32}$$

Additionally, the PEC boundary requires that the Green's function yield a value of zero along $y = 0$. This condition may be enforced by adding an additional term to the general

solution.

$$\Phi_p(\xi,0) = \frac{e^{-\sqrt{\xi^2+\alpha^2}|y-y'|}}{2\sqrt{\xi^2+\alpha^2}} + C_3 e^{-\sqrt{\xi^2+\alpha^2}y} = 0$$

$$\Phi_p(\xi,0) = \frac{e^{-\sqrt{\xi^2+\alpha^2}y'}}{2\sqrt{\xi^2+\alpha^2}} + C_3 = 0$$

$$C_3 = -\frac{e^{-\sqrt{\xi^2+\alpha^2}y'}}{2\sqrt{\xi^2+\alpha^2}}$$

$$\Phi_p(\xi,y) = \frac{e^{-\sqrt{\xi^2+\alpha^2}|y-y'|}}{2\sqrt{\xi^2+\alpha^2}} - \frac{e^{-\sqrt{\xi^2+\alpha^2}y'}}{2\sqrt{\xi^2+\alpha^2}} e^{-\sqrt{\xi^2+\alpha^2}y}.$$

Simplifying $\Phi_p(\xi,y)$ gives the following form:

$$\Phi_p(\xi,y) = \frac{e^{-\sqrt{\xi^2+\alpha^2}|y-y'|}}{2\sqrt{\xi^2+\alpha^2}} - \frac{e^{-\sqrt{\xi^2+\alpha^2}(y'+y)}}{2\sqrt{\xi^2+\alpha^2}}. \tag{3.33}$$

Note that (3.33) is scaled to operate as the Dirac delta function, whereas (3.27) has a constant coefficient of $\frac{1}{\sqrt{2\pi}}$. This indicates that the full representation for $\hat{G}^e_\alpha(\xi,y)$ should be

$$\hat{G}^e_\alpha(\xi,y) = \frac{1}{\sqrt{2\pi}}\Phi_p(\xi,y),$$

which has the expanded form

$$\hat{G}^e_\alpha(\xi,y) = \frac{1}{\sqrt{2\pi}}\left(\frac{e^{-\sqrt{\xi^2+\alpha^2}|y-y'|}}{2\sqrt{\xi^2+\alpha^2}} - \frac{e^{-\sqrt{\xi^2+\alpha^2}(y'+y)}}{2\sqrt{\xi^2+\alpha^2}}\right). \tag{3.34}$$

Taking the inverse Fourier transform of $\hat{G}^e_\alpha(\xi,y)$, considering the variation in the x direction, will return the functional form of $G^e_\alpha(x,y)$.

$$\begin{aligned} F^{-1}[\hat{G}^e_\alpha(\xi,y)] = G^e_\alpha(x,y) &= \frac{1}{\sqrt{2\pi}}\int_{-\infty}^{\infty} \hat{G}^e_\alpha(\xi,y) e^{i(x-x')\xi} d\xi \\ &= \frac{1}{2\pi}\int_{-\infty}^{\infty}\left(\frac{e^{-\sqrt{\xi^2+\alpha^2}|y-y'|}}{2\sqrt{\xi^2+\alpha^2}} - \frac{e^{-\sqrt{\xi^2+\alpha^2}(y'+y)}}{2\sqrt{\xi^2+\alpha^2}}\right) e^{i(x-x')\xi} d\xi \end{aligned}$$

Thus the Green's function may be written as

$$G^e_\alpha(x,y) = \frac{1}{4\pi}\int_{-\infty}^{\infty} \frac{e^{-\sqrt{\xi^2+\alpha^2}|y-y'|}}{\sqrt{\xi^2+\alpha^2}} e^{i(x-x')\xi} d\xi - \frac{1}{4\pi}\int_{-\infty}^{\infty} \frac{e^{-\sqrt{\xi^2+\alpha^2}(y'+y)}}{\sqrt{\xi^2+\alpha^2}} e^{i(x-x')\xi} d\xi \tag{3.35}$$

The integral representation of (3.35) may be simplified by following the example in [10]. Substituting $r\cos\phi = x - x'$ and $r\sin\phi = y - y'$, with $r \geq 0$, and $-\pi \leq \phi < \pi$, allows the transformation

$$\frac{1}{4\pi}\int_{-\infty}^{\infty}\frac{\mathrm{e}^{-\sqrt{\xi^2+\alpha^2}|y-y'|}}{\sqrt{\xi^2+\alpha^2}}\mathrm{e}^{\mathrm{i}(x-x')\xi}d\xi = \frac{\mathrm{i}}{4\pi}\int_{C(\phi)}\mathrm{e}^{\mathrm{i}(\mathrm{i}\alpha)r\cos\beta}d\beta,$$

with $C(\phi)$ defined by

$$C(\phi) = \begin{cases} x = -|\phi| & y \text{ from } \mathrm{i}\infty \text{ to } 0, \\ y = 0 & x \text{ from } -|\phi| \text{ to } \pi - |\phi|, \\ x = \pi - |\phi| & y \text{ from } 0 \text{ to } -\mathrm{i}\infty. \end{cases}$$

Referring to [15], this functional form is equivalent to $\left(\frac{\mathrm{i}}{4\pi}\right)\pi H_0^1(\mathrm{i}\alpha r)$. Similarly, substituting $r_i\cos\phi = x - x'$ and $r_i\sin\phi = -y - y'$, with $r \geq 0$, and $-\pi \leq \phi < \pi$, gives

$$\frac{1}{4\pi}\int_{-\infty}^{\infty}\frac{\mathrm{e}^{-\sqrt{\xi^2+\alpha^2}(y+y')}}{\sqrt{\xi^2+\alpha^2}}\mathrm{e}^{\mathrm{i}(x-x')\xi}d\xi = \frac{\mathrm{i}}{4\pi}\int_{C(\phi)}\mathrm{e}^{\mathrm{i}(\mathrm{i}\alpha)r_i\cos\beta}d\beta = \left(\frac{\mathrm{i}}{4\pi}\right)\pi H_0^1(\mathrm{i}\alpha r_i)$$

Thus, (3.35) can be restated as

$$G_\alpha^e(x,y,x',y') = \frac{\mathrm{i}}{4}(H_0^1(\mathrm{i}\alpha r) - H_0^1(\mathrm{i}\alpha r_i)) \tag{3.36}$$

Two forms of the 2-D Green's function are presented in the literature:

$$\text{From [23]: } G_1(\vec{r},\vec{r'}) = \frac{1}{4j}\left[H_0^2(\alpha|\vec{r}-\vec{r'}|) - H_0^2(\alpha|\vec{r}-\vec{r_i'}|)\right]. \tag{3.37}$$

$$\text{From [36]: } G_2(\vec{r},\vec{r'}) = \frac{1}{2\pi}\left[K_0(\alpha|\vec{r}-\vec{r'}|) - K_0(\alpha|\vec{r}-\vec{r_i'}|)\right]. \tag{3.38}$$

With $\vec{r} = (x,y)$ and its image $\vec{r_i} = (x,-y)$. Equation (3.37) is used for time-harmonic 2-D problems and equation (3.38) is seen in time-variant applications. Below, it is shown that (3.36) is equivalent to (3.38), thus the latter representation may be used.

It is noted in [7] that:

$$K_0(kR) = \frac{\pi\mathrm{i}}{2}H_0^1(\mathrm{i}kR).$$

This is adapted from Abramowitz and Stegun [1], item 9.6.4, which states

$$K_\nu(z) = \frac{1}{2}\pi \mathrm{i} e^{\frac{1}{2}\nu\pi\mathrm{i}} H_\nu^1(z e^{\frac{1}{2}\pi\mathrm{i}}) \qquad -\pi < \arg z \leq \frac{\pi}{2},$$
$$K_\nu(z) = -\frac{1}{2}\pi \mathrm{i} e^{-\frac{1}{2}\nu\pi\mathrm{i}} H_\nu^2(z e^{-\frac{1}{2}\pi\mathrm{i}}) \qquad -\frac{\pi}{2} < \arg z \leq \pi.$$

Note that $\alpha|\vec{r} - \vec{r'}|$ and $\alpha|\vec{r} - \vec{r_i'}|$ are both real and non-negative, implying $\arg z = 0$, gives, from (3.38),

$$G_2(\vec{r}, \vec{r'}) = \frac{\mathrm{i}}{4}\left[H_0^1(\mathrm{i}\alpha|\vec{r} - \vec{r'}|) - H_0^1(\mathrm{i}\alpha|\vec{r} - \vec{r_i'}|)\right].$$

Therefore, the derived Green's function in (3.36) is consistent with (3.38) from the literature, as in [36], and will be used as the principal Green's function in this work.

$$G_\alpha^e(\vec{r}, \vec{r'}) = \frac{1}{2\pi}\left[K_0(\alpha|\vec{r} - \vec{r'}|) - K_0(\alpha|\vec{r} - \vec{r_i'}|)\right]. \tag{3.39}$$

Key properties of the modified Bessel function of the second kind, K_ν, as found in [1], are:

1. $K_0(z) \approx -\ln z$ as $z \to 0$.
2. $\lim_{|z|\to\infty} K_\nu(z) = 0.$
3. $K_\nu(z)$ is real and positive for $\nu > -1$ and $z > 0$.
4. $K_{-\nu}(z) = K_\nu(z)$.
5. $\dfrac{\partial K_\nu(z)}{\partial z} = -\dfrac{1}{2}\left(K_{\nu-1}(z) + K_{\nu+1}(z)\right)$. [40]

These properties are useful for derivations required later in this text and presented here for familiarization.

3.4 Interior Solution

In this section, the exterior solution for u^s is used to construct a Neumann boundary condition for the interior problem. Then we construct the variational formulation for the interior problem, which will be used to solve for interior and aperture fields. Finally, the variational formulation is shown to be well-posed.

3.4.1 Transparent Boundary Condition.

From the discretized problem presented in section 3.2, we seek to find the interior field $u^{n+1} \in \mathbb{H}^1(\Omega)$ which satisfies (3.14), (3.2), and (3.5), summarized by

$$\begin{cases} -\Delta u^{n+1} + \alpha^2 \varepsilon_r u^{n+1} = \alpha^2 \varepsilon_r \tilde{u}^{n+1} & \text{in } \Omega, \\ \dfrac{\partial}{\partial y} u^{tot,n+1}\Big|_{\Gamma^+} = \dfrac{\partial}{\partial y} u^{n+1}\Big|_{\Gamma^-} & \text{on } \Gamma, \\ u^{n+1} = 0 & \text{on } S. \end{cases} \tag{3.40}$$

Note that the continuity condition (1.8) is used as the Neumann boundary condtion. The partial derivative of the external field with respect to y must be evaluated in order to apply this boundary condition. By definition, $\sum_{i=1}^{k} u_i^{n+1} = u^{n+1}$. Furthermore, let $u_i^{n+1} \in \mathrm{H}^1(\Omega_i)$ represent the solution to (3.40) restricted to Ω_i such that for $i = 1, 2, ..., k$,

$$\begin{cases} -\Delta u_i^{n+1} + \alpha^2 \varepsilon_r u_i^{n+1} = \alpha^2 \varepsilon_r \tilde{u}^{n+1} & \text{in } \Omega_i, \\ \dfrac{\partial}{\partial y} u^{tot,n+1}\Big|_{\Gamma_i^+} = \dfrac{\partial}{\partial y} u_i^{n+1}\Big|_{\Gamma_i^-} & \text{on } \Gamma_i, \\ u_i^{n+1} = 0 & \text{on } S_i. \end{cases} \tag{3.41}$$

To simplify the Neumann boundary condition, the normal derivative of the scattered field (3.25) is evaluated as $y \to 0$. Note that for the exterior problem, $\hat{n} = -\hat{y}$. The time step superscript is omitted, since this problem is solved at each time step.

$$\begin{aligned} \frac{\partial}{\partial y} u^s(x,y)\Big|_{y=0} &= \lim_{y\to 0} \left[\frac{\partial}{\partial y} \int_{\mathbb{R}^2_+} \alpha^2 G^e_\alpha(\vec{r}, \vec{r'}) \tilde{u}^s(\vec{r'})\, d\vec{r'} - \frac{\partial}{\partial y} \int_\Gamma g(x') \frac{\partial}{\partial(-y')} G^e_\alpha(\vec{r}, \vec{r'})\, dx' \right] \\ &= \alpha^2 \int_{\mathbb{R}^2_+} \frac{\partial G^e_\alpha}{\partial y}((x,0), \vec{r'}) \tilde{u}^s(\vec{r'}) + G^e_\alpha((x,0), \vec{r'}) \frac{\partial \tilde{u}^s}{\partial y}(\vec{r'})\, d\vec{r'} \\ &\quad - \int_\Gamma \frac{\partial g}{\partial y}(x') \frac{\partial G^e_\alpha}{\partial(-y')}((x,0), \vec{r'}) + g(x') \frac{\partial}{\partial y} \frac{\partial}{\partial(-y')} G^e_\alpha((x,0), \vec{r'})\, dx', \\ &= \alpha^2 \int_{\mathbb{R}^2_+} \frac{\partial G^e_\alpha}{\partial y}((x,0), \vec{r'}) \tilde{u}^s(\vec{r'})\, d\vec{r'} - \int_\Gamma g(x') \frac{\partial}{\partial y} \frac{\partial}{\partial(-y')} G^e_\alpha((x,0),(x',0))\, dx'. \end{aligned}$$

For $y' = 0$,

$$\frac{\partial}{\partial y'} K_0(\alpha|\vec{r} - \vec{r'}|) = -\frac{\partial}{\partial y'} K_0(\alpha|\vec{r} - \vec{r_i'}|).$$

Thus, evaluating one partial derivative of the Green's function (3.39) gives

$$\begin{aligned}\frac{\partial G_\alpha^e}{\partial(-y')}(\vec{r},\vec{r'}) &= \frac{1}{2\pi}\frac{\partial}{\partial(-y')}\left[K_0(\alpha|\vec{r}-\vec{r'}|) - K_0(\alpha|\vec{r}-\vec{r_i'}|)\right], \\ &= -\frac{1}{2\pi}\left[\frac{\partial}{\partial(y')}K_0(\alpha|\vec{r}-\vec{r'}|) - \frac{\partial}{\partial(y')}K_0(\alpha|\vec{r}-\vec{r_i'}|)\right].\end{aligned}$$

Therefore, along Γ_i,

$$\int_{\Gamma_i} g(x')\frac{\partial}{\partial y}\frac{\partial}{\partial(-y')}G_\alpha^e((x,0),(x',0))\,dx' = -\frac{1}{\pi}\int_{\Gamma_i} g(x')\frac{\partial}{\partial y}\frac{\partial}{\partial(y')}K_0(\alpha|x-x'|)\,dx'.$$

Finally, noting the symmetry of the modified Bessel function,

$$\frac{\partial}{\partial y}K_0(\alpha|\vec{r}-\vec{r'}|) = -\frac{\partial}{\partial y'}K_0(\alpha|\vec{r}-\vec{r'}|).$$

Thus, the normal derivative of the scattered field at the ground plane may be simplified to

$$\left.\frac{\partial}{\partial y}u^s(x,y)\right|_{y=0} = \alpha^2\int_{\mathbb{R}^2_+}\frac{\partial G_\alpha^e}{\partial y}((x,0),\vec{r'})\tilde{u}^s(\vec{r'})\,d\vec{r'} - \frac{1}{\pi}\int_\Gamma g(x')\frac{\partial^2 K_0}{\partial y^2}(\alpha|x-x'|)\,dx'. \quad (3.42)$$

For the two-cavity case, letting $g_1 = g|_{\Gamma_1}$ and $g_2 = g|_{\Gamma_2}$, (3.42) can be piecewise defined as

$$\left.\frac{\partial}{\partial y}u^s(x,y)\right|_{y=0} = \begin{cases} \alpha^2\displaystyle\int_{\mathbb{R}^2_+}\frac{\partial G_\alpha^e}{\partial y}((x,0),\vec{r'})\tilde{u}^s(\vec{r'})\,d\vec{r'} - \frac{1}{\pi}\int_{\Gamma_1} g_1(x')\frac{\partial^2 K_0}{\partial y^2}(\alpha|x-x'|)\,dx' & \\ \quad -\dfrac{1}{\pi}\displaystyle\int_{\Gamma_2} g_2(x')\frac{\partial^2 K_0}{\partial y^2}(\alpha|x-x'|)\,dx' & (x,0)\in\Gamma_1, \\ \alpha^2\displaystyle\int_{\mathbb{R}^2_+}\frac{\partial G_\alpha^e}{\partial y}((x,0),\vec{r'})\tilde{u}^s(\vec{r'})\,d\vec{r'} - \frac{1}{\pi}\int_{\Gamma_1} g_1(x')\frac{\partial^2 K_0}{\partial y^2}(\alpha|x-x'|)\,dx' & \\ \quad -\dfrac{1}{\pi}\displaystyle\int_{\Gamma_2} g_2(x')\frac{\partial^2 K_0}{\partial y^2}(\alpha|x-x'|)\,dx' & (x,0)\in\Gamma_2, \\ 0 & (x,0)\in\Gamma^C. \end{cases}$$

Specifically, note that this boundary condition is dependent on the aperture fields from all of the cavities, indicating dependence, or cross-talk, between the fields in each cavity. Additionally, in the upper half plane, $K_0(\alpha|\vec{r}-\vec{r'}|)$ satisfies the modified 2-D wave equation (3.18), allowing the substitution

$$\frac{\partial^2 K_0}{\partial y^2}(\alpha|x-x'|) = \left[\alpha^2 - \frac{\partial^2}{\partial x^2}\right]K_0(\alpha|x-x'|).$$

And thus, the normal derivative of the scattered field at the cavity apertures may be written as

$$\frac{\partial}{\partial y}u^{s,n+1}(x,y)\bigg|_{\Gamma} = \tilde{H}^{n+1}(x) + [T_\alpha g](x), \quad (x,0)\in\Gamma, \tag{3.43}$$

with $\tilde{H} : \mathrm{H}^1(\mathbb{R}^2_+) \to \mathbb{H}^{1/2}(\Gamma)$ and $T_\alpha : \mathbb{H}^{1/2}(\Gamma) \to \mathbb{H}^{-1/2}(\Gamma)$ defined by:

$$\tilde{H}^{n+1}(x) = \alpha^2 \int_{\mathbb{R}^2_+} \frac{\partial G^e_\alpha}{\partial y}((x,0),\vec{r'})\tilde{u}^s(\vec{r'})d\vec{r'}, \tag{3.44}$$

$$[T_\alpha g](x) = \frac{1}{\pi}\int_\Gamma \left[\frac{\partial^2}{\partial x^2} - \alpha^2\right] K_0(\alpha|x-x'|)g(x')dx'. \tag{3.45}$$

Note that the direct coupling between cavities is embedded within the definition of $[T_\alpha g]$ and the time-delayed influence between cavities is captured by $\tilde{H}^{n+1}$.

For the two-cavity case, (3.45) can be expanded as

$$[T_\alpha g](x) = \frac{1}{\pi}\int_{\Gamma_1} \left[\frac{\partial^2}{\partial x^2} - \alpha^2\right] K_0(\alpha|x-x'|)g_1(x')dx' + \frac{1}{\pi}\int_{\Gamma_2} \left[\frac{\partial^2}{\partial x^2} - \alpha^2\right] K_0(\alpha|x-x'|)g_2(x')dx'.$$

Finally, for the total field, referring to (3.3) gives

$$\frac{\partial}{\partial y}u^{tot} = \frac{\partial}{\partial y}u^{inc} + \frac{\partial}{\partial y}u^{ref} + \frac{\partial}{\partial y}u^{s}.$$

Thus, along the ground plane simplifies to the following Neumann boundary condition similar to that found in [36], with the exception that in this case, T_α is a coupled boundary operator over multiple cavities.

$$\frac{\partial}{\partial y}u^{tot}(x,y,t_{n+1})\bigg|_{(x,0)\in(\Gamma)} = 2\frac{\partial u^{inc}}{\partial y}(x,0,t_{n+1}) + \tilde{H}^{n+1}(x) + [T_\alpha g](x). \tag{3.46}$$

Therefore, equation (3.41) can be restated as

$$\begin{cases} -\Delta u_i^{n+1} + \alpha^2\varepsilon_r u_i^{n+1} = \alpha^2\varepsilon_r\tilde{u}^{n+1} & \text{in } \Omega_i, \\ \dfrac{\partial}{\partial y}u_i^{n+1}\bigg|_{\Gamma_i^-} = 2\dfrac{\partial u^{inc}}{\partial y}(x,0,t_{n+1}) + \tilde{H}^{n+1}(x) + [T_\alpha g](x) & \text{on } \Gamma_i, \\ u_i^{n+1} = 0 & \text{on } S_i. \end{cases} \tag{3.47}$$

In order to numerically approximate solutions at each time step, we develop a variational formulation of (3.47) to be implemented wtih the FEM routine.

3.4.2 Linear Sum of Solutions.

At this point, it is important to clarify that the solution, u, to the multiple-cavity problem from (3.47) is not equivalent to the linear sum of single-cavity solutions less the duplicated incident and reflected fields present in each solution. Let w_i represent the zero extension to the multiple-cavity domain Ω of the solution to the problem solved in [36] where only a single cavity is present in a PEC ground plane. For consistency, u_i represents the interior solution for cavity i of the multiple-cavity problem in (3.47).

Theorem 1. *Non-trivial solution u to the multiple-cavity problem is not equal to a linear sum of single-cavity solutions less the duplicated incident and reflected fields.*

$$u \neq -(k-1)(u^{inc} + u^{ref}) + \sum_{i=1}^{k} w_i.$$

Proof. By contradiction, assume that

$$u = -(k-1)(u^{inc} + u^{ref}) + \sum_{i=1}^{k} w_i.$$

Then, for each i, w_i satisfies scalar wave equation (3.1) with boundary conditions

$$\begin{cases} w_i = 0 & \text{on } \Gamma^C \bigcup S_i \bigcup_{j \neq i} \Gamma_j, \\ \lim\limits_{y \to 0+} \dfrac{\partial}{\partial y} w_i(x,y) = \lim\limits_{y \to 0-} \dfrac{\partial}{\partial y} w_i(x,y) & (x,0) \in \Gamma_i. \end{cases} \tag{3.48}$$

The multiple-cavity solution u satisfies the scalar wave equation (3.1) with boundary conditions stated in (3.2).

Without loss of generality, let $k = 2$. Then w_1 and w_2 are each non-trivial solutions to the wave equation (3.1) satisfying (3.48), and $u = w_1 + w_2 - u^{inc} - u^{ref}$ satisfies (3.1) and (3.2). Define

$$w_2^s = w_2 - u^{inc} - u^{ref}.$$

Then, on Γ_1, w_1 fully satisfies the Neumann boundary condition. This implies that

$$\lim_{y \to 0+} \frac{\partial}{\partial y} w_2^s = 0.$$

w_2^s is defined in [36] as

$$w_2^s(\vec{r}) = \alpha^2 \int_0^\infty \int_{-\infty}^\infty G_\alpha^e(\vec{r}, \vec{r'}) \tilde{w}_2^s(\vec{r'})\, d\vec{r'} + \frac{1}{\pi} \int_{\Gamma_2} \frac{\partial}{\partial y} K_0(\alpha|\vec{r} - x'\hat{x}|) g_2(x')\, dx'.$$

Computing the normal derivative for x in Γ_1 gives

$$\lim_{y\to 0+} \frac{\partial}{\partial y} w_2^s(x,y) = \alpha^2 \int_0^\infty \int_{-\infty}^\infty \frac{\partial G_\alpha^e}{\partial y}((x,0), \vec{r'} \tilde{w}_2^s(\vec{r'})\, d\vec{r'} + \frac{1}{\pi} \int_{\Gamma_2} \left(-\alpha^2 + \frac{\partial^2}{\partial x^2}\right) K_0(\alpha|\vec{r} - x'\hat{x}|) g_2(x')\, dx'.$$

The first integral corresponds to $\tilde{H}$, and is only zero when $\tilde{w}_2^s = 0$, which implies that fields on Γ_2 were zero at previous time steps. The second integral corresponds to $T_\alpha(g_2)$, which implies that fields on Γ_2 are zero at the current time step. These conditions together would require that $w_2^s = 0$ for all timesteps, thus contradicting the assumption that u is non-trivial in that for $w_2^s \neq 0$,

$$\lim_{y\to 0+} \frac{\partial}{\partial y} w_2^s \neq 0.$$

Therefore, for $k > 1$, and for all $i = 1, 2, ..., k$, $w_i \neq 0$, the multiple cavity solution is not equal to a linear sum of single-cavity solutions less the duplicated incident and reflected fields.

$$u \neq -(k-1)(u^{inc} + u^{ref}) + \sum_{i=1}^{k} w_i.$$

□

3.4.3 Variational Formulation.

Using the Neumann boundary condition given in (3.46), the interior fields in each of the cavities may be computed as a coupled set of equations at each time step. This formulation follows the development described in [36], but expanded to capture the multiple-cavity interaction.

For each of the k cavities, we define the space of real-valued test functions.

$$V_i = \{v \in \mathrm{H}^1(\Omega_i) : v = 0 \text{ on } S_i\}, \tag{3.49}$$

$$\mathcal{V} = V_1 + V_2 + ... + V_k. \tag{3.50}$$

Note that $\mathcal{V} \subset \mathbb{H}^1(\Omega)$, so integration and multiplication follow the the definitions (1.11) and (1.12), respectively. Let v be a test function in $\mathcal{V}$. Multiplying (3.14) by v and integrating over Ω, gives

$$\int_\Omega \left(-\Delta u^{n+1} + \alpha^2 \varepsilon_r u^{n+1}\right) v \, d\vec{r} = \int_\Omega \alpha^2 \varepsilon_r \tilde{u}^{n+1} v \, d\vec{r},$$

which for k cavities, is expanded as

$$\sum_{i=1}^{k} \int_{\Omega_i} \left(-\Delta u^{n+1} + \alpha^2 \varepsilon_r u^{n+1}\right) v_i \, d\vec{r} = \sum_{i=1}^{k} \int_{\Omega_i} \alpha^2 \varepsilon_r \tilde{u}^{n+1} v_i \, d\vec{r}.$$

Applying Green's theorem on $v_i \Delta u^{n+1}$, gives

$$\int_{\Omega_i} \nabla u^{n+1} \cdot \nabla v_i + \alpha^2 \varepsilon_r u^{n+1} v_i \, d\vec{r} - \int_{\partial\Omega_i} v_i \frac{\partial u^{n+1}}{\partial n} \, dS = \int_{\Omega_i} \alpha^2 \varepsilon_r \tilde{u}^{n+1} v_i \, d\vec{r}.$$

By definition, $v_i = 0$ on S_i, so the boundary integral can be reduced to the aperture Γ_i.

$$\int_{\partial\Omega_i} v_i \frac{\partial u^{n+1}}{\partial n} = \int_{\Gamma_i} v_i \left(2 \frac{\partial u^{inc,n+1}}{\partial y}(x,0) + \tilde{H}^{n+1}(x) + [T_\alpha g](x)\right) dx.$$

Gathering terms dependent on u^{n+1} and g on the left yields the equation

$$\begin{aligned} &\sum_{i=1}^{k} \left(\int_{\Omega_i} \nabla u^{n+1} \cdot \nabla v_i \, d\vec{r} + \int_{\Omega_i} \alpha^2 \varepsilon_r u^{n+1} v_i \, d\vec{r} - \int_{\Gamma_i} [T_\alpha g](x) v_i \, dx \right) \\ &\quad = \sum_{i=1}^{k} \left(\int_{\Omega_i} \alpha^2 \varepsilon_r \tilde{u}^{n+1} v_i \, d\vec{r} + 2 \int_{\Gamma_i} \frac{\partial u^{inc,n+1}}{\partial y} v_i \, dx + \int_{\Gamma_i} \tilde{H}^{n+1} v_i \, dx \right). \end{aligned} \tag{3.51}$$

For the case where $k = 2$, the expansion of the integral in (3.51) containing the operator T_α using (3.45) becomes

$$\begin{aligned} \sum_{i=1}^{2} \int_{\Gamma_i} [T_\alpha g](x) v_i(x) \, dx = &\int_{\Gamma_1} v_1(x) \frac{1}{\pi} \int_{\Gamma_1} \left[\frac{\partial^2}{\partial x^2} - \alpha^2\right] K_0(\alpha|x - x'|) g_1(x') \, dx' \, dx \\ &+ \int_{\Gamma_1} v_1(x) \frac{1}{\pi} \int_{\Gamma_2} \left[\frac{\partial^2}{\partial x^2} - \alpha^2\right] K_0(\alpha|x - x'|) g_2(x') \, dx' \, dx \\ &+ \int_{\Gamma_2} v_2(x) \frac{1}{\pi} \int_{\Gamma_1} \left[\frac{\partial^2}{\partial x^2} - \alpha^2\right] K_0(\alpha|x - x'|) g_1(x') \, dx' \, dx \\ &+ \int_{\Gamma_2} v_2(x) \frac{1}{\pi} \int_{\Gamma_2} \left[\frac{\partial^2}{\partial x^2} - \alpha^2\right] K_0(\alpha|x - x'|) g_2(x') \, dx' \, dx. \end{aligned}$$

This expansion more clearly illustrates the nature of the coupling between the cavities. Next, we define the following inner products for functions f and g in $\mathbb{H}^1(\Omega)$:

$$(\nabla f, \nabla g)_\Omega = \sum_{i=1}^{k} \int_{\Omega_i} \nabla f_i \cdot \nabla \overline{g_i}\, d\vec{r},$$

$$\langle f, g \rangle_\Omega = \sum_{i=1}^{k} \int_{\Omega_i} f_i \overline{g_i}\, d\vec{r},$$

$$\langle f, g \rangle_\Gamma = \sum_{i=1}^{k} \int_{\Gamma_i} f_i \overline{g_i}\, dx.$$

Then, assuming real-valued v, the complex conjugate notation is dropped. Thus, (3.51) can be written as the variational formulation

$$a(u^{n+1}, v) = b^{n+1}(v), \tag{3.52}$$

where

$$a(u, v) = (\nabla u, \nabla v)_\Omega + \alpha^2 \langle \varepsilon_r u, v \rangle_\Omega - \langle [T_\alpha g], v \rangle_\Gamma,$$
$$b^{n+1}(v) = \alpha^2 \langle \varepsilon_r \tilde{u}^{n+1}, v \rangle_\Omega + 2\langle \frac{\partial u^{inc,n+1}}{\partial y}, v \rangle_\Gamma + \langle \tilde{H}^{n+1}, v \rangle_\Gamma.$$

For $k = 2$, (3.52) may be expanded further to

$$\begin{aligned} a(u, v) = {} & (\nabla u_1, \nabla v_1)_{\Omega_1} + (\nabla u_2, \nabla v_2)_{\Omega_2} + \alpha^2 \langle \varepsilon_r u_1, v_1 \rangle_{\Omega_1} + \alpha^2 \langle \varepsilon_r u_2, v_2 \rangle_{\Omega_2} \\ & - \langle [T_\alpha g_1], v_1 \rangle_{\Gamma_1} - \langle [T_\alpha g_2], v_1 \rangle_{\Gamma_1} - \langle [T_\alpha g_1], v_2 \rangle_{\Gamma_2} - \langle [T_\alpha g_2], v_2 \rangle_{\Gamma_2}, \\ b^{n+1}(v) = {} & \alpha^2 \langle \varepsilon_r \tilde{u}^{n+1}, v_1 \rangle_{\Omega_1} + \alpha^2 \langle \varepsilon_r \tilde{u}^{n+1}, v_2 \rangle_{\Omega_2} + 2\langle \frac{\partial u^{inc,n+1}}{\partial y}, v_1 \rangle_{\Gamma_1} + 2\langle \frac{\partial u^{inc,n+1}}{\partial y}, v_2 \rangle_{\Gamma_2} \\ & + \langle \tilde{H}^{n+1}, v_1 \rangle_{\Gamma_1} + \langle \tilde{H}^{n+1}, v_2 \rangle_{\Gamma_2}. \end{aligned}$$

The solution to this variational formulation, u^{n+1}, is based on a known value for u^{inc} and computed values for $\tilde{u}^{n+1}, \tilde{u}^{s,n+1}$. By evaluating u^{n+1} at the apertures, g is found, from which $u^{s,n+1}$ can be determined using the Green's function. Additionally, in the Newmark method, the solution at time step $n + 1$ is used to correct the approximations made based upon time step n data, and make approximations for the next step forward in time. In this fashion,

the Newmark method provides a computational method for numerically approximating $u^{tot}(x, y, t_n)$ for each time step.

3.5 Well-posedness of Single-Cavity Problem

The well-posedness of the single-cavity problem was proved in [36]. The principle theorem upon which the multiple-cavity proof will be based is:

Theorem 2. *Let $V \subset L^2(\Omega)$ be defined as*

$$V = \{u \in H^1(\Omega) : u = 0 \, on \, S\}$$

then the variational problem, (3.52) has a unique solution in V when k = 1.

Additionally, the boundedness of the Dirichlet-to-Neumann operator T^e_α for a single cavity is fundamental to the multiple-cavity proof, and thus presented here for convenience.

Proposition 1. *The operator T^e_α defined by*

$$T^e_\alpha g(x) := \frac{1}{\pi} \int_\Gamma \left(-\alpha^2 + \frac{\partial^2}{\partial x^2} \right) K_0(\alpha|x - x'|) g(x') \, dx', \tag{3.53}$$

is a pseudodifferential operator of order 1 and $T^e_\alpha : H^{1/2}(\Gamma) \to H^{-1/2}(\Gamma)$ is bounded. Moreover $\langle T^e_\alpha g, g \rangle_\Gamma$ is nonpositive for any $g \in H^{1/2}(\Gamma)$.

3.6 Well-posedness of Two-Cavity Problem

Theorem 3. *Let $\mathcal{V}$ be defined as in (3.49) - (3.50), then the variational formulation (3.51) has a unique solution in $\mathcal{V}$ when k = 2.*

In order to prove theorem 3, we first prove the following lemmas which will satisfy the Lax-Milgram theorem.

Lemma 1. *The operator $T_\alpha : \mathbb{H}^{1/2}(\Gamma_1 \cup \Gamma_2) \to \mathbb{H}^{-1/2}(\Gamma_1 \cup \Gamma_2)$ is bounded.*

Proof. For any $g \in \mathbb{H}^{1/2}(\Gamma_1 \cup \Gamma_2)$,

$$T_\alpha g(x) = \frac{1}{\pi} \int_{\Gamma_1 \cup \Gamma 2} \left[\frac{\partial^2}{\partial x^2} - \alpha^2 \right] K_0(\alpha|x - x'|) g(x') dx'.$$

Consider the piecewise sum

$$T_\alpha g(x) = \begin{cases} T_{1,1}(x) + T_{1,2}(x) & x \in \Gamma_1, \\ T_{2,1}(x) + T_{2,2}(x) & x \in \Gamma_2, \end{cases}$$

with $T_{i,j}$ is defined by,

$$T_{i,j}(x) = \frac{1}{\pi} \int_{\Gamma_j} \left[\frac{\partial^2}{\partial x^2} - \alpha^2 \right] K_0(\alpha|x - x'|) g(x') dx', \; x \in \Gamma_i.$$

$T_{1,1}$ and $T_{2,2}$ are the single-cavity operators, (3.53), shown to be bounded in [36]. Therefore,

$$\|T_{1,1}\|_{\mathrm{H}^{-1/2}(\Gamma_1)} \leq c_1 \|g\|_{\mathrm{H}^{1/2}(\Gamma_1)}, \tag{3.54}$$

$$\|T_{2,2}\|_{\mathrm{H}^{-1/2}(\Gamma_2)} \leq c_2 \|g\|_{\mathrm{H}^{1/2}(\Gamma_2)}. \tag{3.55}$$

For $x \neq x'$,

$$\left[\frac{\partial^2}{\partial x^2} - \alpha^2 \right] K_0(\alpha|x - x'|) = \frac{\alpha}{|x - x'|} K_1(\alpha|x - x'|),$$

which is strictly positive and decreasing as the distance, $|x - x'|$, increases. Let

$$d(\Gamma_1, \Gamma_2) := \min_{\substack{x_1 \in \Gamma_1 \\ x_2 \in \Gamma_2}} (|x_1 - x_2|).$$

Then, it is clear that

$$\|T_{1,2}\|_{\mathrm{H}^{-1/2}(\Gamma_1)} \leq c_3 \|g\|_{\mathrm{H}^{1/2}(\Gamma_2)}, \tag{3.56}$$

$$\|T_{2,1}\|_{\mathrm{H}^{-1/2}(\Gamma_2)} \leq c_3 \|g\|_{\mathrm{H}^{1/2}(\Gamma_1)}, \tag{3.57}$$

where,

$$c_3 = \frac{\alpha K_1(\alpha d(\Gamma_1, \Gamma_2))}{\pi d(\Gamma_1, \Gamma_2)}.$$

Therefore,

$$\begin{aligned}
\|T_\alpha g\|^2_{\mathbb{H}^{-1/2}(\Gamma_1\cup\Gamma_2)} &= \|T_\alpha g\|^2_{\mathrm{H}^{-1/2}(\Gamma_1)} + \|T_\alpha g\|^2_{\mathrm{H}^{-1/2}(\Gamma_2)} \\
&= \|T_{1,1} + T_{1,2}\|^2_{\mathrm{H}^{-1/2}(\Gamma_1)} + \|T_{2,1} + T_{2,2}\|^2_{\mathrm{H}^{-1/2}(\Gamma_2)} \\
&\leq \|T_{1,1}\|^2_{\mathrm{H}^{-1/2}(\Gamma_1)} + \|T_{1,2}\|^2_{\mathrm{H}^{-1/2}(\Gamma_1)} \\
&\quad + 2\|T_{1,1}\|_{\mathrm{H}^{-1/2}(\Gamma_1)}\|T_{1,2}\|_{\mathrm{H}^{-1/2}(\Gamma_1)} \\
&\quad + \|T_{2,1}\|^2_{\mathrm{H}^{-1/2}(\Gamma_2)} + \|T_{2,2}\|^2_{\mathrm{H}^{-1/2}(\Gamma_2)} \\
&\quad + 2\|T_{2,1}\|_{\mathrm{H}^{-1/2}(\Gamma_2)}\|T_{2,2}\|_{\mathrm{H}^{-1/2}(\Gamma_2)}.
\end{aligned}$$

Applying inequalities (3.54 - 3.57) to the above yields

$$\begin{aligned}
\|T_\alpha g\|^2_{\mathbb{H}^{-1/2}(\Gamma_1\cup\Gamma_2)} \leq\ & c_1^2\|g\|^2_{\mathrm{H}^{1/2}(\Gamma_1)} + c_3^2\|g\|^2_{\mathrm{H}^{1/2}(\Gamma_2)} \\
&+ 2c_1c_3\|g\|_{\mathrm{H}^{1/2}(\Gamma_1)}\|g\|_{\mathrm{H}^{1/2}(\Gamma_2)} \\
&+ c_3^2\|g\|^2_{\mathrm{H}^{1/2}(\Gamma_1)} + c_2^2\|g\|^2_{\mathrm{H}^{1/2}(\Gamma_2)} \\
&+ 2c_2c_3\|g\|_{\mathrm{H}^{1/2}(\Gamma_1)}\|g\|_{\mathrm{H}^{1/2}(\Gamma_2)}.
\end{aligned}$$

Thus

$$\begin{aligned}
\|T_\alpha g\|^2_{\mathbb{H}^{-1/2}(\Gamma_1\cup\Gamma_2)} &\leq (c_1^2 + c_3^2)\|g\|^2_{\mathrm{H}^{1/2}(\Gamma_1)} + (c_2^2 + c_3^2)\|g\|^2_{\mathrm{H}^{1/2}(\Gamma_2)} \\
&\quad + (c_1c_3 + c_2c_3)\|g\|^2_{\mathbb{H}^{1/2}(\Gamma_1\cup\Gamma_2)} \\
&\leq C\|g\|^2_{\mathbb{H}^{1/2}(\Gamma_1\cup\Gamma_2)}.
\end{aligned}$$

Therefore, $T_\alpha : \mathbb{H}^{1/2}(\Gamma_1 \cup \Gamma_2) \to \mathbb{H}^{-1/2}(\Gamma_1 \cup \Gamma_2)$ is bounded. □

Lemma 2. *The inner product $\langle T_\alpha g, g\rangle_{\Gamma_1\cup\Gamma_2}$ is non-positive for all $g \in \mathbb{H}^{1/2}(\Gamma_1 \cup \Gamma_2)$.*

Proof. Let $g_0 \in \mathrm{H}^{1/2}(\mathbb{R})$ defined by

$$g_0(x) = \begin{cases} g(x) & x \in \Gamma_1 \cup \Gamma_2, \\ 0 & \text{otherwise,} \end{cases}$$

such that $\langle T_\alpha g, g\rangle_{\Gamma_1\cup\Gamma_2} = \langle T_\alpha g_0, g_0\rangle_{\mathbb{R}}$. Then

$$\begin{aligned}\langle T_\alpha g_0, g_0\rangle_{\mathbb{R}} &= \int_{\mathbb{R}} [T_\alpha g_0](x)\overline{g_0}(x)\,dx,\\ &= \int_{\mathbb{R}} \frac{1}{\pi}\int_{\mathbb{R}} g_0(x')\frac{\partial^2 K_0}{\partial^2 x}(\alpha|x-x'|)\,dx'\overline{g_0}(x)\,dx\\ &\quad - \int_{\mathbb{R}} \frac{\alpha^2}{\pi}\int_{\mathbb{R}} g_0(x')K_0(\alpha|x-x'|)\,dx'\overline{g_0}(x)\,dx.\end{aligned} \tag{3.58}$$

Note that $g_0(x)$ has compact support in $\mathbb{R}$, and that

$$\frac{\partial}{\partial x}K_0(\alpha|x-x'|) = -\frac{\partial}{\partial x'}K_0(\alpha|x-x'|).$$

Integration by parts is applied twice to the first double integral in (3.58), giving

$$\begin{aligned}&\frac{1}{\pi}\int_{\mathbb{R}}\int_{\mathbb{R}} \overline{g}_0(x)\frac{\partial^2 K_0}{\partial x^2}(\alpha|x-x'|)g_0(x')\,dx'\,dx\\ &\qquad = -\frac{1}{\pi}\int_{\mathbb{R}}\int_{\mathbb{R}} \frac{\partial\overline{g}_0}{\partial x}(x)\frac{\partial K_0}{\partial x}(\alpha|x-x'|)g_0(x')\,dx'\,dx\\ &\qquad = \frac{1}{\pi}\int_{\mathbb{R}}\int_{\mathbb{R}} \frac{\partial\overline{g}_0}{\partial x}(x)\frac{\partial K_0}{\partial x'}(\alpha|x-x'|)g_0(x')\,dx'\,dx\\ &\qquad = -\frac{1}{\pi}\int_{\mathbb{R}}\int_{\mathbb{R}} K_0(\alpha|x-x'|)\overline{g}_0'(x)g_0'(x')\,dx'\,dx.\end{aligned}$$

Thus, using $\Gamma = \Gamma_1 \cup \Gamma_2$ for brevity,

$$\langle T_\alpha g_0, g_0\rangle_{\mathbb{R}} = \langle T_\alpha g, g\rangle_\Gamma = I_1 + I_2, \tag{3.59}$$

with

$$\begin{aligned}I_1 &= -\frac{\alpha^2}{\pi}\int_\Gamma\int_\Gamma K_0(\alpha|x-x'|)\overline{g}_0(x)g_0(x')\,dx'\,dx,\\ I_2 &= -\frac{1}{\pi}\int_\Gamma\int_\Gamma K_0(\alpha|x-x'|)\overline{g}_0'(x)g_0'(x')\,dx'\,dx.\end{aligned}$$

The method used in [36] is applied, included here for completeness, to show that I_1 and I_2 from (3.65) are both non-positive. Define $\tilde{\Gamma}$ to be a smooth closed curve such that $\{\Gamma_1 \cup \Gamma_2\} \subset \tilde{\Gamma}$ and $\tilde{g} \in \mathrm{H}^{1/2}(\tilde{\Gamma})$. Also, define the function

$$w(x) = \int_{\tilde{\Gamma}} K_0(\alpha|x-x'|)\tilde{g}(x')\,dx' \quad x \in \mathbb{R}^2.$$

Note that $w(x)$ is a solution the 2-D wave equation for $x \notin \tilde{\Gamma}$,

$$-\Delta w + \alpha^2 w = 0 \text{ for } x \in \mathbb{R}^2 \backslash \tilde{\Gamma}.$$

Additionally, if $\tilde{g}$ is regarded as a current on the contour $\tilde{\Gamma}$, with $w(x)$ being an integral form solution to the wave equation with an electric source current, then it is clear that the following boundary condition holds:

$$\hat{n} \times (\vec{H}_1 - \vec{H}_2) = \vec{J},$$

with $\hat{n}$ the unit normal to the surface pointing into region 1 and $\vec{J}$ the current present on the boundary. Then, defining exterior and interior limit functions

$$w_e(x) = \lim_{p \to x} w(p) \quad p \text{ exterior to } \tilde{\Gamma},$$

$$w_i(x) = \lim_{q \to x} w(q) \quad q \text{ interior to } \tilde{\Gamma}.$$

Thus, the boundary condition is expressed as

$$\frac{\partial w_e}{\partial n} - \frac{\partial w_i}{\partial n} = \tilde{g} \qquad \text{for } x \in \tilde{\Gamma}.$$

Similarly, there is no magnetic source present, so $w_e - w_i = 0$ for $x \in \tilde{\Gamma}$, indicating that $w_e = w_i = w$ for $x \in \tilde{\Gamma}$.

Evaluating the normal derivative gives

$$\begin{aligned} \frac{\partial w}{\partial n}(x) &= \frac{\partial}{\partial n} \int_{\tilde{\Gamma}} K_0(\alpha|x - x'|)\tilde{g}(x')\, dx' \\ &= \int_{\tilde{\Gamma}} \frac{\partial}{\partial n} K_0(\alpha|x - x'|)\tilde{g}(x'). \end{aligned}$$

Applying Green's theorem gives, with $A \subset \mathbb{R}^2$ used to denote the region enclosed by $\tilde{\Gamma}$,

$$\frac{\partial w}{\partial n}(x) = \int_A 2\nabla K_0(\alpha|x - x'|) \cdot \nabla \tilde{g}(x') + \Delta K_0(\alpha|x - x'|)\tilde{g}(x') + K_0(\alpha|x - x'|)\Delta \tilde{g}(x') dA.$$

Furthermore, it is clear that the following inequality is true:

$$\begin{aligned} 0 &\leq \int_{\mathbb{R}^2} |\nabla w|^2 + \alpha^2 |w|^2 dx \\ &= \int_{\mathbb{R}^2} \nabla \overline{w} \cdot \nabla w + \alpha^2 \overline{w} w dx. \end{aligned}$$

Define D_{ext} and D_{int} to be the exterior and interior regions with respect to $\tilde{\Gamma}$. Then, applying Green's theorem gives

$$\begin{aligned}
0 &\leq \int_{D_{ext}} \nabla\overline{w} \cdot \nabla w + \alpha^2 \overline{w} w dx + \int_{D_{int}} \nabla\overline{w} \cdot \nabla w + \alpha^2 \overline{w} w dx \\
&= \int_{D_{ext}} -\overline{w}\Delta w + \alpha^2 \overline{w} w dx + \int_{D_{int}} -\overline{w}\Delta w + \alpha^2 \overline{w} w dx \\
&\quad + \int_{\tilde{\Gamma}} w \frac{\partial}{\partial n}(\overline{w}_e - \overline{w}_i) dx \\
&= \int_{\mathbb{R}^2} \overline{w}\left(-\Delta w + \alpha^2 w\right) dx + \int_{\tilde{\Gamma}} w\overline{\tilde{g}} dx \\
&= \int_{\tilde{\Gamma}} w\overline{\tilde{g}} dx \\
&= \int_{\tilde{\Gamma}} \overline{\tilde{g}} \int_{\tilde{\Gamma}} K_0(\alpha|x - x'|)\tilde{g}(x')\, dx' dx. \qquad (3.60)
\end{aligned}$$

Thus, if we define the function $\tilde{g} \in \mathrm{H}^{1/2}(\tilde{\Gamma})$ to be the extension of g onto $\tilde{\Gamma}$,

$$\tilde{g}(x) = \begin{cases} g(x) & x \in \Gamma \\ 0 & x \in \tilde{\Gamma} \setminus \Gamma, \end{cases}$$

the following inequalities follow from (3.60):

$$\begin{aligned}
0 &\leq \int_{\Gamma} \overline{g}(x) \int_{\Gamma} K_0(\alpha|x - x'|) g(x')\, dx' dx, \\
0 &\geq -\frac{\alpha^2}{\pi} \int_{\Gamma} \overline{g}(x) \int_{\Gamma} K_0(\alpha|x - x'|) g(x')\, dx' dx \\
&= I_1.
\end{aligned}$$

Thus, I_1 is non-positive. By similar argument, if we define the function $\tilde{g}$ to be the extension of g' onto $\tilde{\Gamma}$, as

$$\tilde{g}(x) = \begin{cases} g' & x \in \Gamma \\ 0 & x \in \tilde{\Gamma} \setminus \Gamma, \end{cases}$$

it becomes clear from (3.60) that

$$\begin{aligned} 0 &\leq \int_\Gamma \overline{g'}(x) \int_\Gamma K_0(\alpha|x-x'|) g'(x')\, dx' dx, \\ 0 &\geq -\frac{1}{\pi} \int_\Gamma \overline{g'}(x) \int_\Gamma K_0(\alpha|x-x'|) g'(x')\, dx' dx \\ &= I_2. \end{aligned}$$

Thus, I_2 is non-positive.

To summarize,

$$0 \geq I_1,$$

$$0 \geq I_2.$$

Therefore, $\langle T_\alpha g, g\rangle_{\Gamma_1 \cup \Gamma_2}$ is non-positive for all $g \in \mathbb{H}^{1/2}(\Gamma_1 \cup \Gamma_2)$. □

The following lemma proves coercivity of $a(\cdot,\cdot)$

Lemma 3. *There exist positive constants c and C both in $\mathbb{R}$ such that $a(u,u) \geq c\|u\|^2_{\mathbb{H}^1(\Omega)}$ $\forall u \in \mathbb{H}^1(\Omega)$ and $|a(u,v)| \leq C\|u\|_{\mathbb{H}^1(\Omega)}\|v\|_{\mathbb{H}^1(\Omega)}$ $\forall u, v \in \mathbb{H}^1(\Omega)$.*

Proof.

$$\begin{aligned} a(u,u) &= \langle \nabla u, \nabla u\rangle_\Omega + \alpha^2 \langle \varepsilon_r u, u\rangle_\Omega - \langle T_\alpha u, u\rangle_\Gamma. \\ &\geq \langle \nabla u, \nabla u\rangle_\Omega + \alpha^2 \langle \varepsilon_r u, u\rangle_\Omega \\ &\geq \min_{\vec{r}\in\Omega}[1, \alpha^2 \varepsilon_r(\vec{r})]\, (\langle \nabla u, \nabla u\rangle_\Omega + \langle u, u\rangle_\Omega) \\ &\geq c\left(\|u\|^2_{\mathrm{H}^1(\Omega_1)} + \|u\|^2_{\mathrm{H}^1(\Omega_2)}\right) \\ &= c\|u\|^2_{\mathbb{H}^1(\Omega)}, \end{aligned}$$

with

$$c = \min_{\vec{r}\in\Omega_1\cup\Omega_2}[1, \alpha^2 \varepsilon_r(\vec{r})].$$

Therefore, $a(u,u) \geq c\|u\|^2_{\mathbb{H}^1(\Omega)}$ $\forall u \in \mathbb{H}^1(\Omega)$.

For any $u,\ v \in \mathbb{H}^1(\Omega)$ such that u_i, v_i refer to the restrictions of u and v to cavity domain Ω_i, the operator a can be expanded as

$$\begin{aligned}
|a(u,v)| &= |\langle \nabla u_1, \nabla v_1\rangle_{\Omega_1} + \langle \nabla u_2, \nabla v_2\rangle_{\Omega_2} + \alpha^2\langle \varepsilon_r u_1, v_1\rangle_{\Omega_1} + \alpha^2\langle \varepsilon_r u_2, v_2\rangle_{\Omega_2} \\
&\quad - \langle [T_\alpha u_1], v_1\rangle_{\Gamma_1} - \langle [T_\alpha u_2], v_1\rangle_{\Gamma_1} - \langle [T_\alpha u_1], v_2\rangle_{\Gamma_2} - \langle [T_\alpha u_2], v_2\rangle_{\Gamma_2}|, \\
&\leq |\langle \nabla u_1, \nabla v_1\rangle_{\Omega_1} + \langle \nabla u_2, \nabla v_2\rangle_{\Omega_2} + \alpha^2\langle \varepsilon_r u_1, v_1\rangle_{\Omega_1} + \alpha^2\langle \varepsilon_r u_2, v_2\rangle_{\Omega_2}| \\
&\quad + | - \langle [T_\alpha u_1], v_1\rangle_{\Gamma_1} - \langle [T_\alpha u_2], v_1\rangle_{\Gamma_1} - \langle [T_\alpha u_1], v_2\rangle_{\Gamma_2} - \langle [T_\alpha u_2], v_2\rangle_{\Gamma_2}|.
\end{aligned}$$

Applying the triangle inequality, gives

$$\begin{aligned}
|a(u,v)| &\leq |\langle \nabla u_1, \nabla v_1\rangle_{\Omega_1}| + |\alpha^2\langle \varepsilon_r u_1, v_1\rangle_{\Omega_1}| \\
&\quad + |\langle \nabla u_2, \nabla v_2\rangle_{\Omega_2}| + \alpha^2|\langle \varepsilon_r u_2, v_2\rangle_{\Omega_2}| \\
&\quad + | - \langle [T_\alpha u_1], v_1\rangle_{\Gamma_1}| + | - \langle [T_\alpha u_1], v_2\rangle_{\Gamma_2}| \\
&\quad + | - \langle [T_\alpha u_2], v_1\rangle_{\Gamma_1}| + | - \langle [T_\alpha u_2], v_2\rangle_{\Gamma_2}|.
\end{aligned}$$

The Cauchy-Schwarz inequality gives, for $i = 1,\ 2$,

$$\begin{aligned}
|\langle \nabla u_i, \nabla v_i\rangle_{\Omega_i}| &\leq \|\nabla u_i\|_{L^2(\Omega_i)}\|\nabla v_i\|_{L^2(\Omega_i)}, \\
&\leq \|u_i\|_{\mathrm{H}^1(\Omega_i)}\|v_i\|_{\mathrm{H}^1(\Omega_i)}. \\
|\alpha^2\langle \varepsilon_r u_i, v_i\rangle_{\Omega_i}| &\leq \alpha^2\|\varepsilon_r u_i\|_{L^2(\Omega_i)}\|v_i\|_{L^2(\Omega_i)}, \\
&\leq c_1\|u_i\|_{L^2(\Omega_i)}\|\ v_i\|_{L^2(\Omega_i)}, \\
&\leq c_1\|u_i\|_{\mathrm{H}^1(\Omega_i)}\|v_i\|_{\mathrm{H}^1(\Omega_i)}.
\end{aligned}$$

Applying Lemma 1 and the Trace theorem, the aperture inner products satisfy the following inequalities for $i = 1,\ 2$ and $j = 1,\ 2$:

$$\begin{aligned}
\langle [T_\alpha u_i], v_j\rangle_{\Gamma_j} &\leq \langle c\|u_i\|_{\mathrm{H}^{1/2}(\Gamma_i)}, v_j\rangle_{\Gamma_j}, \\
&\leq c_2\|u_i\|_{\mathrm{H}^{1/2}(\Gamma_i)}\langle 1, v_j\rangle_{\Gamma_j}, \\
&\leq c_2\|u_i\|_{\mathrm{H}^{1/2}(\Gamma_i)}\|v_j\|_{\mathrm{H}^{1/2}(\Gamma_j)}, \\
&\leq c_3\|u_i\|_{\mathrm{H}^1(\Omega_i)}\|v_j\|_{\mathrm{H}^1(\Omega_j)}.
\end{aligned}$$

Thus,

$$|a(u,v)| \leq c_4 \sum_{i=1}^{2} \|u_i\|_{\mathrm{H}^1(\Omega_i)} \|v_i\|_{\mathrm{H}^1(\Omega_i)} + c_5 \sum_{i=1}^{2} \sum_{j=1}^{2} \|u_i\|_{\mathrm{H}^1(\Omega_i)} \|v_j\|_{\mathrm{H}^1(\Omega_j)},$$

$$\leq C \|u\|_{\mathbb{H}^1(\boldsymbol{\Omega_1})} \|v\|_{\mathbb{H}^1(\Omega_1)}.$$

Therefore, $|a(u,v)| \leq C\|u\|_{\mathbb{H}^1(\Omega)} \|v\|_{\mathbb{H}^1(\Omega)}$ $\forall u, v \in \mathbb{H}^1(\Omega)$, which concludes the proof. □

Proof of Theorem 3. By Lemmas 1 - 3 we have that the operator $a(\cdot,\cdot)$ is coercive and bounded. Therefore, the Lax-Milgram theorem gives that there exists a unique solution $u^{n+1} \in \mathcal{V} \subset \mathbb{H}^1(\Omega)$ to the variational problem in (3.51) when $k = 2$. This proves the theorem. □

3.7 Well-posedness of Multiple-Cavity Problem

In this section, the well-posedness of the variational formulation for $k > 2$ is established. The development and formulation closely follows the method for $k = 2$ in section 3.6.

Theorem 4. *Let $\mathcal{V}$ be defined as in (3.49) - (3.50), then the variational formulation (3.51) has a unique solution in $\mathcal{V}$ when $k > 2$.*

In order to prove theorem 4, we first prove the following lemmas which will satisfy the Lax-Milgram theorem as in the previous section.

Lemma 4. *The operator $T_\alpha : \mathbb{H}^{1/2}(\Gamma) \to \mathbb{H}^{-1/2}(\Gamma)$ is bounded.*

Proof. For any $g \in \mathbb{H}^{1/2}(\Gamma)$,

$$T_\alpha g(x) = \frac{1}{\pi} \int_\Gamma \left[\frac{\partial^2}{\partial x^2} - \alpha^2 \right] K_0(\alpha|x - x'|) g(x') dx'.$$

Holding fixed g, define $T_{i,j}$ as,

$$T_{i,j}(x) = \frac{1}{\pi} \int_{\Gamma_j} \left[\frac{\partial^2}{\partial x^2} - \alpha^2 \right] K_0(\alpha|x - x'|) g(x') dx', \; x \in \Gamma_i.$$

Note that $T_{i,i}$ is exactly the single-cavity operator, (3.53), shown to be bounded in [36]. Therefore, for each $i = 1, 2, ..., k$, there exists a $c_{ii} < \infty$ such that

$$\|T_{i,i}\|_{\mathrm{H}^{-1/2}(\Gamma_i)} \leq c_{ii}\|g\|_{\mathrm{H}^{1/2}(\Gamma_i)}. \tag{3.61}$$

We may rewrite $T_\alpha g(x)$ as the piecewise sum:

$$T_\alpha g(x) = \sum_{j=1}^{k} T_{i,j}(x), \quad x \in \Gamma_i.$$

For $x \neq x'$,

$$\left[\frac{\partial^2}{\partial x^2} - \alpha^2\right] K_0(\alpha|x - x'|) = \frac{\alpha}{|x - x'|} K_1(\alpha|x - x'|),$$

which is strictly positive and decreasing as the distance, $|x - x'|$, increases. Let $d(\Gamma_i, \Gamma_j)$ represent the smallest distance between apertures Γ_i and Γ_j. Formally,

$$d(\Gamma_i, \Gamma_j) := \min_{\substack{x_1 \in \Gamma_i \\ x_2 \in \Gamma_j}} (|x_1 - x_2|),$$

It is clear that for $i \neq j$,

$$\|T_{i,j}\|_{\mathrm{H}^{-1/2}(\Gamma_i)} \leq c_{ij}\|g\|_{\mathrm{H}^{1/2}(\Gamma_j)}, \tag{3.62}$$

where

$$c_{ij} = \frac{\alpha K_1(\alpha d(\Gamma_i, \Gamma_j))}{\pi d(\Gamma_i, \Gamma_j)}.$$

Therefore,

$$\begin{aligned}
\|T_\alpha g\|^2_{\mathbb{H}^{-1/2}(\Gamma)} &= \sum_{i=1}^{k} \|T_\alpha g\|^2_{\mathrm{H}^{-1/2}(\Gamma_i)} \\
&= \sum_{i=1}^{k} \left\| \sum_{j=1}^{k} T_{i,j} \right\|^2_{\mathrm{H}^{-1/2}(\Gamma_i)} \\
&\leq \sum_{i=1}^{k} \sum_{m=1}^{k} \sum_{n=1}^{k} \|T_{i,m}\|_{\mathrm{H}^{-1/2}(\Gamma_i)} \|T_{i,n}\|_{\mathrm{H}^{-1/2}(\Gamma_i)}
\end{aligned}$$

Applying inequalities (3.61 - 3.62) to the above yields

$$\|T_\alpha g\|^2_{\mathbb{H}^{-1/2}(\Gamma)} \leq \sum_{i=1}^{k}\sum_{m=1}^{k}\sum_{n=1}^{k} c_{im}c_{in}\|g\|_{\mathrm{H}^{1/2}(\Gamma_m)}\|g\|_{\mathrm{H}^{1/2}(\Gamma_n)}. \tag{3.63}$$

Noting that for each i,

$$\|g_i\|_{\mathrm{H}^{1/2}(\Gamma_i)} \leq \|g\|_{\mathbb{H}^{1/2}(\Gamma)},$$

Then, as (3.63) is composed of a finite sum of constant coefficients multiplied by $\|g_i\|_{\mathrm{H}^{1/2}(\Gamma_i)}$, it is clear that there exists a $C < \infty$ that satisfies

$$\|T_\alpha g\|^2_{\mathbb{H}^{-1/2}(\Gamma)} \leq C\|g\|^2_{\mathbb{H}^{1/2}(\Gamma)}.$$

Therefore, $T_\alpha : \mathbb{H}^{1/2}(\Gamma) \to \mathbb{H}^{-1/2}(\Gamma)$ is bounded. □

Lemma 5. *The inner product $\langle T_\alpha g, g\rangle_\Gamma$ is non-positive for all $g \in \mathbb{H}^{1/2}(\Gamma)$.*

Proof. Let $g_0 \in \mathrm{H}^{1/2}(\mathbb{R})$ defined by

$$g_0(x) = \begin{cases} g(x) & x \in \Gamma, \\ 0 & \text{otherwise,} \end{cases}$$

such that $\langle T_\alpha g, g\rangle_\Gamma = \langle T_\alpha g_0, g_0\rangle_{\mathbb{R}}$. Then,

$$\begin{aligned} \langle T_\alpha g_0, g_0\rangle_{\mathbb{R}} &= \int_{\mathbb{R}} [T_\alpha g_0](x)\overline{g_0}(x)\,dx, \\ &= \int_{\mathbb{R}} \frac{1}{\pi}\int_{\mathbb{R}} g_0(x')\frac{\partial^2 K_0}{\partial^2 x}(\alpha|x-x'|)\,dx'\overline{g_0}(x)\,dx \\ &\quad - \int_{\mathbb{R}} \frac{\alpha^2}{\pi}\int_{\mathbb{R}} g_0(x')K_0(\alpha|x-x'|)\,dx'\overline{g_0}(x)\,dx. \end{aligned} \tag{3.64}$$

Note that $g_0(x)$ has compact support in $\mathbb{R}$, and that

$$\frac{\partial}{\partial x}K_0(\alpha|x-x'|) = -\frac{\partial}{\partial x'}K_0(\alpha|x-x'|).$$

Integration by parts is applied twice to the first double integral in (3.64), giving

$$\begin{aligned}
&\frac{1}{\pi}\int_{\mathbb{R}}\int_{\mathbb{R}}\overline{g}_0(x)\frac{\partial^2 K_0}{\partial x^2}(\alpha|x-x'|)g_0(x')\,dx'\,dx \\
&\qquad = -\frac{1}{\pi}\int_{\mathbb{R}}\int_{\mathbb{R}}\overline{g}_0'(x)\frac{\partial K_0}{\partial x}(\alpha|x-x'|)g_0(x')\,dx'\,dx \\
&\qquad = \frac{1}{\pi}\int_{\mathbb{R}}\int_{\mathbb{R}}\overline{g}_0'(x)\frac{\partial K_0}{\partial x'}(\alpha|x-x'|)g_0(x')\,dx'\,dx \\
&\qquad = -\frac{1}{\pi}\int_{\mathbb{R}}\int_{\mathbb{R}}K_0(\alpha|x-x'|)\overline{g}_0'(x)g_0'(x')\,dx'\,dx.
\end{aligned}$$

Thus,

$$\langle T_\alpha g_0, g_0\rangle_{\mathbb{R}} = \langle T_\alpha g, g\rangle_\Gamma = I_1 + I_2, \tag{3.65}$$

with,

$$\begin{aligned}
I_1 &= -\frac{\alpha^2}{\pi}\int_\Gamma\int_\Gamma K_0(\alpha|x-x'|)\overline{g}_0(x)g_0(x')\,dx'\,dx, \\
I_2 &= -\frac{1}{\pi}\int_\Gamma\int_\Gamma K_0(\alpha|x-x'|)\overline{g}_0'(x)g_0'(x')\,dx'\,dx.
\end{aligned}$$

The method used in [36] is applied, as in section 3.6, to show that I_1 and I_2 are both non-positive.

$$I_1 \le 0,$$

$$I_2 \le 0.$$

Therefore, $\langle T_\alpha g, g\rangle_\Gamma = I_1 + I_2$ is non-positive for all $g \in \mathbb{H}^{1/2}(\Gamma)$. □

The following lemma proves coercivity of $a(\cdot,\cdot)$

Lemma 6. *There exist positive constants c and C both in $\mathbb{R}$ such that $a(u,u) \ge c\|u\|^2_{\mathbb{H}^1(\Omega)}$ $\forall u \in \mathbb{H}^1(\Omega)$ and $|a(u,v)| \le C\|u\|_{\mathbb{H}^1(\Omega)}\|v\|_{\mathbb{H}^1(\Omega)}$ $\forall u, v \in \mathbb{H}^1(\Omega)$.*

Proof.

$$
\begin{aligned}
a(u,u) &= \langle \nabla u, \nabla u\rangle_{\Omega} + \alpha^2 \langle \varepsilon_r u, u\rangle_{\Omega} - \langle T_{\alpha} u, u\rangle_{\Gamma}. \\
&\geq \langle \nabla u, \nabla u\rangle_{\Omega} + \alpha^2 \langle \varepsilon_r u, u\rangle_{\Omega} \\
&\geq \min_{\vec{r}\in\Omega}[1, \alpha^2 \varepsilon_r(\vec{r})]\, (\langle \nabla u, \nabla u\rangle_{\Omega} + \langle u, u\rangle_{\Omega}) \\
&\geq c\left(\sum_{i=1}^{k} \|u\|^2_{\mathrm{H}^1(\Omega_i)}\right) \\
&= c\|u\|^2_{\mathbb{H}^1(\Omega)},
\end{aligned}
$$

with

$$
c = \min_{\vec{r}\in\Omega}[1, \alpha^2 \varepsilon_r(\vec{r})].
$$

Therefore, $a(u,u) \geq c\|u\|^2_{\mathbb{H}^1(\Omega)}\ \forall u \in \mathbb{H}^1(\Omega)$.

For any $u,\ v \in \mathbb{H}^1(\Omega)$ such that u_i, v_i refer to the restrictions of u and v to cavity domain Ω_i, the operator a can be expanded as

$$
\begin{aligned}
|a(u,v)| = \Bigg| \sum_{i=1}^{k} \langle \nabla u_i, \nabla v_i\rangle_{\Omega_i} + \alpha^2 \langle \varepsilon_r u_i, v_i\rangle_{\Omega_i} - \langle [T_{\alpha} u], v_i\rangle_{\Gamma_i} \Bigg|, \\
\Bigg| \sum_{i=1}^{k} \langle \nabla u_i, \nabla v_i\rangle_{\Omega_i} + \alpha^2 \langle \varepsilon_r u_i, v_i\rangle_{\Omega_i} \Bigg| + \Bigg| - \sum_{i=1}^{k} \sum_{j=1}^{k} \langle [T_{\alpha} u_j], v_i\rangle_{\Gamma_i} \Bigg|.
\end{aligned}
$$

Applying the triangle inequality, gives

$$
\begin{aligned}
|a(u,v)| \leq \sum_{i=1}^{k} \left(|\langle \nabla u_i, \nabla v_i\rangle_{\Omega_i}| + |\alpha^2 \langle \varepsilon_r u_1, v_1\rangle_{\Omega_1}| \right) \\
+ \sum_{i=1}^{k} \sum_{j=1}^{k} | - \langle [T_{\alpha} u_j], v_i\rangle_{\Gamma_i}|.
\end{aligned}
$$

The Cauchy-Schwarz inequality gives, for $i = 1, 2, ..., k$,

$$\begin{aligned}
|\langle \nabla u_i, \nabla v_i \rangle_{\Omega_i}| &\leq \|\nabla u_i\|_{L^2(\Omega_i)} \|\nabla v_i\|_{L^2(\Omega_i)}, \\
&\leq \|u_i\|_{\mathrm{H}^1(\Omega_i)} \|v_i\|_{\mathrm{H}^1(\Omega_i)}. \\
|\alpha^2 \langle \varepsilon_r u_i, v_i \rangle_{\Omega_i}| &\leq \alpha^2 \|\varepsilon_r u_i\|_{L^2(\Omega_i)} \|v_i\|_{L^2(\Omega_i)}, \\
&\leq c_i \|u_i\|_{L^2(\Omega_i)} \| v_i\|_{L^2(\Omega_i)}, \\
&\leq c_i \|u_i\|_{\mathrm{H}^1(\Omega_i)} \|v_i\|_{\mathrm{H}^1(\Omega_i)}.
\end{aligned}$$

Applying lemma 4 and the Trace theorem, the aperture inner products satisfy the following inequalities for $i = 1, 2, ..., k$ and $j = 1, 2, ..., k$:

$$\begin{aligned}
\langle [T_\alpha u_i], v_j \rangle_{\Gamma_j} &\leq \langle c_2 \|u_i\|_{\mathrm{H}^{1/2}(\Gamma_i)}, v_j \rangle_{\Gamma_j}, \\
&\leq c_2 \|u_i\|_{\mathrm{H}^{1/2}(\Gamma_i)} \langle 1, v_j \rangle_{\Gamma_j}, \\
&\leq c_2 \|u_i\|_{\mathrm{H}^{1/2}(\Gamma_i)} \|v_j\|_{\mathrm{H}^{1/2}(\Gamma_j)}, \\
&\leq c_3 \|u_i\|_{\mathrm{H}^1(\Omega_i)} \|v_j\|_{\mathrm{H}^1(\Omega_j)}.
\end{aligned}$$

Thus,

$$\begin{aligned}
|a(u, v)| &\leq c_4 \sum_{i=1}^{k} \|u_i\|_{\mathrm{H}^1(\Omega_i)} \|v_i\|_{\mathrm{H}^1(\Omega_i)} \\
&\quad + c_5 \sum_{i=1}^{k} \sum_{j=1}^{k} \|u_i\|_{\mathrm{H}^1(\Omega_i)} \|v_j\|_{\mathrm{H}^1(\Omega_j)}, \\
&\leq C \|u\|_{\mathbb{H}^1(\Omega)} \|v\|_{\mathbb{H}^1(\Omega)}.
\end{aligned}$$

Therefore, $|a(u, v)| \leq C \|u\|_{\mathbb{H}^1(\Omega)} \|v\|_{\mathbb{H}^1(\Omega)}$ $\forall u, v \in \mathbb{H}^1(\Omega)$, which concludes the proof. □

Proof of Theorem 4. By Lemmas 4 - 6 we have that the operator $a(\cdot, \cdot)$ is coercive and bounded. Therefore, the Lax Milgram theorem gives that there exists a unique solution $u^{n+1} \in \mathcal{V} \subset \mathbb{H}^1(\Omega)$ to the variational problem in (3.51). This proves the theorem. □

IV. Numerical Simulation and Analysis

In this chapter, the time-discretization and implementation of the numerical model using the FE-BI method are described.

4.1 Finite Element Approximation

Define the space

$$\mathbb{H}^1_S(\Omega) = \{f \in \mathbb{H}^1(\Omega) : f = 0 \text{ on } S\}.$$

Let $\mathcal{T}$ be the subspace of linear functions in $\mathbb{H}^1_S(\Omega)$ defined by a set of R nodes $\{p_k\}_{k=1}^R$ and N basis functions $\{\phi_i\}_{i=1}^N$ such that any function f in $\mathcal{T}$ may be represented by

$$f = \sum_{i=1}^{N} c_i \phi_i.$$

The problem we seek to solve is: given u^n, find $u^{n+1} \in \mathcal{T}$ which solves the variational formulation (3.51). Following the method in [36], the variational formulation (3.51) is discretized to the matrix equation,

$$[K + M + P]U^{n+1} = F^{n+1}, \tag{4.1}$$

where, U^{n+1} is the coefficient vector defined by

$$u^{n+1} = \sum_{j=1}^{N} U_j^{n+1} \phi_j.$$

4.1.1 Left-hand Side.

The entries of matrices K, M, and P are determined for basis elements ϕ in the following manner:

$$\begin{aligned} K_{ij} &= \int_\Omega \Delta\phi_i \cdot \Delta\phi_j dA \\ M_{ij} &= \alpha^2 \int_\Omega \varepsilon_r \phi_i \phi_j dA \\ P_{ij} &= -\int_\Gamma \phi_i \left(T_\alpha \phi_j\right) dS. \end{aligned} \tag{4.2}$$

Matrix P is mostly zeros with entries only in positions corresponding to aperture nodes. For clarity, we denote Λ_i as the aperture segment from x_i to x_{i+1}. Noting the compact support for ϕ_i, we apply integration by parts to (3.45) to yield

$$P_{ij} = \frac{\alpha^2}{\pi} \int_{\Lambda_i} \phi_i(x) \int_{\Lambda_j} K_0(\alpha|x - x'|)\phi_j(x')dx'dx + \frac{1}{\pi} \int_{\Lambda_i} \frac{\partial \phi_i}{\partial x}(x) \int_{\Lambda_j} K_0(\alpha|x - x'|)\frac{\partial \phi_j}{\partial x'}(x')dx'dx.$$

When $i \neq j$, both integrals in P_{ij} may be approximated by standard quadrature methods, as was shown in [36]. The midpoint approximation gives

$$P_{ij} \approx \left(\frac{4 + \alpha^2|\Lambda_i||\Lambda_j|}{4\pi}\right) K_0(\alpha|\xi_i - \xi_j|), \tag{4.3}$$

where $\xi_i = \frac{x_i + x_{i+1}}{2}$. However, when $i = j$, the integrals in P_{ij} are singular and are approximated as

$$P_{ij} \approx \left(\frac{4 + \alpha^2|\Lambda_i|}{2\alpha\pi}\right) \int_0^{\frac{\alpha|\Lambda_i|}{2}} K_0(\tau)d\tau. \tag{4.4}$$

As was done in [36], referring to [1], the integral in (4.4) may be numerically evaluated by

$$\int_0^y K_0(\tau)\, d\tau = \left[-\left(\gamma_0 + \ln\frac{y}{2}\right) y \sum_{k=0}^{\infty} \frac{(y/2)^{2k}}{(k!)^2(2k+1)} + y \sum_{k=0}^{\infty} \frac{(y/2)^{2k}}{(k!)^2(2k+1)^2} + y \sum_{k=1}^{\infty} \frac{(y/2)^{2k}}{(k!)^2(2k+1)} \left(\sum_{m=1}^{k} \frac{1}{m}\right)\right],$$

where $y = \dfrac{\alpha|\Lambda_i|}{2}$ and γ_0 is Euler's constant. The sums in this expansion converge rapidly for small values of y, i.e. $y < 2$. Thus, (4.3) and (4.4) provide a method for approximating the aperture integral in (4.2).

4.1.2 Right-hand Side.

The right-hand side of (4.1) is dependent only on known or pre-computed values.

$$\begin{aligned} F_j^{n+1} &= b^{n+1}(\phi_j) \\ &= \alpha^2 \int_\Omega \varepsilon_r \tilde{u}^{n+1}\phi_j dA + \int_\Gamma \phi_j \left(2\frac{\partial u^{inc}}{\partial y} + \tilde{H}^{n+1}\right) dS. \end{aligned} \tag{4.5}$$

Matrix F^{n+1} in (4.5) is computed at every timestep and is dependent on $\tilde{u}^{n+1}$. Below, we detail the method used to construct this matrix.

Assuming that in Ω,

$$\tilde{u}^{n+1} \approx \sum_{j=1}^{N} \tilde{U}_j^{n+1} \phi_j,$$

the interior integral of (4.5) may be approximated by

$$\alpha^2 \int_{\Omega} \varepsilon_r \tilde{u}^{n+1} \phi_j dA \approx [M\tilde{U}^{n+1}]_j.$$

The aperture integral of (4.5) is approximated in much the same fashion as was done for P in (4.3) and (4.4). Using the midpoint approximation gives

$$\int_{\Gamma} \phi_j \left(2\frac{\partial u^{inc}}{\partial y} + \tilde{H}^{n+1} \right) dS \approx \frac{|\Lambda_j|}{2} \left(2\frac{\partial u^{inc}}{\partial y}(\xi_j, 0) + \tilde{H}^{n+1}(\xi_j) \right).$$

The incident field and its derivative are known from initial information. Next, we describe how $\tilde{H}$ is approximated. An alternative numerical algorithm to approximate hypersingular integrals for electromagetic cavity applications is presented in [41] which reduces error to $O(h^2)$. The method detailed below follows the steps outlined in [36]. Evaluating the partial derivative of (3.39) and substituting into (3.44) gives

$$\tilde{H}^{n+1}(\xi_j) = \frac{\alpha^3}{\pi} \int_{\mathbb{R}^2_+} \frac{y'}{|(\xi_j, 0) - \vec{r'}|} K_1(\alpha|(\xi_j, 0) - \vec{r'}|) \tilde{u}^{s,n+1}(\vec{r'}) d\vec{r'}.$$

The integrand in $\tilde{H}$ exhibits exponential decay as $|\vec{r'}|$ increases and hypersingularity as $\vec{r'} \to (\xi_j, 0)$. In light of these attributes, we establish a numerical integration over a truncated region which does not require evaluation at $\vec{r'} = (\xi_j, 0)$.

Let the region of integration be rectangular, defined by $x' \in [-X, X], y' \in (0, Y]$, where X and Y are suitably large constants.

$$\tilde{H}^{n+1}(\xi_j) \approx \frac{\alpha^3}{\pi} \int_{-X}^{X} \int_{0}^{Y} \frac{y'}{|(\xi_j, 0) - \vec{r'}|} K_1(\alpha|(\xi_j, 0) - \vec{r'}|) \tilde{u}^{s,n+1}(x', y') dy' dx'.$$

As was done in [36], the exterior integral may be approximated by partitioning $[-X, X]$ into L intervals donoted X_l and $[0, Y]$ into M intervals denoted Y_m each with lengths $|X_l|$, $|Y_m|$,

respectively. Letting $R_{lm} = X_l \times Y_m$, $|R_{lm}| = |X_l||Y_m|$ denoting the area of the rectangle R_{lm}, and letting λ_{lm} denote the midpoint of R_{lm}, gives

$$\tilde{H}^{n+1}(\xi_j) \approx \frac{\alpha^3}{\pi} \sum_{l=1}^{L} \sum_{m=1}^{M} |R_{lm}| \frac{\lambda_{lm} \cdot \hat{y}}{|\xi_j \hat{x} - \lambda_{lm}|} K_1(\alpha|\xi_j \hat{x} - \lambda_{lm}|) \tilde{u}^{s,n+1}(\lambda_{lm}). \tag{4.6}$$

In order to use this method, the midpoint values of $\tilde{u}^{s,n+1}(\lambda_{lm})$ should be computed in addition to the nodal values of $u^{s,n+1}(x, y)$.

4.1.3 Matrix Construction.

When filled, the non-zero elements of the matrix $[K + M + P]$ exhibits the banded diagonal feature common to the finite element method with additional non-zero elements to capture the coupling between aperture elements induced by the operator T_α. For the case with c cavities, this matrix may be viewed as a collection of smaller matrices. Let $[K + M]_i$ represent the parts of K and M which are non-zero in Ω_i. Also let $[P]_{a,b}$ represent the members $P_{i,j}$ where $\Lambda_i \subseteq \Gamma_a$, and $\Lambda_j \subseteq \Gamma_b$. When combined, the matrix $[K + M]$ will be arranged in the following manner:

$$\begin{bmatrix} [K+M]_1 & [0] & \dots & [0] & [0] \\ [0] & [K+M]_2 & \ddots & [0] & [0] \\ \vdots & \ddots & \ddots & \ddots & \vdots \\ [0] & [0] & \ddots & [K+M]_{c-1} & [0] \\ [0] & [0] & \dots & [0] & [K+M]_c \end{bmatrix}$$

Commonly, the submatrices, $[K + M]_i$, will be banded diagonal and symmetric. This, of course, depends on the choice of basis functions. In the case of linear nodal basis functions on triangular elements, the resulting matrices $[K + M]_i$ are banded tridiagonal and positive definite. The $[P]$ matrix is different in form to $[K+M]$, but still maintains useful properties.

The layout of $[P]$ is:

$$\begin{bmatrix} [P]_{1,1} & [P]_{1,2} & [P]_{1,3} & \dots & [P]_{1,c} \\ [P]_{2,1} & [P]_{2,2} & [P]_{2,3} & \dots & [P]_{2,c} \\ \vdots & \vdots & \vdots & \ddots & \vdots \\ [P]_{c,1} & [P]_{c,2} & [P]_{c,3} & \dots & [P]_{c,c} \end{bmatrix}$$

As defined, an element of $[P]_{a,b}$ will only be non-zero if the corresponding nodes are found on the apertures Γ_a and Γ_b. Additionally, each $[P]_{a,b}$ is symmetric and $[P]_{a,b} = [P]_{b,a}$. Therefore $[P]$ is also symmetric.

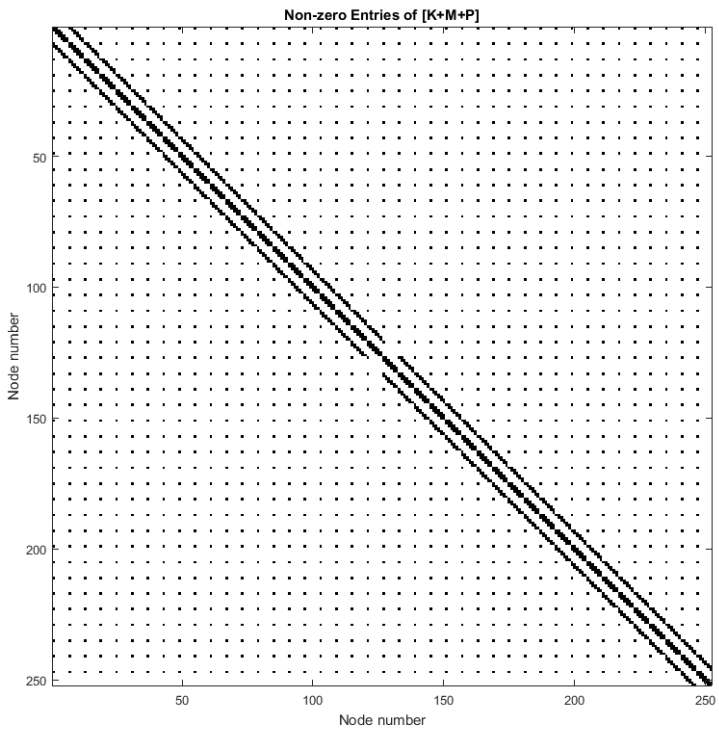

Figure 4.1: Non-zero entries of finite element matrix illustrating coupling

For the two-cavity case, the non-zero elements of the matrix $[K + M + P]$ illustrated in Figure 4.1, for equally-sized cavities, show the banded diagonal feature common to the

finite element method. The additional non-zero elements indicate the coupling between aperture elements induced by the operator T_α.

4.2 Scattered Field Approximation

A critical step in the computational process is the approximation of the scattered field u^s in the exterior region. Not only is the solution of u^s at some time T the intended output of this numerical simulation, but the scattered field at each time step is an important factor in the boundary condition, as seen in the approximation of $\tilde{H}^{n+1}$ in (4.6). Given $u^{s,n}$ data, $\tilde{u}^{s,n+1}$ is computed directly with (3.12). After solving the interior problem for u^{n+1}, enforcing the condition $u^{n+1}(x,0) = u^{s,n+1}(x,0)$, $(x,0) \in \Gamma$, provides the required data for the second integral in (3.25).

The computational challenge then is in computing the integral form of the scattered field, which requires computing the Green's function for the truncated computational area. This is accomplished efficiently by approximating the integration as a matrix multiplication. Define the exterior computational region by

$$\mathcal{D}^{ext} = \{(x,y) \in \mathbb{R}^2 : |x| \le X, 0 \le y \le Y\}.$$

Let X_l, Y_m, and λ_{lm}, $l = 1, 2, ..., L$, $m = 1, 2, ..., M$, as used in (4.6), describe LM grid squares covering $\mathcal{D}^{ext}$. Then there are $(L+1)(M+1)$ corner points and LM center points at which the values of $u^{s,n+1}$ are to be approximated. Assuming equal spacing in x with length s, we have $N_\Gamma = \sum_{i=1}^{k} \frac{|\Gamma_i|}{s}$ aperture segments Λ_i with midpoints $(\xi_j, 0)$, $j = 1, 2, ..., N_\Gamma$. Then

for each center point, $\vec{r} = \lambda_{lm}$, the scattered field integrals can be discretized as

$$\begin{aligned} u^{s,n+1}(\lambda_{lm}) &= \int_{\mathbb{R}^2_+} G^e_\alpha(\lambda_{lm}, \vec{r'})\alpha^2 \tilde{u}^{s,n+1}(\vec{r'})\, d\vec{r'} - \int_\Gamma u^{s,n+1}(\vec{r'}) \frac{\partial G^e_\alpha}{\partial n}(\lambda_{lm}, \vec{r'})\, dx', \\ &= \sum_{i=1}^{L}\sum_{j=1}^{M} \int_{X_i}\int_{Y_j} G^e_\alpha(\lambda_{lm}, \vec{r'})\alpha^2 \tilde{u}^{s,n+1}(\vec{r'})\, d\vec{r'} - \sum_{k=1}^{N_\Gamma} \int_{\Lambda_k} g(x') \frac{\partial G^e_\alpha}{\partial n}(\lambda_{lm}, (x', 0))\, dx', \\ &\approx \sum_{i=1}^{L}\sum_{j=1}^{M} |X_i||Y_j| G^e_\alpha(\lambda_{lm}, \lambda_{ij})\alpha^2 \tilde{u}^{s,n+1}(\lambda_{ij}) - \sum_{k=1}^{N_\Gamma} |\Lambda_k| g(\xi_k) \frac{\partial G^e_\alpha}{\partial n}(\lambda_{lm}, (\xi_k, 0)). \end{aligned}$$

By appropriately re-indexing the input values of $\tilde{u}^{s,n+1}$ into an $LM \times 1$ vector $[\tilde{U}^s]$, and g into an $N_\Gamma \times 1$ vector $[g]$, this integration becomes a matrix multiplication. Define matrix $[G]$ as an $LM \times LM$ matrix with entries

$$[G]_{N_{ij}, N_{lm}} = |X_i||Y_j|\alpha^2 G^e_\alpha(\lambda_{lm}, \lambda_{ij}).$$

Also, define $[Gn]$ as an $N_\Gamma \times LM$ matrix with entries

$$[Gn]_{k, N_{lm}} = |\Lambda_k| \frac{\partial G^e_\alpha}{\partial n}(\lambda_{lm}, (\xi_k, 0)).$$

Thus, $u^{s,n+1}$ is approximated by $[G][\tilde{U}^s] - [G_n][g]$. The same general method is used to approximate the scattered field at the corner points, adjusting for increased count and partial grid squares around the edges.

4.3 Algorithm Overview

Below is an overview of the computational algorithm used.

1. Input initial conditions. This is the initialization step where the incident field, step size, computational domain, etc. are defined. Assume that initial fields inside cavities are equal to zero.

2. Build Matrices: $K = \langle \nabla\phi_i, \nabla\phi_j \rangle_{\mathbf{\Omega}}$, $M = \alpha^2 \langle \varepsilon_r \phi_i, \phi_j \rangle_{\mathbf{\Omega}}$, $P = -\langle T\phi_i, \phi_j \rangle_{\mathbf{\Gamma}}$. These matrices are fixed and do not change with each time step. Additionally, in this step, the integration matrices $[G]$ and $[Gn]$ are constructed.

3. Loop for each time step:

   (a) Calculate predictions $\tilde{u}$ for interior and exterior regions.

   (b) Compute right-hand side vector F^{n+1}.

   (c) Solve $(K + M + P)u^{n+1} = F^{n+1}$ for intereior and aperture fields u^{n+1}.

   (d) Compute solution for exterior field $u^{s,n+1}$.

   (e) Correct time derivatives for interior and exterior regions.

   (f) Record required data from interior, exterior, or aperture fields.

4. Conduct post-processing and analysis; generate plots and save collected data.

V. Numerical Results

In this section we present examples of numerical tests conducted for one, two, and three rectangular cavities embedded in the ground plane. The first set of examples use a continuous incident wave and the second set use a Gaussian wave as the incident field. All tests are conducted at normal incidence. The time scale, consistent with [36], is light-meters, i.e. the time it takes light to travel 1 meter in free space, which is $\frac{1}{c}$ sec or 3.336×10^{-9} sec. A uniform triangular mesh with node spacing, $r = 0.05$ m is used. For the Newmark method the time increment, $h = 0.05$ light-meters, $\gamma = 0.9$, and $\beta = 0.25(0.5 + \gamma)^2$. Polarization of the incident fields is TM^z, indicating that wave propagation and the magnetic field will be fully described in the xy-plane plane, and the electric field will be entirely z-directed, but described as a function of x and y. The area above the ground plane will be considered free space $\mathbb{R}^2_+ = \{x, y \in \mathbb{R}^2 : y > 0\}$ with homogeneous parameters ε_0, μ_0 denoting the permittivity and permeability of free space. A simple example is illustrated in Figure 5.1.

For all tests, aperture fields were recorded for each time step and for some tests, exterior fields along a semi-circle with radius 3 m centered at the origin were collected as well. For each test, cavities were 1 m wide with depth of either 0.25 m or 5 m. Cavities were either unfilled ($\varepsilon_r = 1$), or filled with non-magnetic ($\mu_r = \mu_0$), dielectric material with $\varepsilon_r = 2$ or $\varepsilon_r = 4$. Figure 5.2 shows the computational grid, exterior field capture points, and field values at $t = 6.75$ LM from a three-cavity test using depth $= (0.25, 5, 0.25)$ and $\varepsilon_r = (2, 2, 2)$.

Throughout the discussion of results, we will refer to *influence* of additional cavities when refering to aperture fields. Specifically, we define this as the difference between the

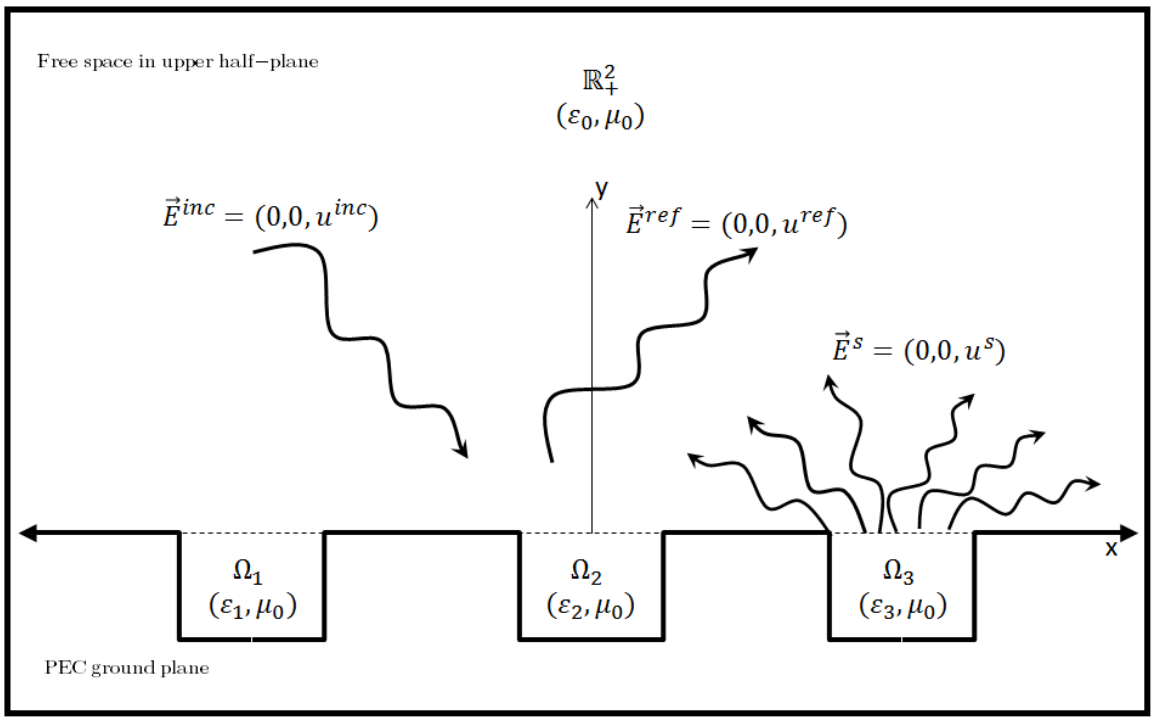

Figure 5.1: Three cavity environment

computed solution when only one cavity is present in the ground plane and the computed solution when multiple cavities present, with respect to the same point in time and space.

5.1 Continuous Wave

For the continuous wave example, the incident electric field has a wavelength of 1 m. Using scaled time units, the incident field is described by

$$u^{inc}(x, y, t) = \mathrm{Re}\left\{e^{i2\pi(t-y)}\right\}.$$

The first test conducted was a validation test with single rectangular cavity, width = 1 m, depth = 0.25 m. These results are shown in figure 5.3 and compared with published results from [36] as seen in figure 5.4. It is noted that some differences exist between our computed solutions and the reference solutions. However, the principle shape and

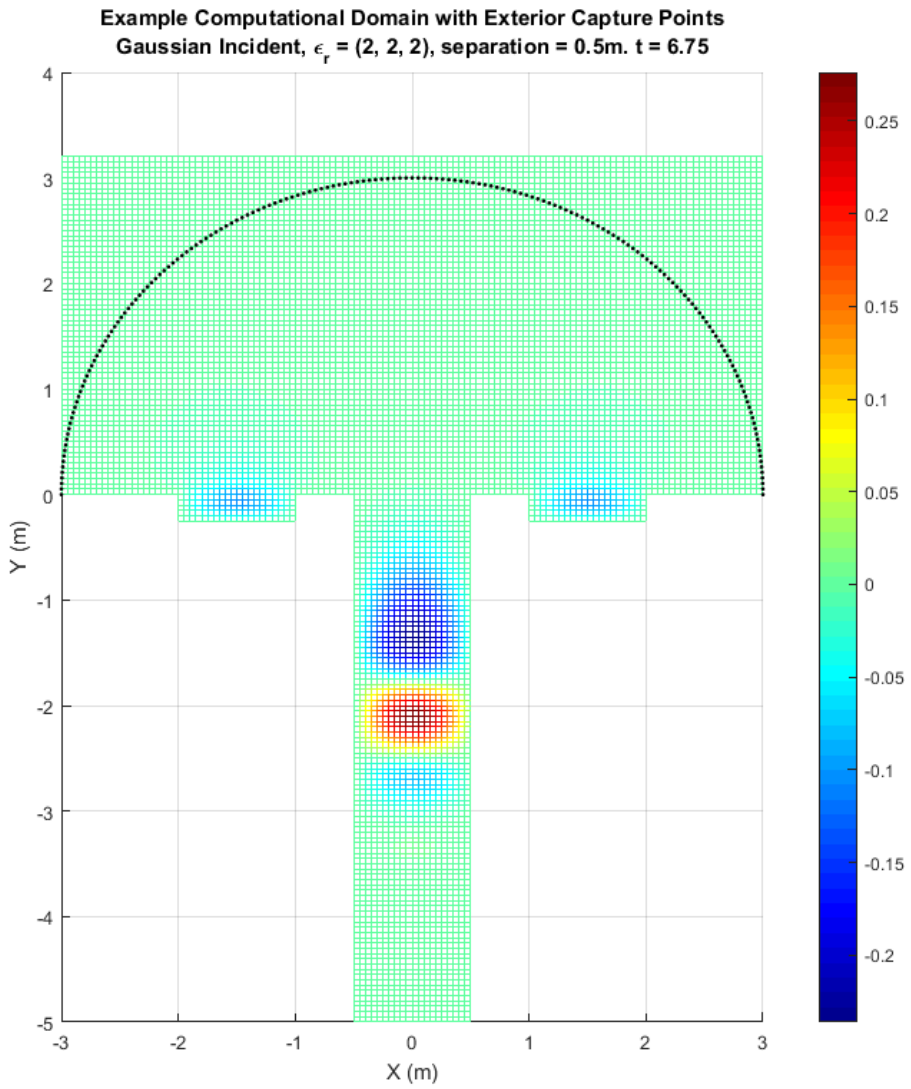

Figure 5.2: Example of computational domain

period are consistent. Additionally, the late-time stability of the numerical routine was investigated by allowing the simulation to run for 120 LM. The results shown in figure 5.5 demonstrate that this routine is stable, not demonstrating the late-time linear growth often associated with the Newmark method [8]. In the same plots, note that a stable periodic state is acheived more quickly in the unfilled cavity (approx. 5 LM) than in the filled cavity (approx. 20LM). This is related to the speed of propagation through the medium and

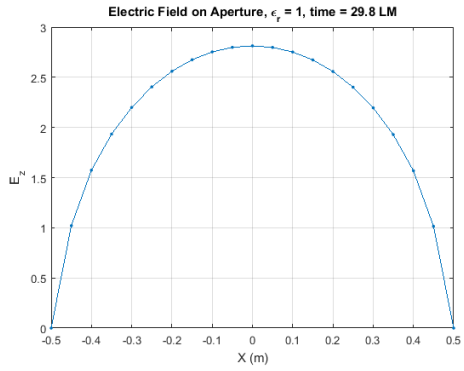

(a) Single-cavity solution with $\varepsilon_r = 1$.

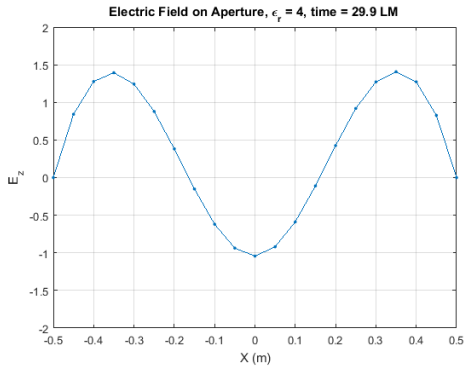

(b) Single-cavity solution with $\varepsilon_r = 4$.

Figure 5.3: Computed single-cavity results, continuous incident wave.

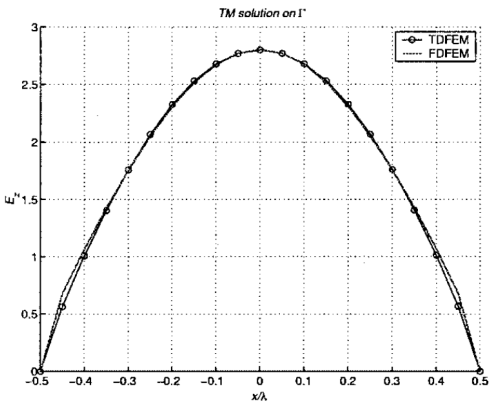

(a) Single-cavity solution with $\varepsilon_r = 1$.

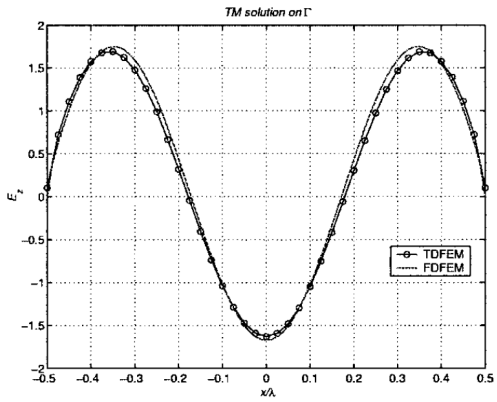

(b) Single-cavity solution with $\varepsilon_r = 4$.

Figure 5.4: Solutions published in [36].

the depth of the cavity. Because the computational model initializes with fields inside the cavities set to zero, it is expected that a relatively small number of cycles will be required before acheiving the periodic solution.

After demonstrating that single-cavity solutions are stable for the applied numerical method, we next conducted tests with two cavities. Combining the two single-cavity tests into one, we use two identical cavities, width = 1 m, depth = 0.25 m, separated by 1 m, with cavity 1 unfilled and cavity 2 filled with dielectric having $\varepsilon_r = 4$. To denote multiple

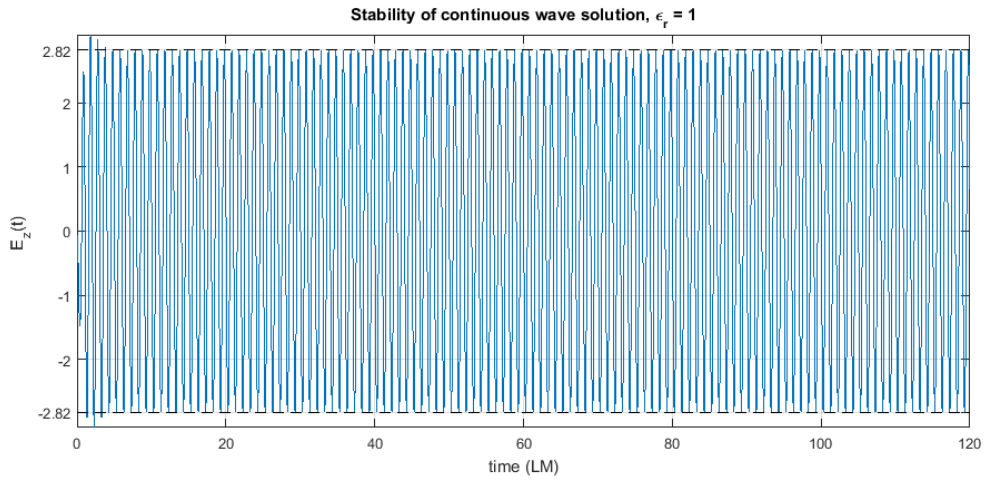

(a) Single-cavity solution with $\varepsilon_r = 1$.

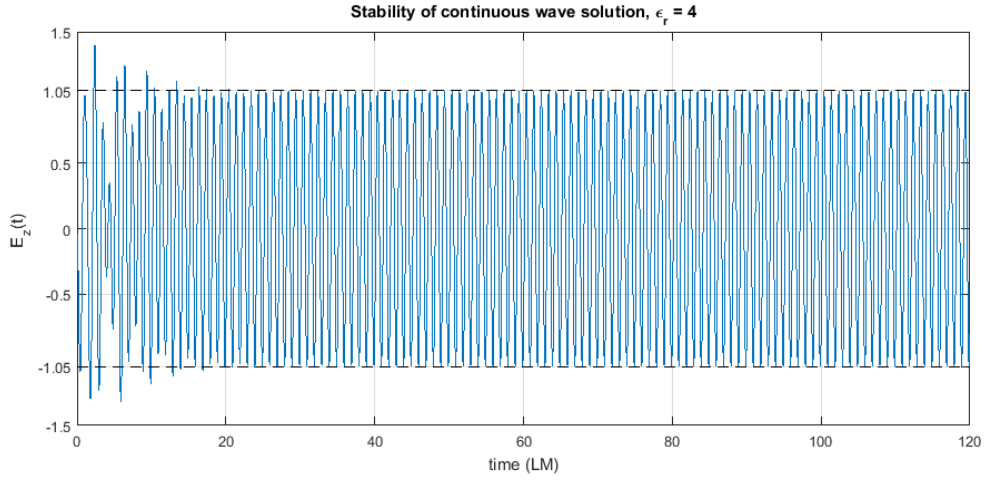

(b) Single-cavity solution with $\varepsilon_r = 4$.

Figure 5.5: Aperture fields at (0,0), continuous incident wave.

cavity parameters, we adopt the convention

$$\text{parameter} = (\text{cavity } 1,\ \text{cavity } 2, ...,\ \text{cavity } k),$$

where parameters are listed from left to right by cavity. For example, in this case: $\varepsilon_r = (1, 4)$, width = (1m, 1m), depth = (0.25m, 0.25m).

In figure 5.6, one cycle of the periodic response is shown alongside a single-time step cross section of the fields. Note that the two-cavity solutions strongly resemble the single-cavity solutions. This indicates that the effect of the coupling, or cross-talk, between the cavities is relatively weak at this distance.

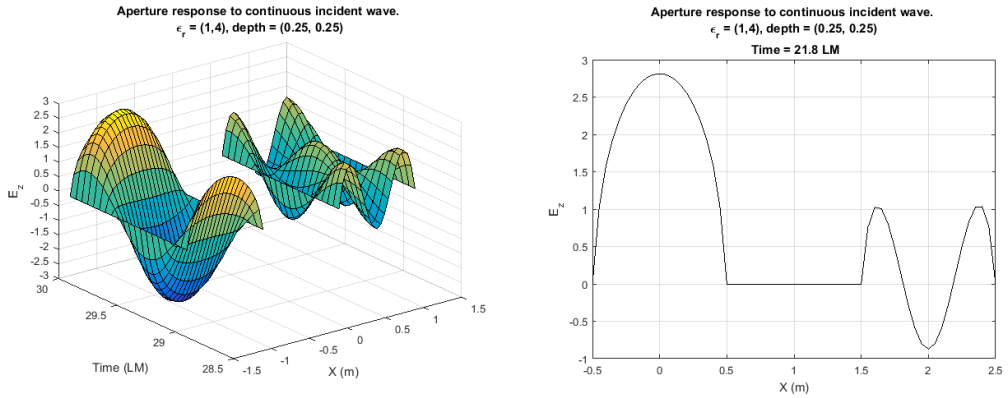

(a) Aperture electric field over one cycle.

(b) Aperture electric field at t=21.8.

Figure 5.6: Aperture electric field, continuous incident field.

In order to identify the effects of coupling between cavities, the computed single-cavity solutions were subtracted from the multi-cavity solutions. The difference between solutions is attributed to the existence of additional cavities. Figure 5.7 shows the difference in aperture fields found in two tests, the first conducted with a separation of 0.1 m, the second with a separation of 1 m. Note that at 0.1 m, the maximum influence is approximately 4×10^{-2} and at 1 m, the maximum influence is approximately 1×10^{-3}.

Additional tests were run at a variety of distances to determine the effect of separation distance on the strength of coupling. We use maximum absolute value of influence as a metric for describing strength of interaction as a function of distance. Figure 5.8 summarizes the influence between an unfilled cavity (cavity 1), and one filled with material have $\varepsilon_r = 4$ (cavity 2). Figure 5.9 shows results from tests run with identical cavities, both

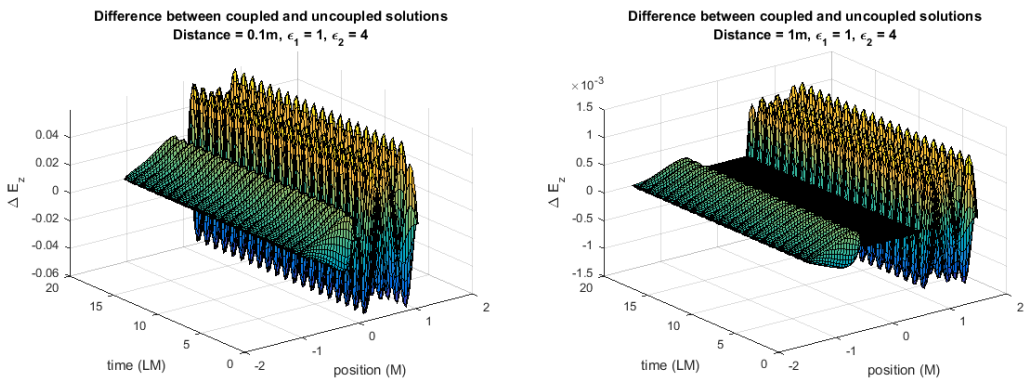

(a) Difference from coupling at 10 cm. (b) Difference from coupling at 1 m.

Figure 5.7: Calculated effects of coupling on solutions at two different distances.

filled with material having $\varepsilon_r = 2$. Both figures demonstrate that coupling between cavities, as measured by aperture fields exponentially diminishes as distance increases.

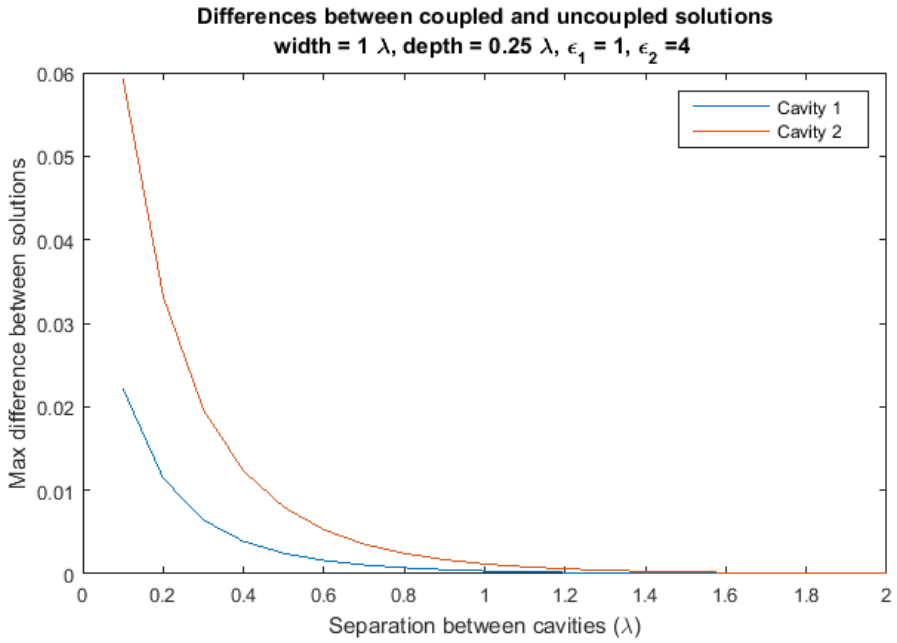

Figure 5.8: Interaction between cavities, $\varepsilon_1 = \varepsilon_0$, $\varepsilon_2 = 4\varepsilon_0$.

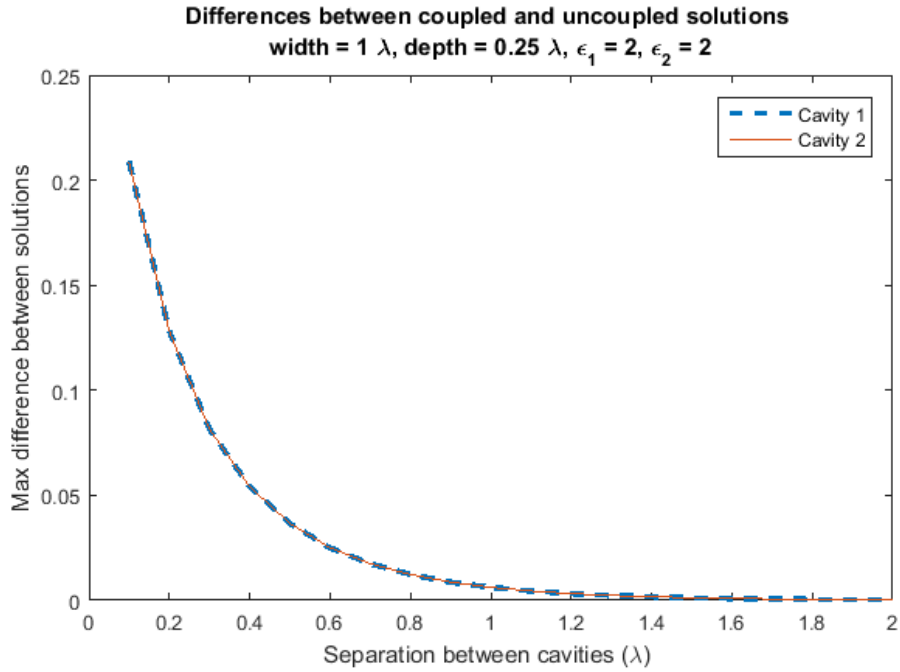

Figure 5.9: Interaction between identical cavities $\varepsilon_r = 2$.

In an attempt to scale the influence factor based on the strength of the second cavity, we propose the following method. Define $E^1_{\varepsilon_r}$ as the reference response for one cavity filled with material having permittivity of ε_r, and $E^2_{\varepsilon_r}(d,\ M)$ be the two-cavity response as a function of d, the distance to the second cavity, and M, the maximum absolute value of the reference response of the second cavity. Then, we examine the scaled influence factor

$$C_{\varepsilon_r}(d,\ M) = \frac{\max_{x\in\Gamma_1,\, t\in[20,T]} \left(\left| E^2_{\varepsilon_r}(d,\ M) - E^1_{\varepsilon_r} \right| \right)}{M}.$$

In figure 5.10, the scaled influence factor, $C_{\varepsilon_r}(d,\ M)$ is plotted for $d \in [.05, .5, 1]$ and using the same geometry and parameters as in figure 5.6. Additionally, multiples of e^{-4d} are plotted for comparison. In looking at influence in this way, it is clear that the effect diminishes exponentially as a function of distance between cavities. The scale factor does not bring the influence plots directly together, but does reduce the observed distance between them.

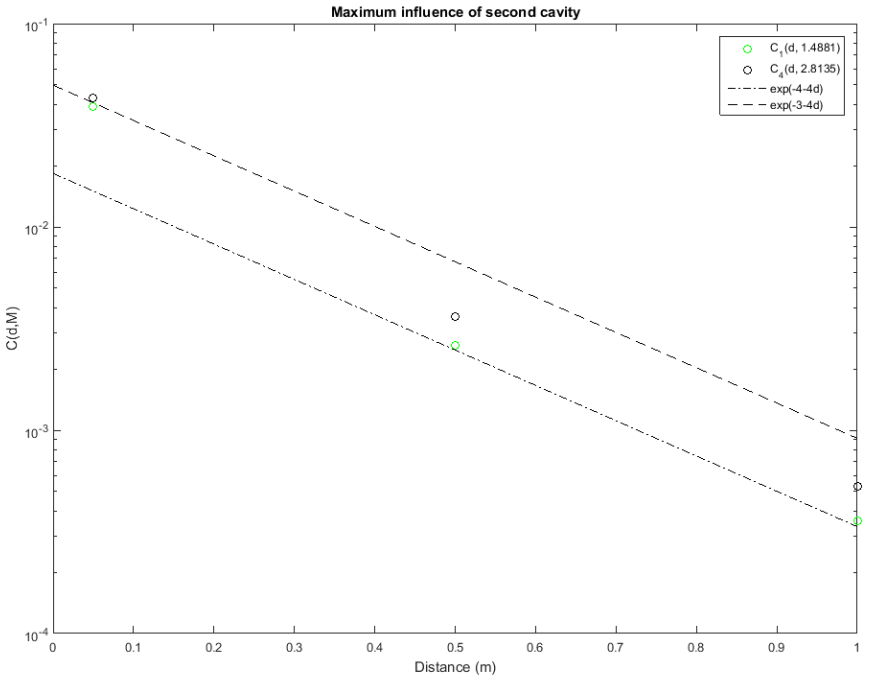

Figure 5.10: Scaled maximum influence of second cavity.

Figure 5.12 shows the response from three rectangular cavities separated by only 0.05 m. In this example, the outer cavities are 1 m $\times$ 5 m, filled with material having $\varepsilon_r = 4$, and the center cavity is 1 m $\times$ 0.25 m, and unfilled. When compared to figure 5.13, which had greater separation between the cavities, figure 5.12 demonstrates a slight skewing of the aperture fields due to the interaction between the cavities.

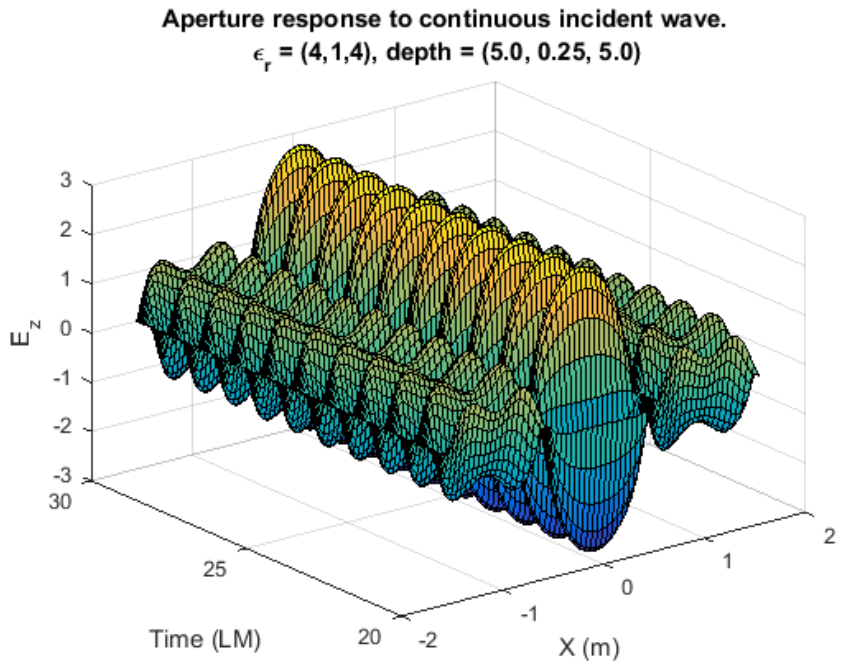

Figure 5.11: Periodic aperture fields for three close cavities.

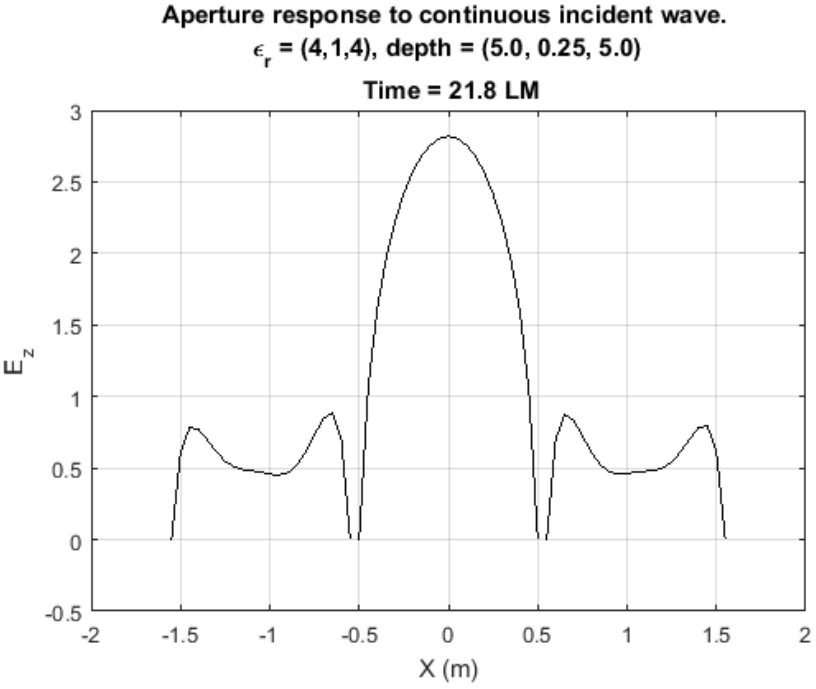

Figure 5.12: Cross section of aperture fields for three close cavities.

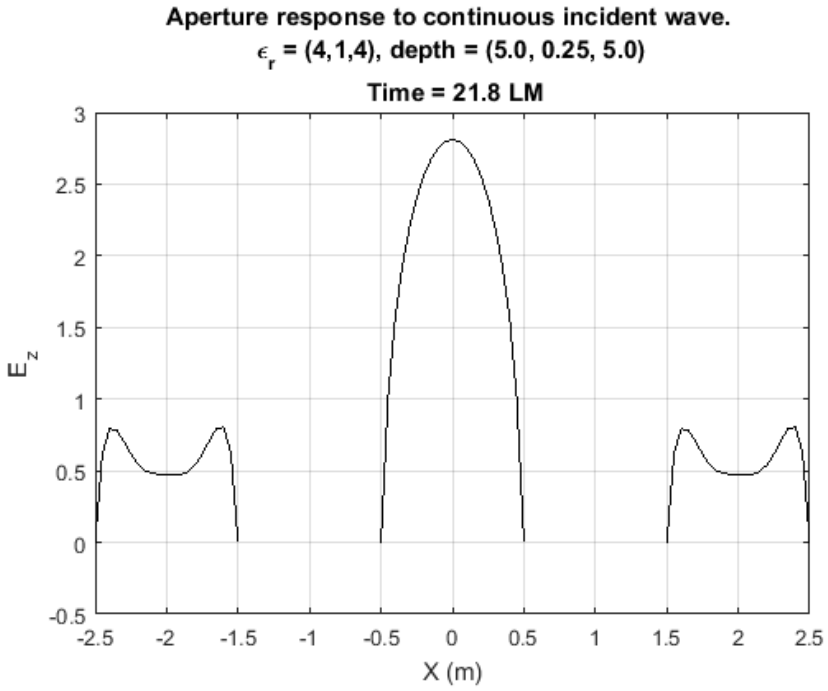

Figure 5.13: Aperture fields for three cavities separated by 1 m.

5.2 Gaussian Pulse

For the Gaussian wave example, the incident electric field is described by

$$u^{inc}(x, y, t) = A\frac{4}{T\sqrt{\pi}}e^{-\tau^2},$$

with

$$\tau = \frac{4(t - t_0 + x\cos\theta_{inc} + y\sin\theta_{inc})}{T}, \quad \theta_{inc} \in [\pi/2, \pi].$$

The parameter T in the defining equation of the Gaussian is used to control the width of the pulse. For example, 5.14 demonstrates the different waves generated for $T = 1$, 2, and 4. t_0 defines the time at which the wave will reach its maximum at the origin, and θ_{inc} is the angle of incidence.

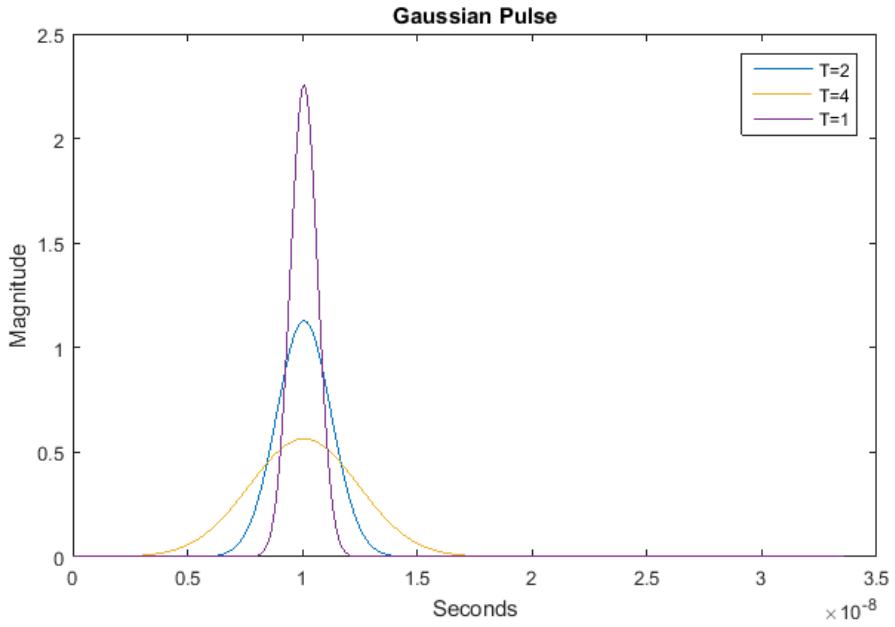

Figure 5.14: Gaussian wave for different T values.

For the following numerical examples, parameters for the incident field are as follows: $T = 2$, $A = 1$, $\theta_{inc} = \frac{\pi}{2}$, and $t_0 = 3$. These parameters are chosen to be the same as were used in [36].

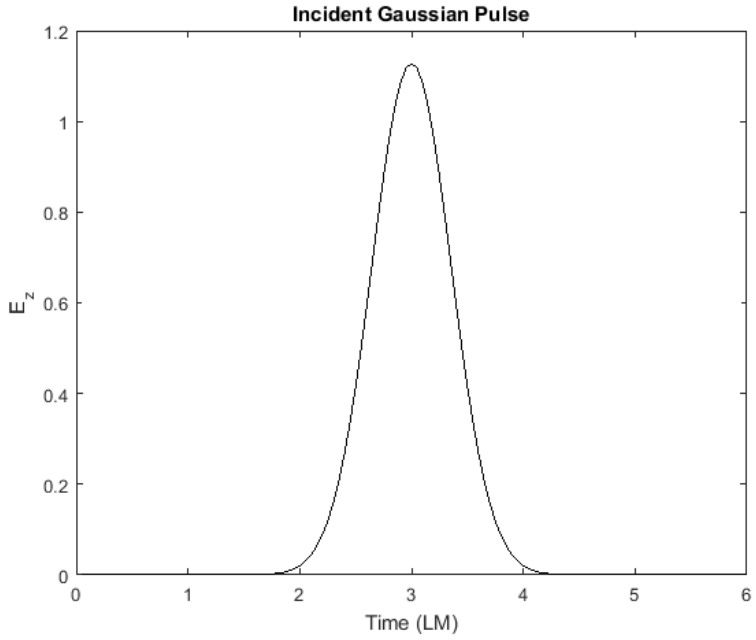

Figure 5.15: Gaussian pulse at cavity aperture.

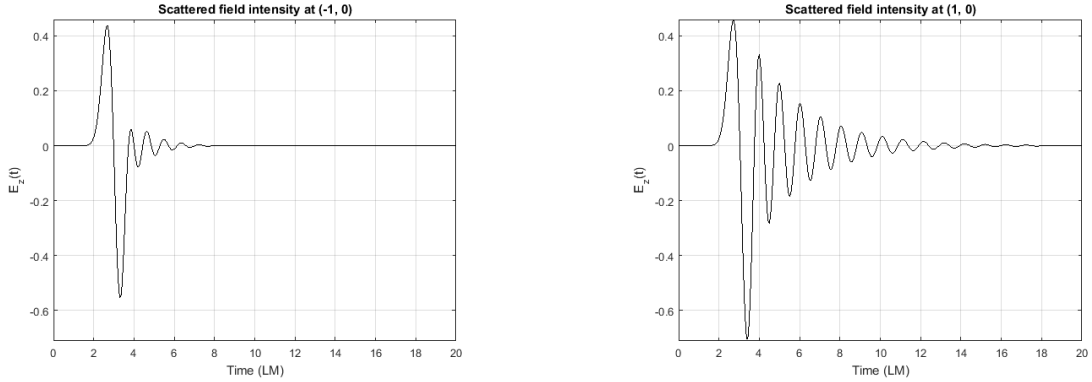

(a) TM solution for aperture 1, $\varepsilon_r = 1$.

(b) TM solution for aperture 2, $\varepsilon_r = 2$.

Figure 5.16: Field values at midpoints of apertures.

For the following two-cavity numerical examples, cavity 1 is unfilled, $\varepsilon_r = 1$, and cavity 2 is filled with non-magnetic dielectric material having $\varepsilon_r = 2$.

Figure 5.16 illustrates that the rates of decay are consistent with reference plots found in [36]. Additionally, figure 5.17(a) shows the spectral content of the incident pulse as well as responses from a single 1 m $\times$ 0.25 m cavity given different dielectric fillings. In the

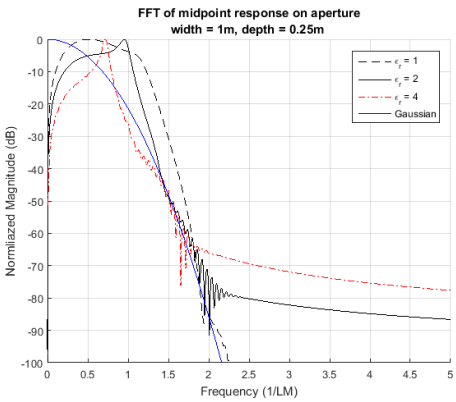

(a) Normalized fast Fourier transform of aperture fields sampled at midpoint.

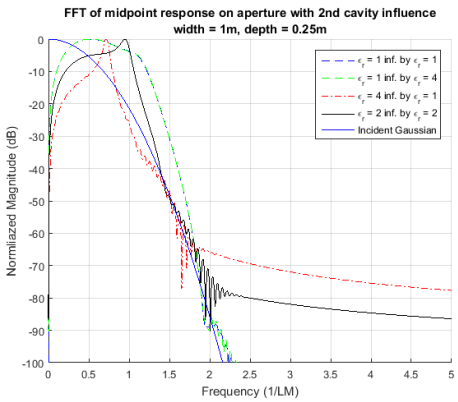

(b) Normalized fast Fourier transform of coupled aperture fields sampled at midpoint.

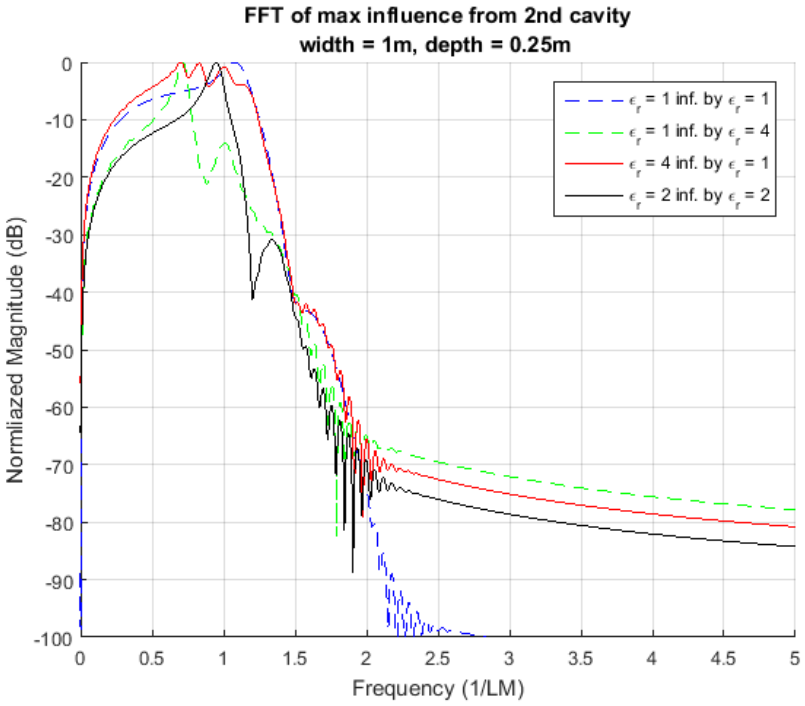

(c) Normalized fast Fourier transform of influence from 2nd cavity.

Figure 5.17: Spectral content of one cavity and two cavity solutions.

filled cavities, there is a visible spike in the plot; this corresponds to the primary resconant frequency. Note the peak at $1/LM$ for $\varepsilon_r = 2$, this is consistent with the observed resonance with time between peaks of approximately 1 light-meter. This response is expected, as it

takes the primary peak 1 light meter to propagate 0.25 m down and 0.25 m back in a medium of this type. The plotting tools and interpretation of the FFT were greatly informed by discussions with Mr. Hirsch Chizever.

Figure 5.17(b) shows the response from the same cavity as in 5.17(a), but with the influence of a second cavity with separation of only 0.05 m. Even at this proximity, the effect of the coupling is dominated by the primary effects of the scattering from the cavity. However, when the single-cavity response is subtracted from the two-cavity response, the influence of the second cavity may be analyzed separately. The spectral content of the influence is shown in figure 5.17(c).

Figure 5.18 shows the field strength at the aperture midpoint for a deep cavity (5m). In this experiment, all three cavities were filled with non-magnetic dielectric material having permittivity $\varepsilon_r = 2\varepsilon_0$. Cavities 1 and 3 were shallow, having depth of 0.25 m and the center cavity, cavity 2 was deep, having depth of 5 m. Notice that influence from the cross-talk is graphically imperceptible as would be expected due to the relative strength of the interaction compared to the strength of the primary response. To better visualize the influence of the additional cavities and the dependence of influence strength on distance between cavities, the one-cavity solution was subtracted from the three cavity solutions as shown in figure 5.19.

Additionally, exterior fields along the semi-circle of radius 3 m were sampled for different cavity spacings. Figures 5.20 and 5.21 show the observed field strength for angles of $\pi/2$ and $\pi/4$, respectively. The strength of the observed fields depends primarily on proximity of the cavity aperture to the sampling point.

To further examine the interaction between cavities, exterior fields were computed for one cavity at a time, and the three-cavity problem. We use u^s to refer to the multiple-cavity

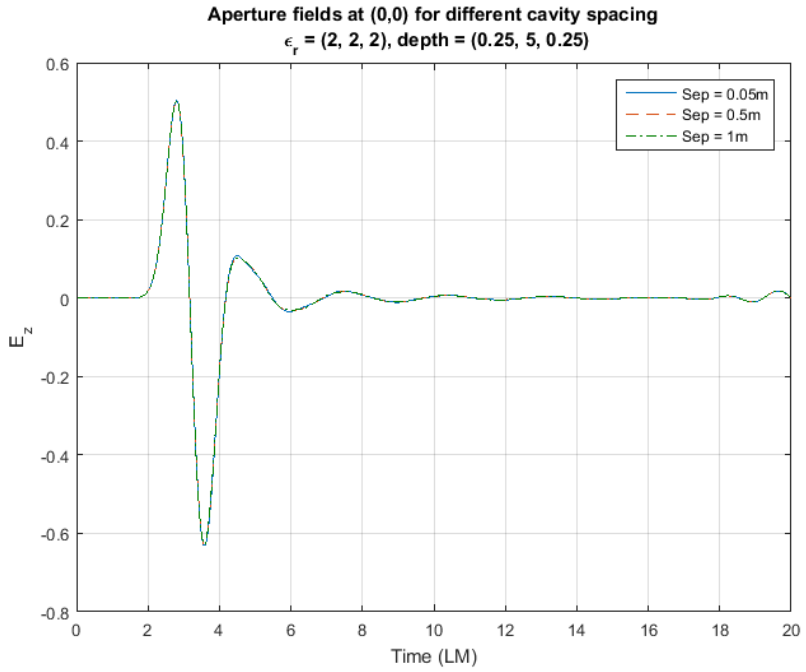

Figure 5.18: Aperture fields at midpoint of deep (5m) cavity.

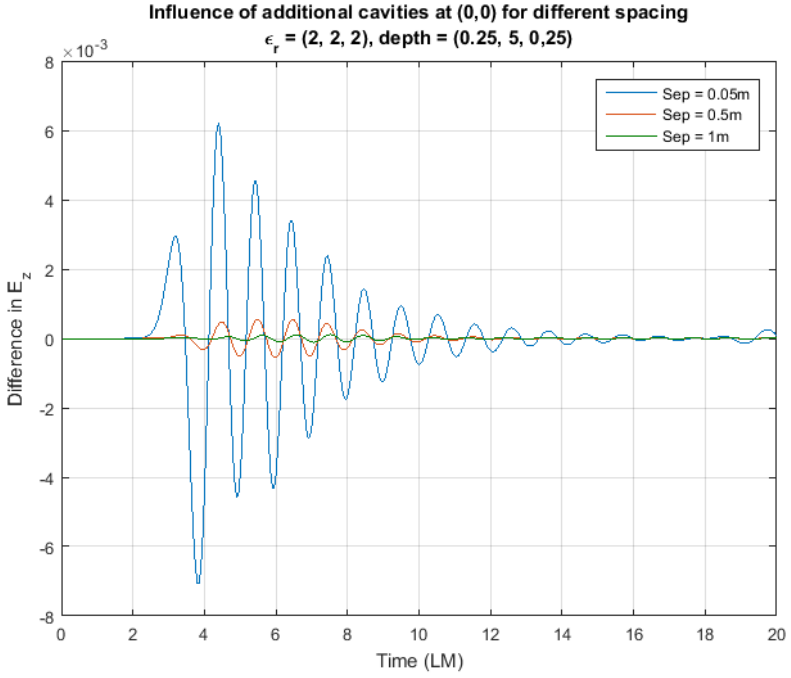

Figure 5.19: Difference in aperture fields for deep (5m) cavity.

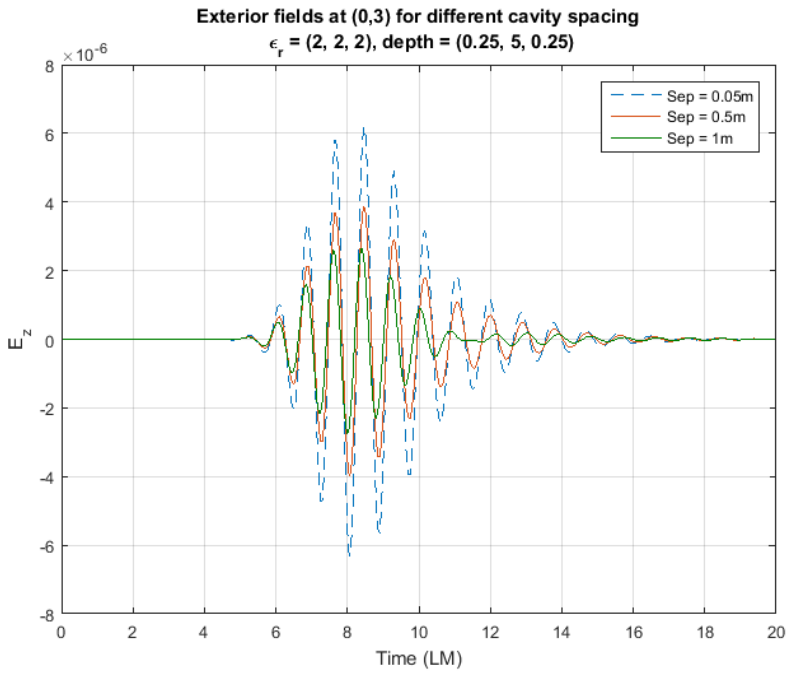

Figure 5.20: Exterior fields at $\theta = \pi/2$.

solution for the scattered field and $u^s_{\Omega_i}$ to denote the scattered field computed for just one cavity defined by Ω_i embedded in the ground plane. The linear construction of the solution is:

$$\hat{u}^s = u^s_{\Omega_1} + u^s_{\Omega_2} + u^s_{\Omega_3}.$$

We consider the question, how well does $\hat{u}^s$ approximate u^s? Figure 5.22 shows how closely the fields might be approximated by using a linear sum of single-cavity solutions. As expected, primary effects were nearly additive, because the magnitude of the interaction is small compared to the cavity response. However, late time fields are not well approximated. Figure 5.23 illustrates the difference between the linear sum and the three cavity solution which captures interactions between cavities. Note that from 6 sec to 11 sec, the difference is a small proportion (approx. 3%) of the solution. However, at later times, the interaction between cavities accounts for a growing proportion of the observed fields. For example,

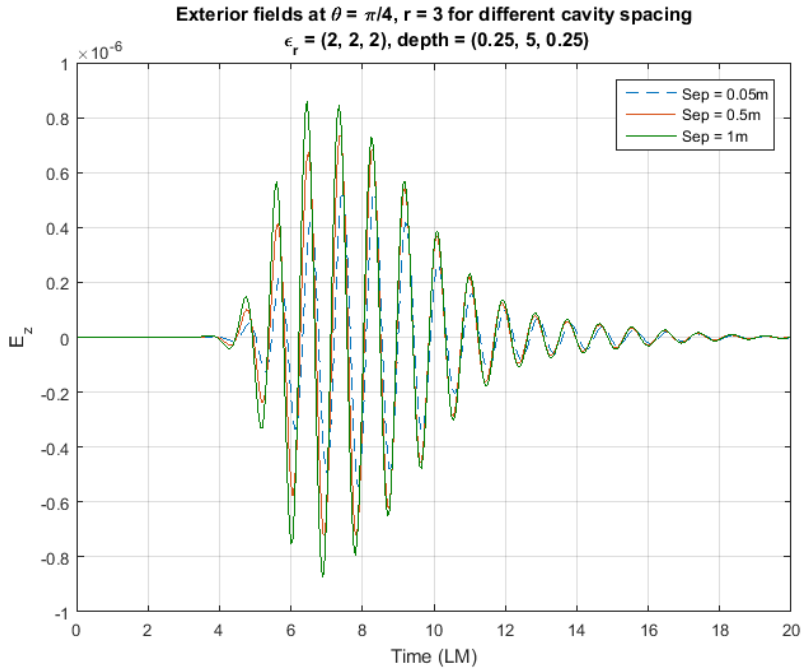

Figure 5.21: Exterior fields at $\theta = \pi/4$.

at time = 14.65 LM, the error in the linear sum is approximately 10% and at time = 19.35 LM, the error grows to nearly 120%.

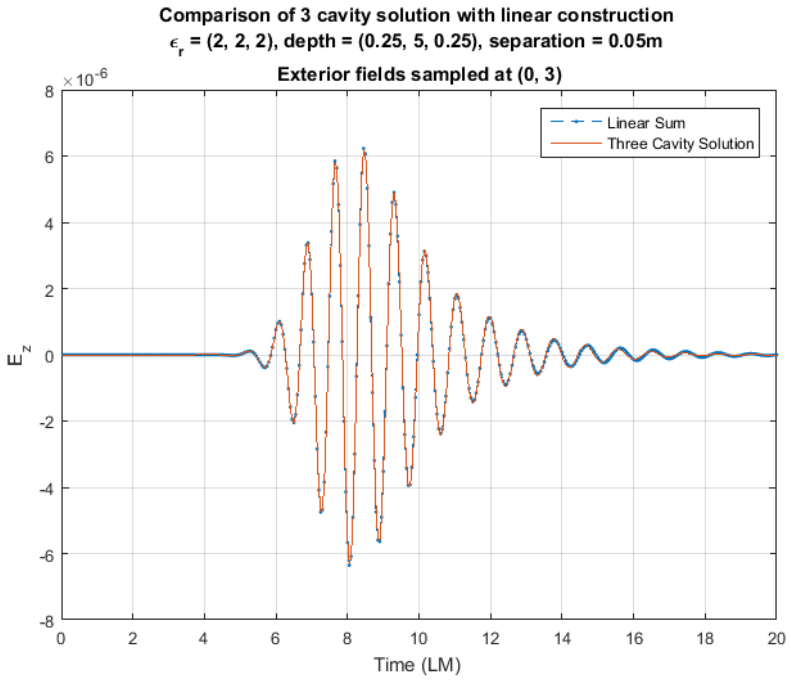

Figure 5.22: Comparison of exterior fields at $\theta = \pi/2$.

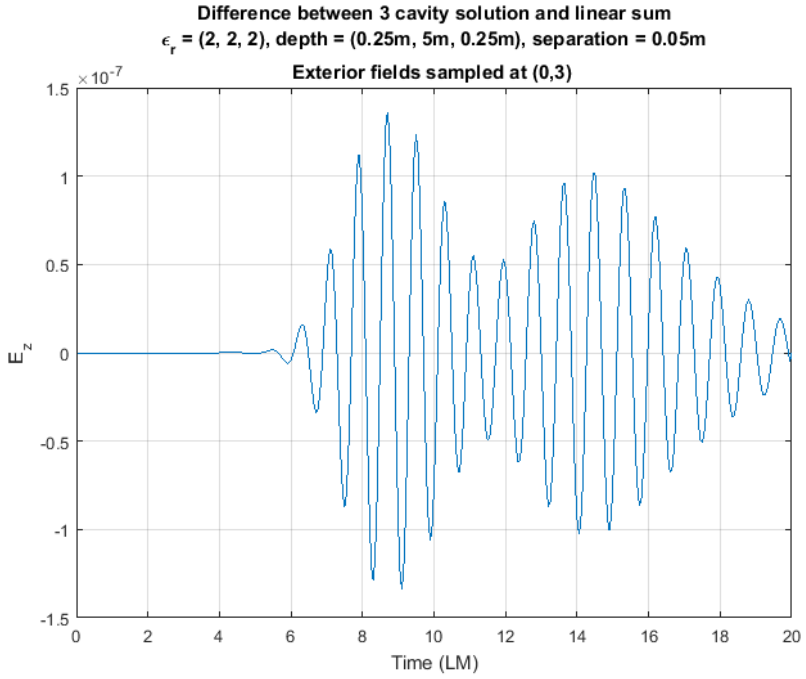

Figure 5.23: Difference in exterior fields at $\theta = \pi/2$.

VI. Conclusions and Future Work

In this work, we have shown that the discretized multiple-cavity TM^z problem has a well-posed variational formulation at each time step, constructed a stable numerical model, and compared results from different number, spacing, and depth of cavities. The well-posedness of the variational formulation was demonstrated by proving that the requirements for the Lax-Milgram theorem were satisfied, therefore guaranteeing a unique solution in the chosen solution space. The numerical model utilized the FE-BI method to solve for interior and exterior fields at each discretized time step. The implicit Newmark method was applied to step through time to ensure stability of solutions. Finally, various numerical tests were conducted to compare the influence of coupling between cavities. In doing these tests, multiple-cavity solutions were compared to single-cavity solutions and linear constructions thereof to demonstrate the relative strength of the cross-talk and its effect on the full-field solution.

The scope of this work was limited to TM^z polarization and a PEC ground plane. Future work should broaden applications to include impedence ground planes, and expand solutions to TE^z polarity. Furthermore, additional methods should be developed to enhance the numerical efficiency of the computational routine, as well as apply the model to shapes other than rectangles.

6.1 Conclusions

In conclusion, I have presented a well-posed numerical method for simulating the scattered field from a TM^z incident field on a cavity embedded in a PEC ground plane. The problem was first discretized with the Newmark method, which transformed the transient wave equation into a forced 2-D Helmholtz equation at each time step.

After discretizing the problem, I developed the boundary integral method and Green's function for analytically describing the exterior scattered field as a function of the aperture fields and prior time step data. The Green's function and boundary integrals were consistent with previously published results, with expected differences due to their application to multiple scatterers.

Next, the boundary integral form of the scattered field was used to develop aperture boundary conditions for the multiple-cavity interior problem. The partial derivative of the scattered field normal to the apertures was used to enforce continuity conditions across the transparent boundary on the aperture. Thus, I developed the DtN operator to couple the exterior and interior solutions. This DtN operator was similar in form to existing examples, but different in that it captured directly the coupling between apertures and enforced this coupling on the interior field solutions.

Once the aperture boundary condition was defined, at each time step, the interior problem was posed as a forced Helmholtz equation with boundary data. This boundary value problem was transformed into a variational formulation in order to solve using the FEM. The principle contribution in this work is to show that this multiple-cavity variational formulation is well-posed. This proof utilized the Lax-Milgram theorem and was presented for the two-cavity case as well as the multiple ($k > 2$) cavity case.

Having proved that the variational formulation is well-posed, focus then shifted to the development and implementation of the numerical model. The Newmark method when applied to discretize the problem, generated the forcing data for the Helmholtz problem. For each step in time, the boundary integral was approximated to compute exterior field data. The DtN operator was approximated as a matrix multiplication to accelerate computation of the boundary data. Finally, FEM was used at each time step to solve for interior and aperture fields. Aperture fields were then used an inputs for

the boundary integral to generate exterior fields, and in this way the computational model stepped through time.

Numerical tests were conducted using a continuous incident field. These tests were useful for validating computed results and characterizing the maximum difference between single-cavity and multiple-cavity solutons. The difference, described as influence between the cavities, was shown to be very sensitive to the distance separating the cavities from one another. This information is valuable, because for sufficiently distant cavities, one may justify simply adding together scattered fields found from single-cavity solvers, as the influence between distant cavities may be negligible in the overall solution. Thus, this analysis provides a basis for determining criteria for when simplifying assumptions of additivity can be made.

Additionally, numerical tests were conducted using a Gaussian incident wave. These tests are the primary application for which the transient solver for multiple cavities was designed. Existing time-harmonic solvers are insufficient for modeling Gaussing waves, since they must be run at a discrete set of frequencies, generally selected from the Fourier transform of the Gaussian wave. By using this method, multiple frequencies are modeled at the same time, providing a more complete picture of the scattering from multiple cavities.

For the Gaussian tests, I examined differences between single-cavity and multiple-cavilty solutions on aperture fields. As with continuous tests, the magnitude of the influence was shown to be dependent on distance separating the cavities. Additionally, the transient nature of the solutions was shown in the additional time-lag of the difference fields caused by increased distance between cavities. Furthermore, exterior fields were modeled along a semi-circle of radius 3 m centered at the origin. These data were compared to explicitly demonstrate the breakdown in simply adding together single-cavity solutions to approximate the mutliple-cavity response. Specifically, the influence of the cross-talk

dominated the later-time scattered fields, where single-cavity fields had already diminished below the strength of the echoes from coupled cavities.

6.2 Future Work

Future work should continue to improve the numerical efficiency of the method, broaden applications to include impedence ground planes, and expand solutions to TE^z polarity.

One way to improve numerical efficience of the FE-BI solver applied to a multiple-cavity finite element matrix would be to apply specific matrix methods to reduce the computational cost of solving the multiple-cavity matrix which grows in a block-like manner as additional cavities are added. For large problems, iterative solvers may be applied to decrease the overall complexity of inverting the FEM matrix. Another improvement would be to use an adaptive mesh to improve accuracy of solutions without requiring a vastly greater number of nodes.

Improvements to numerical accuracy may also be made by using higher-order polynomial basis functions which will reduce the overall error from projecting the solution into the function space spanned by finite-element basis functions. Additional tests may be conducted to determine the optimal selection of parameters β and γ for the Newmark discretization.

In terms of broadening applications, the first step might be to extend results to the TE^z polarity. This will provide a method for modeling scattering returns from a far greater set of incident fields, because in free-space, all incident fields may be decomposed into a linear combination of TE^z and TM^z components. By modelling full-fields, more complex media may be used to fill cavities and their effects on the total scattered field could be better understood.

Additionally, three-dimensional cavities may be modeled using similar methods. These models would allow for even greater flexibility in cavity geometry and filler media.

The FE-BI method was applied to transient scattering from a cavity in an impedence ground plane in [7]. This method may be adapted to the multiple cavity problem to provide greater flexibility in modeling real-world scattering problems which do not have true-PEC materials.

In all, there is no shortage of potential applications for modeling multiple cavities. Each variation is sufficiently complex that it would be a worthwile endeavor and would contribute to the quickly growing body of research in the field of CEM.

Appendix A: Finite Element Matrix Construction

Using a triangular mesh and finite elements defined on each triangle, the variational formulation (3.52) can be discretized to compute a solution. Define a finite element space $\mathcal{T}^N$ with basis functions $\{\phi_i\}_{i=1}^N$ such that for any $f \in \mathcal{T}^N$, $f = \sum_1^N c_i\phi_i$. Define the projection operator $P_{\mathcal{T}^N}$ such that

$$P_{\mathcal{T}^N}(g) = v \iff \|g - v\|_{\mathbb{H}^1(\mathbf{\Omega})} = \min_{w\in\mathcal{T}^N} \|g - w\|_{\mathbb{H}^1(\mathbf{\Omega})}.$$

Let the solution $u \in \mathbb{H}^1(\mathbf{\Omega})$ be projected onto our finite element space $\mathcal{T}^{\mathcal{N}}$ by projection operator $P_{\mathcal{T}^N}$ giving

$$u^n(x, y) = P_{\mathcal{T}^N}[u(x, y, t_n)].$$

Similarly,

$$u(x, y, t_n) = u^n(x, y) + \epsilon(x, y), \quad \epsilon \in [\mathcal{T}^N]^\perp.$$

Then our the variational formulation $a(u, v) = b(v)$ can be discretized in the following way. Let $v = \sum_{i=1}^N \phi_i$ and $u^n = \sum_{i=1}^N c_i\phi_i$.

$$\begin{aligned}
(\nabla u^n, \nabla v)_{\Omega_1} &= \int_{\Omega_1} \left(\nabla \sum_{i=1}^N c_i\phi_i\right) \cdot \left(\nabla \sum_{j=1}^N \phi_j\right) d\vec{r}, \\
&= \sum_{i=1}^N c_i \int_{\Omega_1} (\nabla\phi_i) \cdot \left(\nabla \sum_{j=1}^N \phi_j\right) d\vec{r}, \\
&= \sum_{i=1}^N c_i \sum_{j=1}^N \int_{\Omega_1} \nabla\phi_i \cdot \nabla\phi_j \, d\vec{r}.
\end{aligned}$$

$$\begin{aligned}
\langle u^n, v\rangle_{\Omega_1} &= \int_{\Omega_1} \left(\sum_{i=1}^N c_i\phi_i\right)\left(\sum_{j=1}^N \phi_j\right) d\vec{r}, \\
&= \sum_{i=1}^N c_i \int_{\Omega_1} \phi_i \left(\sum_{j=1}^N \phi_j\right) d\vec{r}, \\
&= \sum_{i=1}^N c_i \sum_{j=1}^N \int_{\Omega_1} \phi_i\phi_j \, d\vec{r}.
\end{aligned}$$

For the aperture elements, a subset of the basis functions are non-zero. These functions will be denoted $\{\phi_i^\Gamma\}_{i=1}^{N_\Gamma}$.

$$g = \sum_{i=1}^{N_{\Gamma_1}} c_i \phi_i^{\Gamma_1} + \sum_{m=1}^{N_{\Gamma_2}} c_m \phi_m^{\Gamma_2}$$

$$\langle g, v \rangle_{\Gamma_1 \cup \Gamma_2} = \int_{\Gamma_1} \left(\sum_{i=1}^{N_{\Gamma_1}} c_i \phi_i^{\Gamma_1} \right) \left(\sum_{j=1}^{N_{\Gamma_1}} \phi_j^{\Gamma_1} \right) dx + \int_{\Gamma_2} \left(\sum_{n=1}^{N_{\Gamma_2}} c_n \phi_n^{\Gamma_2} \right) \left(\sum_{m=1}^{N_{\Gamma_2}} \phi_m^{\Gamma_2} \right) dx,$$

Using this aperture inner product, we replace g with $T_\alpha g$ to see the form of the final term in the bilinear operator $a(u, v)$ in (3.51).

In this implementation, linear nodal basis functions are defined over the triangulations in Ω_1 and Ω_2. Assuming node map of the form:

$$[\text{Tri}] = \begin{bmatrix} p_{1,1} & p_{1,2} & p_{1,3} \\ p_{2,1} & p_{2,2} & p_{2,3} \\ \vdots & \vdots & \vdots \\ p_{N_{Tri},1} & p_{N_{Tri},2} & p_{N_{Tri},3} \end{bmatrix},$$

the i^{th} row contains the global node references for the three vertices of the i^{th} triangular element, Tri^i, arranged in a counter-clockwise manner. The basis functions for a given triangular element Tri^e will be defined such that

$$\phi^e(x, y) = \sum_{j=1}^{3} \psi_j^e,$$

This common basis set is well-described in [13, 23].

$$\psi_i^e(x, y) = \begin{cases} \dfrac{1}{2\Delta^e}(a_i^e + b_i^e x + c_i^e y) & (x, y) \in \text{Tri}^e, \\ 0 & \text{otherwise.} \end{cases}, \quad i = 1, 2, 3$$

Coefficients are given by the following equations:

$$\begin{aligned} a_1^e &= x_2^e y_3^e - x_3^e y_2^e & b_1^e &= y_2^e - y_3^e & c_1^e &= x_3^e - x_2^e \\ a_2^e &= x_3^e y_1^e - x_1^e y_3^e & b_2^e &= y_3^e - y_1^e & c_2^e &= x_1^e - x_3^e \\ a_3^e &= x_1^e y_2^e - x_2^e y_1^e & b_3^e &= y_1^e - y_2^e & c_3^e &= x_2^e - x_1^e \end{aligned}.$$

Δ^e represents the triangular area of the e^{th} element given by

$$\Delta^e = \frac{1}{2}\begin{vmatrix} 1 & x_1^e & y_1^e \\ 1 & x_2^e & y_2^e \\ 1 & x_3^e & y_3^e \end{vmatrix} = \frac{1}{2}(b_1^e c_2^e - b_2^e c_1^e).$$

Using these basis elements, the inner product $(\nabla u, \nabla v)_\Omega$ can be written as a summation of the form

$$\sum_e \sum_{i=1}^{3} \sum_{j=1}^{3} u_i \int_{Tri^e} \nabla\psi_i^e \cdot \nabla\psi_j^e \, dA = \sum_e \sum_{i=1}^{3} \sum_{j=1}^{3} u_i^e \frac{1}{4\Delta^e}(b_i^e b_j^e + c_i^e c_j^e).$$

This has an equivalent matrix representation of $[K^\Delta][u^\Delta]$ where, $[K^\Delta]$ is a $3N_{TRI} \times 3N_{TRI}$ matrix and $[u^\Delta]$ is a $3N_{TRI} \times 1$ matrix with components

$$K^\Delta_{[3(e-1)+i,\,3(e-1)+j]} = \frac{1}{4\Delta^e}(b_i^e b_j^e + c_i^e c_j^e), \quad u^\Delta_{[3(e-1)+i]} = u_i^e = u(x_i^e, y_i^e).$$

Similarly, the inner product $(u, v)_\Omega$ can be written as

$$\sum_e \sum_{i=1}^{3} \sum_{j=1}^{3} u_i \int_{Tri^e} \psi_i^e \psi_j^e \, dA = \sum_e \sum_{i=1}^{3} \sum_{j=1}^{3} u_i^e \frac{\Delta^e}{12}(1 + \delta_{ij}),$$

where δ_{ij} represents the Kronecker delta. This also can be written as a matrix multiplication of the form $[D^\Delta][u^\Delta]$ with $[M^\Delta]$, a $3N_{TRI} \times 3N_{TRI}$ matrix, and $[u]$ as before.

$$M^\Delta_{[3(e-1)+i,\,3(e-1)+j]} = \frac{\Delta^e}{12}(1 + \delta_{ij}).$$

The aperture functions may also be approximated with linear basis functions. We define linear elements of Γ, Γ^e, such that $\Gamma = \bigcup_e \Gamma^e$, and associated basis functions,

$$\phi^{\Gamma^e}(x) = \sum_{j=1}^{2} \psi_j^{\Gamma^e}(x).$$

$$\psi_1^{\Gamma^e} = \begin{cases} \dfrac{x_2^{\Gamma_e} - x}{x_2^{\Gamma_e} - x_1^{\Gamma_e}} & x \in \Gamma^e \\ 0 & \text{otherwise.} \end{cases} \qquad \psi_2^{\Gamma^e} = \begin{cases} \dfrac{x - x_1^{\Gamma_e}}{x_2^{\Gamma_e} - x_1^{\Gamma_e}} & x \in \Gamma^e \\ 0 & \text{otherwise.} \end{cases}$$

Then the aperture inner product, $\langle u, v \rangle_\Gamma$, may be seen as the discrete sum

$$\sum_{\Gamma^e} \sum_{i=1}^{2} \sum_{j=1}^{2} u_i^{\Gamma_e} \int_{\Gamma^e} \psi_i^{\Gamma_e} \psi_j^{\Gamma_e} \, dx = \sum_{\Gamma^e} \sum_{i=1}^{2} \sum_{j=1}^{2} u_i^{\Gamma_e} \frac{x_2^{\Gamma_e} - x_1^{\Gamma_e}}{6} (1 + \delta_{ij})$$

Using triangular elements, the entire surface Γ will be covered by those elements which have two nodes on the aperture. Thus, by appropriately matching node and element indices, this inner product may be written as a sparse matrix $[G^\Delta]$, with dimensions matching those of $[K^\Delta]$ and $[M^\Delta]$. The matrices $[K^\Delta]$, $[M^\Delta]$, and $[G^\Delta]$ are all $3N_{TRI} \times 3N_{TRI}$ in dimension, which is much larger than the actual number of points in the grid. Finally, by enforcing continuity requirements at the matching grid points, these matrices may be reduced to the number of individual points where we aim to know the function value. For example, a nine-point grid with x points $[-1, 0, 1]$ and y points $[-2, -1, 0]$ would generate eight triangular elements as shown in Figure A.1, with nodes shown in Table A.1.

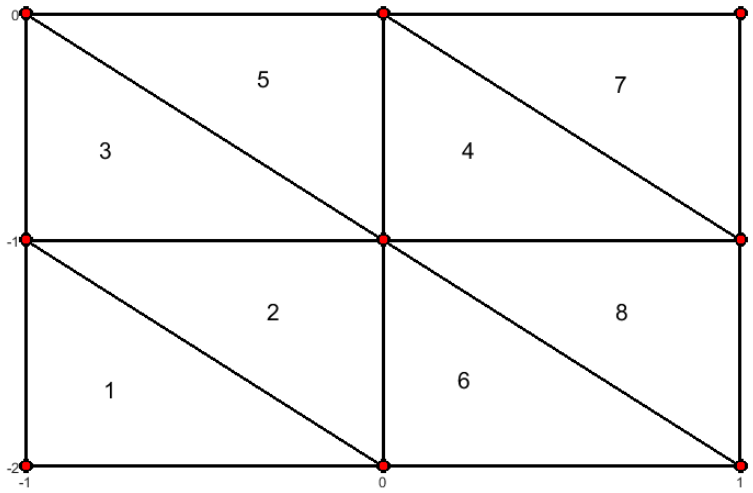

Figure A.1: Delaunay Triangulation

Building matrices in the manner described above to generate $[K^\Delta]$, $[M^\Delta]$, and $[G^\Delta]$, would yield dimension 24×24 matrices. An example matrix is shown below for $[M^\Delta]$. Note the duplication of u values in $[u^\Delta]$.

Table A.1: Example Triangulation

e	$(x,y)_1^e$	$(x,y)_2^e$	$(x,y)_3^e$
1	(-1, -2)	(0, -2)	(-1, -1)
2	(0, -2)	(0, -1)	(-1, -1)
3	(-1, -1)	(0, -1)	(-1, 0)
4	(0, -1)	(1, -1)	(0, 0)
5	(-1, 0)	(0, -1)	(0, 0)
6	(0, -2)	(1, -2)	(0, -1)
7	(0, 0)	(1, -1)	(1, 0)
8	(0, -1)	(1, -2)	(1, -1)

$$[M^{\Delta}][u^{\Delta}] = \begin{bmatrix} \frac{\Delta^1}{6} & \frac{\Delta^1}{12} & \frac{\Delta^1}{12} & 0 & 0 & 0 & \cdots & 0 & 0 & 0 \\ \frac{\Delta^1}{12} & \frac{\Delta^1}{6} & \frac{\Delta^1}{12} & 0 & 0 & 0 & \cdots & 0 & 0 & 0 \\ \frac{\Delta^1}{12} & \frac{\Delta^1}{12} & \frac{\Delta^1}{6} & 0 & 0 & 0 & \cdots & 0 & 0 & 0 \\ 0 & 0 & 0 & \frac{\Delta^2}{6} & \frac{\Delta^2}{12} & \frac{\Delta^2}{12} & \cdots & 0 & 0 & 0 \\ 0 & 0 & 0 & \frac{\Delta^2}{12} & \frac{\Delta^2}{6} & \frac{\Delta^2}{12} & \cdots & 0 & 0 & 0 \\ 0 & 0 & 0 & \frac{\Delta^2}{12} & \frac{\Delta^2}{12} & \frac{\Delta^2}{6} & \cdots & 0 & 0 & 0 \\ & \vdots & & & \vdots & & \ddots & & \vdots & \\ 0 & 0 & 0 & 0 & 0 & 0 & \cdots & \frac{\Delta^8}{6} & \frac{\Delta^8}{12} & \frac{\Delta^8}{12} \\ 0 & 0 & 0 & 0 & 0 & 0 & \cdots & \frac{\Delta^8}{12} & \frac{\Delta^8}{6} & \frac{\Delta^8}{12} \\ 0 & 0 & 0 & 0 & 0 & 0 & \cdots & \frac{\Delta^8}{12} & \frac{\Delta^8}{12} & \frac{\Delta^8}{6} \end{bmatrix} \begin{bmatrix} u(-1,-2) \\ u(0,-2) \\ u(-1,-1) \\ u(0,-2) \\ u(0,-1) \\ u(-1,-1) \\ \vdots \\ u(0,-1) \\ u(1,-2) \\ u(1,-1) \end{bmatrix}$$

However, by enforcing the continuity requirements and noting that in this case, the areas, Δ^e of each triangle are equal, this is reduced to

$$[M][u] = \begin{bmatrix} \frac{\Delta}{6} & \frac{\Delta}{12} & 0 & \frac{\Delta}{12} & 0 & 0 & 0 & 0 & 0 \\ \frac{\Delta}{12} & \frac{\Delta}{2} & \frac{\Delta}{12} & \frac{\Delta}{6} & \frac{\Delta}{6} & 0 & 0 & 0 & 0 \\ 0 & \frac{\Delta}{12} & \frac{\Delta}{3} & 0 & \frac{\Delta}{6} & \frac{\Delta}{12} & 0 & 0 & 0 \\ \frac{\Delta}{12} & \frac{\Delta}{6} & 0 & \frac{\Delta}{2} & \frac{\Delta}{6} & 0 & \frac{\Delta}{12} & 0 & 0 \\ 0 & \frac{\Delta}{6} & \frac{\Delta}{6} & \frac{\Delta}{6} & \Delta & \frac{\Delta}{6} & \frac{\Delta}{6} & \frac{\Delta}{6} & 0 \\ 0 & 0 & \frac{\Delta}{12} & 0 & \frac{\Delta}{6} & \frac{\Delta}{2} & 0 & \frac{\Delta}{6} & \frac{\Delta}{12} \\ 0 & 0 & 0 & \frac{\Delta}{12} & \frac{\Delta}{6} & 0 & \frac{\Delta}{3} & \frac{\Delta}{12} & 0 \\ 0 & 0 & 0 & 0 & \frac{\Delta}{6} & \frac{\Delta}{6} & \frac{\Delta}{12} & \frac{\Delta}{2} & \frac{\Delta}{12} \\ 0 & 0 & 0 & 0 & 0 & \frac{\Delta}{12} & 0 & \frac{\Delta}{12} & \frac{\Delta}{6} \end{bmatrix} \begin{bmatrix} u(-1,-2) \\ u(-1,-1) \\ u(-1,0) \\ u(0,-2) \\ u(0,-1) \\ u(0,0) \\ u(1,-2) \\ u(1,-1) \\ u(1,0) \end{bmatrix}$$

Where now, $[M]$ is a 9×9 and $[u]$ is a 9×1 matrix. The same reduction method may be applied to $[K^{\Delta}]$ and $[G^{\Delta}]$ to create the right-sized matrices constrained by continuity at the nodes.

Appendix B: MATLAB Code

This appendix includes the primary MATLAB script used to run the three-cavity simulations, as well as a representative sample of subroutines used within the main script.

B.1 Three Cavity Main Script

This is the primary script used to run the simulations.

```
%function ThreeCav(w1, w2, w3, d1, d2, d3, sep1, sep2, onoff, EPS)
%ThreeCav is an extension of the MultiScat function for 3 cavities.
%plane waves scaled to lambda = 1 meter
%time scaled to unit = light-meter in free space
w1 = 1; w2 = 1; w3 = 1; d1 = .25; d2 = .25; d3= .25; sep1 = .05; sep2 = .05;
onoff = [ 1, 1, 1 ]; % 1 is on, 0 is off, [ cav1, cav2, cav3 ]
EPS = [4, 1, 4];
%% Step one - Define the geometry

isgauss =1 %either 1 for gaussian impulse or 0 for continuous wave.
r = 1/20;    %grid spacing
h = r;      %time step
%computational domain limits in x
x = -(w1+w2+w3+sep1+sep2+2)/2:r:(w1+w2+w3+sep1+sep2+2)/2;
y = 0:r:3.2; %computational domain limit in +y
Tfinal = 20  % end time

%% Define points for geometry.
a1 = -w2/2-sep1-w1; %left(x) of cav 1
b1 = -w2/2-sep1;  %right(x) of cav 1

a2 = -w2/2;   %left(x) of cav 2
```

```
b2 = w2/2;   %right(x) of cav 2

a3 = w2/2+sep1;   %left(x) of cav 3
b3 = w2/2+sep1+w3;   %right(x) of cav 3

y1L = -d1;  %bottom(y) of cav 1
y2L = -d2;  %bottom(y) of cav 2
y3L = -d3;  %bottom(y) of cav 3

y1 = 0:-r:y1L;  %y values in cav 1
y2 = 0:-r:y2L;  %y values in cav 2
y3 = 0:-r:y3L;  %y values in cav 3

%in case grid spacing doesn't perfectly match end points:
[~,x1]=min(abs(a1 - x));  %index in x of left side of cav1
[~,x2]=min(abs(b1 - x));  %index in x of right side of cav1
[~,x3]=min(abs(a2 - x));  %index in x of left side of cav2
[~,x4]=min(abs(b2 - x));  %index in x of right side of cav2
[~,x5]=min(abs(a3 - x));  %index in x of left side of cav3
[~,x6]=min(abs(b3 - x));  %index in x of right side of cav3
[~,ymin1]=min(abs(y1L - y1));  %id for lowest y in cav1.
[~,ymin2]=min(abs(y2L - y2));  %id for lowest y in cav2.
[~,ymin3]=min(abs(y3L - y3));  %id for lowest y in cav3.
%define cavity meshes
[xin1,yin1] = meshgrid( x(x1:x2), y1);
[xin2,yin2] = meshgrid( x(x3:x4), y2);
[xin3,yin3] = meshgrid( x(x5:x6), y3);
[xout,yout] = meshgrid(x,y);
[LY,LX] = size(xout);
Ny1 = length(yin1(:,1));
Ny2 = length(yin2(:,1));
Ny3 = length(yin3(:,1));
```

```
%% establish test points for exterior scattered fields
D = 1.5; % parameter for ellipse distance from cavities
%rad = max(abs([a1,b2]))+D; %general sizing
rad = 3;
%rady = D; %general sizing
rady = 1.5;
angle = pi/180*(0:180);
extpoints= zeros(181,4);
%ellipse
    extpoints2(:,:)=[rad*cos(angle)', rady*sin(angle)',angle',...
        sqrt((rad*cos(angle)').^2 +(rady*sin(angle)').^2) ];
%circle
    extpoints(:,:)=[rad*cos(angle)', rad*sin(angle)',angle',rad*ones(181,1) ];
extpoints2(end,2)= 0; %hard code for error correction;
extpoints(end,2)= 0; %hard code for error correction;
%% build triangulations
Tri1 = delaunay(xin1,yin1);
Tri2 = delaunay(xin2, yin2);
Tri3 = delaunay(xin3, yin3);
% Get length of Tri vector (#of triangles)
[L1,~] = size(Tri1);
[L2, ~] = size(Tri2);
[L3, ~] = size(Tri3);

%% Set Fill Material Permittivity
% matrix setup allows for inhomogeneous dielectric filling
 epsr1T =( epsr1(Tri1(:,1))+epsr1(Tri1(:,2))+epsr1(Tri1(:,3)))/3;
 epsr1 = (EPS(1))*ones(size(xin1));
 epsr2 = (EPS(2)) * ones(size(xin2));
 epsr2T =( epsr2(Tri2(:,1))+epsr2(Tri2(:,2))+epsr2(Tri2(:,3)))/3;
  epsr3 = (EPS(3)) * ones(size(xin3));
```

```
 epsr3T =( epsr3(Tri3(:,1))+epsr3(Tri3(:,2))+epsr3(Tri3(:,3)))/3;
%% Establish linear basis vectors
%Refer to Jin, 2014, page 83-84

%phi has form 1/(2*area) (a+bx+cy)
aele1 = [xin1(Tri1(:,2)).*yin1(Tri1(:,3))-xin1(Tri1(:,3)).*yin1(Tri1(:,2)),...
            xin1(Tri1(:,3)).*yin1(Tri1(:,1))-xin1(Tri1(:,1)).*yin1(Tri1(:,3)),...
            xin1(Tri1(:,1)).*yin1(Tri1(:,2))-xin1(Tri1(:,2)).*yin1(Tri1(:,1))];

bele1 = [yin1(Tri1(:,2))-yin1(Tri1(:,3)),...
            yin1(Tri1(:,3))-yin1(Tri1(:,1)),...
            yin1(Tri1(:,1))-yin1(Tri1(:,2))];

cele1 = [xin1(Tri1(:,3))-xin1(Tri1(:,2)),...
            xin1(Tri1(:,1))-xin1(Tri1(:,3)),...
            xin1(Tri1(:,2))-xin1(Tri1(:,1))];

area1 = 1/2*(bele1(:,1).*cele1(:,2)-bele1(:,2).*cele1(:,1));
center1 = [(xin1(Tri1(:,1))+xin1(Tri1(:,2))+xin1(Tri1(:,3)))/3,...
        (yin1(Tri1(:,1))+yin1(Tri1(:,2))+yin1(Tri1(:,3)))/3];

%phi has form a+bx+cy
aele2 = [xin2(Tri2(:,2)).*yin2(Tri2(:,3))-xin2(Tri2(:,3)).*yin2(Tri2(:,2)),...
            xin2(Tri2(:,3)).*yin2(Tri2(:,1))-xin2(Tri2(:,1)).*yin2(Tri2(:,3)),...
            xin2(Tri2(:,1)).*yin2(Tri2(:,2))-xin2(Tri2(:,2)).*yin2(Tri2(:,1))];

bele2 = [yin2(Tri2(:,2))-yin2(Tri2(:,3)),...
            yin2(Tri2(:,3))-yin2(Tri2(:,1)),...
            yin2(Tri2(:,1))-yin2(Tri2(:,2))];

cele2 = [xin2(Tri2(:,3))-xin2(Tri2(:,2)),...
            xin2(Tri2(:,1))-xin2(Tri2(:,3)),...
```

```
            xin2(Tri2(:,2))-xin2(Tri2(:,1))];

area2 = 1/2*(bele2(:,1).*cele2(:,2)-bele2(:,2).*cele2(:,1));
center2 = [(xin2(Tri2(:,1))+xin2(Tri2(:,2))+xin2(Tri2(:,3)))/3,...
        (yin2(Tri2(:,1))+yin2(Tri2(:,2))+yin2(Tri2(:,3)))/3];

%phi has form a+bx+cy
aele3 = [xin3(Tri3(:,2)).*yin3(Tri3(:,3))-xin3(Tri3(:,3)).*yin3(Tri3(:,2)),...
            xin3(Tri3(:,3)).*yin3(Tri3(:,1))-xin3(Tri3(:,1)).*yin3(Tri3(:,3)),...
            xin3(Tri3(:,1)).*yin3(Tri3(:,2))-xin3(Tri3(:,2)).*yin3(Tri3(:,1))];

bele3 = [yin3(Tri3(:,2))-yin3(Tri3(:,3)),...
            yin3(Tri3(:,3))-yin3(Tri3(:,1)),...
            yin3(Tri3(:,1))-yin3(Tri3(:,2))];

cele3 = [xin3(Tri3(:,3))-xin3(Tri3(:,2)),...
            xin3(Tri3(:,1))-xin3(Tri3(:,3)),...
            xin3(Tri3(:,2))-xin3(Tri3(:,1))];

area3 = 1/2*(bele3(:,1).*cele3(:,2)-bele3(:,2).*cele3(:,1));
center3 = [(xin3(Tri3(:,1))+xin3(Tri3(:,2))+xin3(Tri3(:,3)))/3,...
        (yin3(Tri3(:,1))+yin3(Tri3(:,2))+yin3(Tri3(:,3)))/3];


 [row,col]=size(xin1);
Nnode1 = row*col;  %Gives total number of nodes in Cav1
 [row,col]=size(xin2);
Nnode2 = row*col; %Gives total number of nodes in Cav2
 [row,col]=size(xin3);
Nnode3 = row*col; %Gives total number of nodes in Cav3
 clear row col
```

```
 %% Find edges for PEC Condition

S1L = find(xin1==x(x1));
S1R = find(xin1==x(x2));
S1B = find(yin1==yin1(ymin1));
S2L = find(xin2==x(x3));
S2R = find(xin2==x(x4));
S2B = find(yin2==yin2(ymin2));
S3L = find(xin3==x(x5));
S3R = find(xin3==x(x6));
S3B = find(yin3==yin3(ymin3));

 S1= [S1L; S1B; S1R];
 S2= [S2L; S2B; S2R];
 S3= [S3L; S3B; S3R];

  %%%%% cut off one cavity or another by making PEC condition at aperture.
%%%%
 if onoff(1) ==0
  S1AP = find(yin1 == 0);
   S1= [S1L; S1B; S1R; S1AP];
 end
 if onoff(2) == 0
 S2AP = find(yin2 == 0);
    S2= [S2L; S2B; S2R; S2AP];
 end
  if onoff(3) == 0
 S3AP = find(yin3 == 0);
    S3= [S3L; S3B; S3R; S3AP];
  end

 %% Input initial conditions
```

```
% Establish NEWMARK constants beta and gamma.
%  gamma = sqrt(2)-.5; %Original Parameter
%  beta= .25*(.5+gamma)^2;
 gamma = .9;
 beta= .49;
    alpha = sqrt(1/(beta*h^2));
% theta is incidence angle from ground plane
theta=pi/2;
t0=0; %parameter for starting time.
if isgauss == 0
k = (2*pi);
else
    k = 1;
end

%%identify aperture segments
Seg1=zeros(L1,5);
Seg2=zeros(L2,5);
Seg3=zeros(L3,5);

for n = 1:L1
    temp = find(yin1(Tri1(n,:)) == 0);
    if length(temp)>1;
        Seg1(n,1:5) = [Tri1(n,temp),n,temp];
    end
end
%segs on 2.
for n = 1:L2
    temp = find(yin2(Tri2(n,:)) == 0);
    if length(temp)>1;
        Seg2(n,1:5) = [Tri2(n,temp),n,temp];
    end
```

```
end
%segs on 3.
for n = 1:L3
    temp = find(yin3(Tri3(n,:)) == 0);
    if length(temp)>1;
        Seg3(n,1:5) = [Tri3(n,temp),n,temp];
    end
end

if isgauss ==0
u0  = planewave(theta,k, xout,yout,t0,1);
uref0=-planewave(theta,k, xout,-yout,t0,1);
U0=u0+uref0;
%timestep 1, t = h
t = h;
ut  = planewave(theta,k, xout,yout,t,1);

dyUt = -2*k*1i*sin(theta).*ut; %@aperture
else
    %parameters for gausswave
    T=2;
    T0 = 3;

u0 = gausswave(t0,T0,T,xout,yout,theta);
uref0= -gausswave(t0,T0,T,xout,-yout,theta);
U0=u0+uref0;
%timestep 1, t = h
t = h;
ut = gausswave(t,T0,T,xout,yout,theta);
%ureft= -gausswave(t,T0,T,xout,-yout,theta);
%Ut = ut+ureft;
dyUt = k*(-16)*sin(theta)*4*(t-T0+xout(1,:)*cos(theta)...
```

```
    +yout(1,:)*sin(theta))/T^2.*ut(1,:); %
end
%calculate T matrix values
%using algorithm as in Van2002
 Tfunc= -(ThreeCavT(xin1(1,:),xin2(1,:),xin3(1,:),alpha));

 %% Build K
 beta1=epsr1T*alpha^2;
 beta2=epsr2T*alpha^2;
 beta3=epsr3T*alpha^2;
 % K will hold < grad phi, grad phi > +  alpha^2 * <epsr * phi, phi> - T.
 K = zeros(Nnode1+Nnode2+Nnode3);
%Kphiphi is just the <phi, phi> part of K.
 Kphiphi = zeros(size(K));
%Kgamma is <phi_gamma, phi_gamma>
 Kgamma = zeros(size(K));
%Kphiphi is  <epsr dot phi, phi> part of K.
 Keps = zeros(size(K));
 %Input basic components K, Kphiphi, Kgamma.
 %Cav1
 for n =1:L1;
     if Seg1(n,3)>0
         for i = 1:2
             for j = 1:2
                 if i == j
                del = 1;
                 else
                del = 0;
                 end
          Kgamma(Tri1(n,Seg1(n,3+i)),Tri1(n,Seg1(n,3+j)))=...
        r/6*(1+del)...
        +Kgamma(Tri1(n,Seg1(n,3+i)),Tri1(n,Seg1(n,3+j)));
```

```
            end
        end
    end


    for i = 1:3
        for j = 1:3
            if i == j
                del = 1;
            else
                del = 0;
            end
            %fill in K
            K(Tri1(n,i),Tri1(n,j)) = K(Tri1(n,i),Tri1(n,j))+...
                1/(4*area1(n))*(bele1(n, i)*bele1(n,j)+cele1(n, i)*cele1(n,j))+...
                area1(n)/12*beta1(n)*(1+del);
            Keps(Tri1(n,i),Tri1(n,j)) =  Keps(Tri1(n,i),Tri1(n,j))+...
                area1(n)/12*beta1(n)*(1+del);
            Kphiphi(Tri1(n,i),Tri1(n,j))=Kphiphi(Tri1(n,i),Tri1(n,j))+...
                area1(n)/12*(1+del);
        end
    end
end
 %Cav2
    for n =1:L2;

            if Seg2(n,3)>0
        for i = 1:2
            for j = 1:2
                if i == j
               del = 1;
                else
```

```
                del = 0;
                 end
         Kgamma(Nnode1+Tri2(n,Seg2(n,3+i)),Nnode1+Tri2(n,Seg2(n,3+j)))=...
        r/6*(1+del)...
        +Kgamma(Nnode1+Tri2(n,Seg2(n,3+i)),Nnode1+Tri2(n,Seg2(n,3+j)));
             end
         end
            end

        for i = 1:3
            for j = 1:3
            if i == j
                del = 1;
            else
                del = 0;
            end
            %fill in K
            K(Nnode1+Tri2(n,i),Nnode1+Tri2(n,j)) =...
          K(Nnode1+Tri2(n,i),Nnode1+Tri2(n,j))+...
                1/(4*area2(n))*(bele2(n, i)*bele2(n,j)+cele2(n, i)*cele2(n,j))+...
                area2(n)/12*beta2(n)*(1+del);
             Keps(Nnode1+Tri2(n,i),Nnode1+Tri2(n,j)) =...
         Keps(Nnode1+Tri2(n,i),Nnode1+Tri2(n,j))+...
               area2(n)/12*beta2(n)*(1+del);
            Kphiphi(Nnode1+Tri2(n,i),Nnode1+Tri2(n,j)) =...
         Kphiphi(Nnode1+Tri2(n,i),Nnode1+Tri2(n,j))+...
                area2(n)/12*(1+del);
            end
        end
    end
%Cav3
    for n =1:L3;
```

```
        if Seg3(n,3)>0
    for i = 1:2
        for j = 1:2
            if i == j
           del = 1;
            else
           del = 0;
            end
    Kgamma(Nnode1+Nnode2+Tri3(n,Seg3(n,3+i)),...
Nnode1+Nnode2+Tri3(n,Seg3(n,3+j)))=...
r/6*(1+del)+Kgamma(Nnode1+Nnode2+...
Tri3(n,Seg3(n,3+i)),Nnode1+Nnode2+Tri3(n,Seg3(n,3+j)));
        end
    end
       end

   for i = 1:3
       for j = 1:3
       if i == j
           del = 1;
       else
           del = 0;
       end
       %fill in K
       K(Nnode1+Nnode2+Tri3(n,i),Nnode1+Nnode2+Tri3(n,j)) =...
     K(Nnode1+Nnode2+Tri3(n,i),Nnode1+Nnode2+Tri3(n,j))+...
           1/(4*area3(n))*(bele3(n, i)*bele3(n,j)+cele3(n, i)*cele3(n,j))+...
           area3(n)/12*beta3(n)*(1+del);
        Keps(Nnode1+Nnode2+Tri3(n,i),Nnode1+Nnode2+Tri3(n,j)) =...
    Keps(Nnode1+Nnode2+Tri3(n,i),Nnode1+Nnode2+Tri3(n,j))+...
          area3(n)/12*beta3(n)*(1+del);
```

```
            Kphiphi(Nnode1+Nnode2+Tri3(n,i),Nnode1+Nnode2+Tri3(n,j)) =...
          Kphiphi(Nnode1+Nnode2+Tri3(n,i),Nnode1+Nnode2+Tri3(n,j))+...
                area3(n)/12*(1+del);
            end
        end
    end
     %%%%%%%%%%%%%%%%%%%%%%%%%%%%%%%%%%%%%%%%%%%%%%%%%%%%%%%%%%%%
     %%%%%%%%%%%%%%%%%%%%%%%%%%%%%%%%%%%%%%%%%%%%%%%%%%%%%%%%%%%%
%% add coupling from Tfunc.
M=zeros(size(K));
   for n =1:x2-x1
       for m = 1:x2-x1
            for i = 1:2
                for j = 1:2
if  i == j
    del = 1;
else
    %del = 1;
    del = 1;
end

            %fill in K  Ny1*(n+i-2)+1 is the node number of the i'th node
            %on the n'th segment along the aperture.
           M(Ny1*(n+i-2)+1,Ny1*(m+j-2)+1) =M(Ny1*(n+i-2)+1,Ny1*(m+j-2)+1)+...
               Tfunc(n,m)/(2*del);
                end
            end
       end
    end
  %Ap 2 to Ap 2
    for n =1:x4-x3
       for m = 1:x4-x3
```

```
        for i = 1:2
            for j = 1:2
                if  i == j
                    del = 1;
                else
                    del = 1;
                end
        M(Nnode1+Ny2*(n+i-2)+1,Nnode1+Ny2*(m+j-2)+1) =...
    M(Nnode1+Ny2*(n+i-2)+1,Nnode1+Ny2*(m+j-2)+1)+...
           Tfunc(x2-x1+n,x2-x1+m)/(2*del);
            end
        end
   end
end
  %Ap 3 to Ap 3
for n =1:x6-x5
   for m = 1:x6-x5
        for i = 1:2
            for j = 1:2
                if  i == j
                    del = 1;
                else
                    del = 1;
                end
        M(Nnode1+Nnode2+Ny3*(n+i-2)+1,Nnode1+Nnode2+Ny3*(m+j-2)+1) =...
    M(Nnode1+Nnode2+Ny3*(n+i-2)+1,Nnode1+Nnode2+Ny3*(m+j-2)+1)+...
           Tfunc(x2-x1+x4-x3+n,x2-x1+x4-x3+m)/(2*del);
            end
        end
   end
end
```

```
%Ap 1 affects others...
    for n =1:x2-x1
          %Ap 1 to Ap 2
       for m = 1:x4-x3
            for i = 1:2
                for j = 1:2
            M(Ny1*(n+i-2)+1,Nnode1+Ny2*(m+j-2)+1) =...
             M(Ny1*(n+i-2)+1,Nnode1+Ny2*(m+j-2)+1)+...
                    Tfunc(n,x2-x1+m)/2;
                end
            end
       end
         %Ap 1 to Ap 3
       for m = 1:x6-x5
            for i = 1:2
                for j = 1:2
            M(Ny1*(n+i-2)+1,Nnode1+Nnode2+Ny3*(m+j-2)+1) =...
             M(Ny1*(n+i-2)+1,Nnode1+Nnode2+Ny3*(m+j-2)+1)+...
                    Tfunc(n,x2-x1+x4-x3+m)/2;
                end
            end
       end
    end
%Ap2 affects others
    for n =1:x4-x3
         %Ap 2 to Ap 1
       for m = 1:x2-x1
            for i = 1:2
                for j = 1:2
            % Ny1*(n+i-2)+1 is the node number of the i'th node
            %on the n'th segment along the aperture.
            M(Nnode1+Ny2*(n+i-2)+1,Ny1*(m+j-2)+1) =...
```

```
      M(Nnode1+Ny2*(n+i-2)+1,Ny1*(m+j-2)+1) + ...
              Tfunc(x2-x1+n,m)/2;
              end
          end
    end

              %Ap 2 to Ap 3
    for m = 1:x6-x5
          for i = 1:2
              for j = 1:2
          % Ny1*(n+i-2)+1 is the node number of the i'th node
          %on the n'th segment along the aperture.
          M(Nnode1+Ny2*(n+i-2)+1,Nnode1+Nnode2+Ny3*(m+j-2)+1) =...
      M(Nnode1+Ny2*(n+i-2)+1,Nnode1+Nnode2+Ny3*(m+j-2)+1) + ...
              Tfunc(x2-x1+n,x2-x1+x4-x3+m)/2;
              end
          end
    end

end

%Ap3 affects others
for n =1:x6-x5
     %Ap 3 to Ap 1
    for m = 1:x2-x1
          for i = 1:2
              for j = 1:2
          % Ny1*(n+i-2)+1 is the node number of the i'th node
          %on the n'th segment along the aperture.
          M(Nnode1+Nnode2+Ny3*(n+i-2)+1,Ny1*(m+j-2)+1) =...
      M(Nnode1+Nnode2+Ny3*(n+i-2)+1,Ny1*(m+j-2)+1)  + ...
              Tfunc(x2-x1+x4-x3+n,m)/2;
```

```
                end
            end
        end

                %Ap 3 to Ap 2
        for m = 1:x4-x3
            for i = 1:2
                for j = 1:2
            % Ny1*(n+i-2)+1 is the node number of the i'th node
            %on the n'th segment along the aperture.
            M(Nnode1+Nnode2+Ny3*(n+i-2)+1,Nnode1+Ny2*(m+j-2)+1) =...
          M(Nnode1+Nnode2+Ny3*(n+i-2)+1,Nnode1+Ny2*(m+j-2)+1) + ...
                Tfunc(x2-x1+x4-x3+n,x2-x1+m)/2;
                end
            end
        end

    end

 K = K + M;
    clear M
%
 %% clear and fill b

 %%%%%%%%%%%%%%%%  %%%%%%%%%%%%%%%%%%%%%%%%%%%%%%
dy1=(dyUt(1,x1:x2-1)+dyUt(1,x1+1:x2))/2; %H is zero at this point
dy2=(dyUt(1,x3:x4-1)+dyUt(1,x3+1:x4))/2; %H is zero at this point
dy3=(dyUt(1,x5:x6-1)+dyUt(1,x5+1:x6))/2; %H is zero at this point
 b=zeros(Nnode1+Nnode2+Nnode3,1);
 %Ap 1
   for n =1:x2-x1
            for i = 1:2
```

```
            %fill in b  Ny1*(n+i-2)+1 is the node number of the i'th node
            %on the n'th segment along the aperture.
            b(Ny1*(n+i-2)+1) =b(Ny1*(n+i-2)+1)+ dy1(n)*r/2;
            end
            %b(Ny1*(n+i-2)+1) =b(Ny1*(n+i-2)+1)+ (dyUt(1,x1+n-1)+H1mid(n))*r;
                    %this is not very different for normal incidence.
    end
  %Ap 2
   for n =1:x4-x3
            for i = 1:2
            %fill in b  Ny1*(n+i-2)+1 is the node number of the i'th node
            %on the n'th segment along the aperture.
            b(Nnode1+Ny2*(n+i-2)+1) =  b(Nnode1+Ny2*(n+i-2)+1)+dy2(n)*r/2;
            end

   end
     %Ap 3
   for n =1:x6-x5
            for i = 1:2
            %fill in b  Ny1*(n+i-2)+1 is the node number of the i'th node
            %on the n'th segment along the aperture.
            b(Nnode1+Nnode2+Ny3*(n+i-2)+1) =...
          b(Nnode1+Nnode2+Ny3*(n+i-2)+1)+dy3(n)*r/2;
            end

   end
   B2=b;
  %% Input PEC conditions
 for n = 1:length(S1)
K(S1(n),S1(n))=10^100; %forcing u to zero.
 end
 for n = 1:length(S2)
```

```
K(Nnode1+S2(n),Nnode1+S2(n))=10^100;
 end
 for n = 1:length(S3)
K(Nnode1+Nnode2+S3(n),Nnode1+Nnode2+S3(n))=10^100;
 end

  %% build Utilde(1)
Utilde1 = zeros(size(B2)); %starting with all zeros in cavity.
%Uin1tilde and Uin2tilde are sized to match the mesh grid.
Uin1tilde = zeros(size(xin1));
Uin1tilde(:)=Utilde1(1:Nnode1); %time 1
Uin2tilde = zeros(size(xin2));
Uin2tilde(:)=Utilde1(Nnode1+1:Nnode1+Nnode2); %time 1
Uin3tilde = zeros(size(xin3));
Uin3tilde(:) = Utilde1(Nnode1+Nnode2+1:Nnode1+Nnode2+Nnode3); %time 1

UinCavtilde1 = zeros(3*(L1+L2+L3),1);
UinCavtilde1(Tri1(:)) = Uin1tilde(Tri1(:));  %Resizing to fit fele
UinCavtilde1(Tri2(:)+3*L1) = Uin2tilde(Tri2(:)); %Resizing to fit fele
UinCavtilde1(Tri3(:)+3*(L1+L2)) = Uin3tilde(Tri3(:)); %Resizing to fit fele

Uin1=zeros(size(xin1)); %container for U in cavity 1 sized like mesh
Uin1ddot = zeros(size(xin1)); %container for Uddot in cavity 1 sized like mesh
Uin1dot = gamma*h*Uin1ddot;

Uin2=zeros(size(xin2)); %container for U in cavity 2 sized like mesh
Uin2ddot = zeros(size(xin2)); %container for Uddot in cavity 2 sized like mesh
Uin2dot = gamma*h*Uin2ddot;

Uin3=zeros(size(xin3)); %container for U in cavity 2 sized like mesh
Uin3ddot = zeros(size(xin3)); %container for Uddot in cavity 2 sized like mesh
Uin3dot = gamma*h*Uin3ddot;
```

```
%% f is defined by element as epsr * alpha^2 *utilde

% put in the zero conditions:
B2(S1) = 0;
B2(Nnode1+S2) = 0;
B2(Nnode1+Nnode2+S3) = 0;

 %%
 id = 'MATLAB:nearlySingularMatrix';
 warning('off',id); %every matrix division generates warning that :
 %  Warning: Matrix is close to singular or badly scaled.
%  Results may be inaccurate. RCOND = 1.231004e-100.
 %Solving for u @ time h.
%A = real(K\B2);
A = K\B2;

A1 = zeros(size(xin1));  %A1, A2 sized like grid
A1(:)=A(1:Nnode1); %time 1
A2 = zeros(size(xin2));
A2(:)=A(Nnode1+1:Nnode1+Nnode2); %time 1
A3 = zeros(size(xin3));
A3(:)= A(Nnode1+Nnode2+1:Nnode1+Nnode2+Nnode3); %time 1

save1=zeros(round(Tfinal/h,0),length(A1(1,:)));
save2=zeros(round(Tfinal/h,0),length(A2(1,:)));
save3=zeros(round(Tfinal/h,0),length(A3(1,:)));
time=zeros(round(Tfinal/h,0),1);

save1(1,:) = A1(1,:);
save2(1,:) = A2(1,:);
save3(1,:) = A3(1,:);
```

```
time(1) = h;

%%
% calculate the time derivative approximations for time 1
uddotnin1 = alpha^2*(A1-Uin1tilde) ;
uddotnin2 = alpha^2*(A2-Uin2tilde) ;
uddotnin3 = alpha^2*(A3-Uin3tilde) ;
udotnin1 = Uin1dot+(1-gamma)*h*Uin1ddot+gamma*h*uddotnin1;
udotnin2 = Uin2dot+(1-gamma)*h*Uin2ddot+gamma*h*uddotnin2;
udotnin3 = Uin3dot+(1-gamma)*h*Uin3ddot+gamma*h*uddotnin3;

utildenplus1in1=A1+h*udotnin1+(1/2-beta)*h^2*uddotnin1;
utildenplus1in2=A2+h*udotnin2+(1/2-beta)*h^2*uddotnin2;
utildenplus1in3=A3+h*udotnin3+(1/2-beta)*h^2*uddotnin3;
%%
%Calculate Scattered Field uscat1 and uscattilde1
ApFields = [A1(1,1:end),A2(1,1:end),A3(1,1:end)];
ApFieldsTilde = [Uin1tilde(1,1:end),Uin2tilde(1,1:end),Uin3tilde(1,1:end)];

uscat = zeros(size(xout));
uscattilde = zeros(size(xout));
uscat =uscat+ scatfield3(ApFields,1:length(ApFields),x(x1:x2),...
        x(x3:x4),x(x5:x6),xout,yout,alpha);
%%%%%%%%%%%%%%%%%%%%%%%%%%%% adding midpoint evaluations %%%%%%%%%%%
midx = (xout(1,1:end-1)+xout(1, 2:end))/2;
midy = (yout(1:end-1,1)+yout( 2:end,1))/2;
[mx,my] = meshgrid(midx,midy);
uscatmid = scatfield3mid(ApFields,1:length(ApFields),x(x1:x2),...
        x(x3:x4), x(x5:x6),mx,my,alpha);
uscattildemid = zeros(size(uscatmid));
%%%%%%%%%%%%%%%%%%%%%%%%%%%%%%%%%%%%%%%%%%%%%%%%
uscattilde(1,x1:x2)= ApFieldsTilde(1:x2-x1+1);
```

```
uscattilde(1,x3:x4) = ApFieldsTilde(x2-x1+2:(x2-x1+1)+(x4-x3+1));
uscattilde(1,x5:x6) = ApFieldsTilde((x2-x1+1)+(x4-x3+1)+1:end);

uscatddot = alpha^2*(uscat-uscattilde) ;
uscatdot = gamma*h*uscatddot;
%\tilde u ^{s, n+1} outside
uscattildenplus1 = uscat + h* uscatdot + (1/2 - beta) * h^2 * uscatddot;
% First scattered field does not sum over utilde*green's function -- future
% ones will.
%%
%%%%%%%%%%%%% midpoint evaluations %%%%%%%%%%%%%%%%
uscatddotmid = alpha^2*(uscatmid-uscattildemid) ;
uscatdotmid = gamma*h*uscatddotmid;
uscattildenplus1mid = uscatmid + h* uscatdotmid +...
             (1/2 - beta) * h^2 * uscatddotmid;
%%%%%%%%%%%%%%%%%%%%%%%%%%%%%%%%%%%%%%%%%%%%%%%%%%%
%Approximate H
utildevec = zeros(LX*LY,1);
utildevec(:)=uscattildenplus1(:);

%%%%%%%%%%%%% midpoint evaluations %%%%%%%%%%%%%%%%
utildevecmid = zeros((LX-1)*(LY-1),1);
utildevecmid(:)=uscattildenplus1mid(:);
Hmid = MakeHmid(mx,my,[x1:x2,x3:x4,x5:x6],alpha,r);
%%%%%%%%%%%%%%%%%%%%%%%%%%%%%%%%%%%%%%%%%%%%%%%%%%%
H1mid = (Hmid(1:x2-x1,:)*utildevecmid).';
H2mid = (Hmid(x2-x1+2:(x2-x1+1)+(x4-x3+1)-1,:)*utildevecmid).';
H3mid = (Hmid((x2-x1+1)+(x4-x3+1)+1:end-1,:)*utildevecmid).';
%%%%%%%%%%%%%%%%%%%%%%%%%%%%%%%%%%%%%%%%%%%%%%%%%%%
clear str
str(1,:)=[A1(1,:),A2(1,:),A3(1,:)];
```

```
%% test points
Nsteps = round(Tfinal/h,0);
EXT = zeros(181,Nsteps);
EXT2 = zeros(181,Nsteps);
Gsemi = MakeGsemi(xout, yout, extpoints(:,1:2),alpha, r);
Gsemi2 = MakeGsemi(xout, yout, extpoints2(:,1:2),alpha, r);
Gimgsemi = MakeGimgsemi(xout, yout, extpoints(:,1:2),alpha, r);
Gimgsemi2 = MakeGimgsemi(xout, yout, extpoints2(:,1:2),alpha, r);
test = scatfield3semi(ApFields,1:length(ApFields),x(x1:x2),x(x3:x4),...
         x(x5:x6),extpoints(:,1),extpoints(:,2),alpha);
test = test + (Gsemi+Gimgsemi)*utildevec;
test2 = scatfield3semi(ApFields,1:length(ApFields),x(x1:x2),x(x3:x4),...
        x(x5:x6),extpoints2(:,1),extpoints2(:,2),alpha);
test2 = test2 + (Gsemi2+Gimgsemi2)*utildevec;
EXT(:,1) = test;
EXT2(:,1) = test2;
plot(extpoints(:,3),test, extpoints2(:,3),test2)
%%

% Construct dy n+1 where n = 1
if isgauss ==0
    ut  = planewave(theta,k, xout,yout,t,1);
    ut2 =  planewave(theta,k, xout,yout,t+h,1);
    ureft=-planewave(theta,k,xout,-yout,t,1);
    Ut=ut+ureft;
    dyUt = -2*k*1i*sin(theta)*ut2; %@aperture
else
ut = gausswave(t,T0,T,xout,yout,theta);
ut2=gausswave(t+h,T0,T,xout,yout,theta);
ureft= -gausswave(t,T0,T,xout,-yout,theta);
    Ut=ut+ureft;
    %du/dy = -2tau*u*dtau/dy =  -2*4*sin(theta)*tau*u
```

```
    %dyUt = 2(du_inc/dy) = -16*sin(theta)*tau *u.
   dyUt = k*(-16)*sin(theta)*4*(t+h-T0+xout(1,:)*cos(theta)...
        +yout(1,:)*sin(theta))/T^2.*ut2(1,:);
end
%define dy on segments as linear average.
%PDE calls for 2dyU + H, but dyU already has the factor of two included.
%%%%%%%%%%%%%%%% APPLY MIDPOINT FOR H %%%%%%%%%%%%%%%%%%%%%%%%%%%%%%
dy1=(dyUt(1,x1:x2-1)+dyUt(1,x1+1:x2))/2 +H1mid;
dy2=(dyUt(1,x3:x4-1)+dyUt(1,x3+1:x4))/2+H2mid;
dy3=(dyUt(1,x5:x6-1)+dyUt(1,x5+1:x6))/2+H3mid;

b=zeros(Nnode1+Nnode2+Nnode3,1);
 %Ap 1
   for n =1:x2-x1
            for i = 1:2
            %fill in b  Ny1*(n+i-2)+1 is the node number of the i'th node
            %on the n'th segment along the aperture.
            b(Ny1*(n+i-2)+1) =b(Ny1*(n+i-2)+1)+ dy1(n)*r/2;
            end
            %b(Ny1*(n+i-2)+1) =b(Ny1*(n+i-2)+1)+ (dyUt(1,x1+n-1)+H1mid(n))*r;
                    %this is not very different for normal incidence.
    end
  %Ap 2
   for n =1:x4-x3
            for i = 1:2
            %fill in b  Ny1*(n+i-2)+1 is the node number of the i'th node
            %on the n'th segment along the aperture.
            b(Nnode1+Ny2*(n+i-2)+1) =  b(Nnode1+Ny2*(n+i-2)+1)+dy2(n)*r/2;
            end

   end
     %Ap 3
```

```
   for n =1:x6-x5
            for i = 1:2
            %fill in b  Ny1*(n+i-2)+1 is the node number of the i'th node
            %on the n'th segment along the aperture.
            b(Nnode1+Nnode2+Ny3*(n+i-2)+1) =...
          b(Nnode1+Nnode2+Ny3*(n+i-2)+1)+dy3(n)*r/2;
            end

   end
   B2=b;

   %% FU is defined by element as <epsr * alpha^2 *utilde,v.
    %averaged for element by using midpoint values
FU=[reshape(utildenplus1in1,Nnode1,1);...
    reshape(utildenplus1in2,Nnode2,1);...
     reshape(utildenplus1in3,Nnode3,1)];
B2 = B2 + Keps*FU;

% put in the zero conditions:
B2(S1) = 0;
B2(Nnode1+S2) = 0;
B2(Nnode1+Nnode2+S3) = 0;
 %calculate the new fields
 %Solving for u @ time 2h.
A = (K\B2);
A1(:)=A(1:Nnode1); %time 1
A2(:)=A(Nnode1+1:Nnode1+Nnode2); %time 1
A3(:)= A(Nnode1+Nnode2+1:Nnode1+Nnode2+Nnode3); %time 1
%% compute G
fprintf('Building G matrix  ...  ')
G = MakeG(xout,yout, alpha, r);
Gmid = MakeGmid(mx,my,alpha,r);
```

```
fprintf('Building Gimg matrix  ...  ')
G =G- MakeGimg(xout,yout, alpha, r);
Gmid = Gmid - MakeGimgmid(mx,my,alpha,r);

G = alpha^2* G;
Gmid = alpha^2*Gmid;

%pause(.2) %pause allows plots to render

save1(2,:) = A1(1,:);
save2(2,:) = A2(1,:);
save3(2,:) = A3(1,:);
time(2) = 2*h;
fprintf('Entering timestep routine.')
%%%%%%%%%%%%%%%%%%%%%%%%%%%%%%%%%% BEGIN TIME STEPPING HERE %%%%%%%%%%%%%%
for t = 2*h:h:Tfinal-h

% calculate the time derivative approximations for time n
temp1 = uddotnin1;
temp2 = uddotnin2;
temp3 = uddotnin3;
uddotnin1 = alpha^2*(A1-utildenplus1in1) ;
uddotnin2 = alpha^2*(A2-utildenplus1in2) ;
uddotnin3 = alpha^2*(A3-utildenplus1in3) ;
udotnin1 = udotnin1+(1-gamma)*h*temp1+gamma*h*uddotnin1;
udotnin2 = udotnin2+(1-gamma)*h*temp2+gamma*h*uddotnin2;
udotnin3 = udotnin3+(1-gamma)*h*temp3+gamma*h*uddotnin3;
utildenplus1in1=(A1+h*udotnin1+(1/2-beta)*h^2*uddotnin1);
utildenplus1in2=(A2+h*udotnin2+(1/2-beta)*h^2*uddotnin2);
utildenplus1in3=(A3+h*udotnin3+(1/2-beta)*h^2*uddotnin3);
```

```
%Calculate Scattered Field uscat1 and uscattilde1
ApFields = [A1(1,1:end),A2(1,1:end),A3(1,1:end)];
ApFieldsTilde = [Uin1tilde(1,1:end),Uin2tilde(1,1:end),Uin3tilde(1,1:end)];

uscat =scatfield3(ApFields,1:length(ApFields),x(x1:x2),...
        x(x3:x4),x(x5:x6),xout,yout,alpha);
utildevec(:)=uscattildenplus1(:);
uscatR2 = G*utildevec;
uscat(:) = uscat(:) + uscatR2(:);
uscat(1,:)= [zeros(1,x1-1), ApFields(1:x2-x1+1), zeros(1,x3-x2-1),...
        ApFields(x2-x1+2:(x2-x1+1)+(x4-x3+1)), zeros(1,x5-x4-1),...
        ApFields((x2-x1+1)+(x4-x3+1)+1:end),zeros(1,LX-x6)];
%%%%%%%%%%%%%%%%%%%%%%%%%%%% adding midpoint evaluations %%%%%%%%%%%%
uscatmid = scatfield3mid(ApFields,1:length(ApFields),...
        x(x1:x2),x(x3:x4),x(x5:x6),mx,my,alpha);
uscatR2mid = Gmid*utildevecmid;
uscatmid(:) = uscatmid(:)+uscatR2mid(:);

temp4=uscatddot;
% scattered time derivative time 1
uscatddot = alpha^2*(uscat-uscattildenplus1);
%scattered time derivative time 1
uscatdot = uscatdot + (1-gamma)*h*temp4+gamma*h*uscatddot;
%tilde for time 2
uscattildenplus1 = uscat+h*uscatdot+(1/2-beta)*h^2*uscatddot;

%Approximate H
%%%%%%%%%%%%%% midpoint evaluations %%%%%%%%%%%%%%%%
tempmid = uscatddotmid;
uscatddotmid = alpha^2*(uscatmid-uscattildenplus1mid) ;
uscatdotmid = uscatdotmid + (1-gamma)*h*tempmid+gamma*h*uscatddotmid;
```

```
uscattildenplus1mid = uscatmid + h* uscatdotmid + (1/2 - beta)...
                * h^2 * uscatddotmid;
utildevecmid(:)=uscattildenplus1mid(:);
%%%%%%%%%%%%% midpoint evaluations %%%%%%%%%%%%%%%%
H1mid = (Hmid(1:x2-x1,:)*utildevecmid).';
H2mid = (Hmid(x2-x1+2:(x2-x1+1)+(x4-x3+1)-1,:)*utildevecmid).';
H3mid = (Hmid((x2-x1+1)+(x4-x3+1)+1:end-1,:)*utildevecmid).';
%%%%%%%%%%%%%%%%%%%%%%%%%%%%%%%%%%%%%%%%%%%%%%%%%%%
test = scatfield3semi(ApFields,1:length(ApFields),...
    x(x1:x2),x(x3:x4), x(x5:x6),extpoints(:,1),extpoints(:,2),alpha);
test = test + (Gsemi+Gimgsemi)*utildevec;
test2 = scatfield3semi(ApFields,1:length(ApFields),...
    x(x1:x2),x(x3:x4),x(x5:x6),extpoints2(:,1),extpoints2(:,2),alpha);
test2 = test2 + (Gsemi2+Gimgsemi2)*utildevec;
EXT(:,round(t/h,0)) = test;
EXT2(:,round(t/h,0)) = test2;
%plot(extpoints(:,3),test, extpoints2(:,3),test2)
%%%%%%%%%%%%%%%%%%%%%%%%%%%%%%%%%%%%%%%%%%%%%%%%%%%
%%
% Construct dy

if isgauss ==0
    ut  = planewave(theta,k, xout,yout,t+h,1);
    ureft=-planewave(theta,k,xout,-yout,t+h,1);
    Ut=ut+ureft;
    dyUt = -2*k*1i*sin(theta)*ut; %@aperture
else
ut = gausswave(t,T0,T,xout,yout,theta);
ureft= -gausswave(t,T0,T,xout,-yout,theta);
ut2 = gausswave(t+h,T0,T,xout,yout,theta);
    Ut=ut+ureft;
   dyUt = k*(-16)*sin(theta)*4*(t-T0+h+xout(1,:)*cos(theta)...
```

```
        +yout(1,:)*sin(theta)).*ut2(1,:)/T^2;%
end

%%%%%%%%%%%%%%%% APPLY MIDPOINT FOR H %%%%%%%%%%%%%%%%%%%%%%%%%%%%%%
dy1=(dyUt(1,x1:x2-1)+dyUt(1,x1+1:x2))/2 +H1mid;
dy2=(dyUt(1,x3:x4-1)+dyUt(1,x3+1:x4))/2+H2mid;
dy3=(dyUt(1,x5:x6-1)+dyUt(1,x5+1:x6))/2+H3mid;

b=zeros(Nnode1+Nnode2+Nnode3,1);
 %Ap 1
   for n =1:x2-x1
            for i = 1:2
            %fill in b  Ny1*(n+i-2)+1 is the node number of the i'th node
            %on the n'th segment along the aperture.
            b(Ny1*(n+i-2)+1) =b(Ny1*(n+i-2)+1)+ dy1(n)*r/2;
            end
    end
  %Ap 2
   for n =1:x4-x3
            for i = 1:2
            %fill in b  Ny1*(n+i-2)+1 is the node number of the i'th node
            %on the n'th segment along the aperture.
            b(Nnode1+Ny2*(n+i-2)+1) =  b(Nnode1+Ny2*(n+i-2)+1)+dy2(n)*r/2;
            end

   end
     %Ap 3
   for n =1:x6-x5
            for i = 1:2
            %fill in b  Ny1*(n+i-2)+1 is the node number of the i'th node
            %on the n'th segment along the aperture.
            b(Nnode1+Nnode2+Ny3*(n+i-2)+1) = ...
```

```
        b(Nnode1+Nnode2+Ny3*(n+i-2)+1)+dy3(n)*r/2;
            end
    end
    B2=b;

    %% FU is defined by element as <epsr * alpha^2 *utilde,v.
     % averaged for element by using midpoint values
FU=[reshape(utildenplus1in1,Nnode1,1);reshape(utildenplus1in2,Nnode2,1);...
     reshape(utildenplus1in3,Nnode3,1)];
B2 = B2 + Keps*FU;

% put in the zero conditions:
B2(S1) = 0;
B2(Nnode1+S2) = 0;
B2(Nnode1+Nnode2+S3) = 0;
 %calculate the new fields
 %Solving for u @ time 2h.
A = K\B2;
A1(:)=A(1:Nnode1); %time 1
A2(:)=A(Nnode1+1:Nnode1+Nnode2); %time 1
A3(:)= A(Nnode1+Nnode2+1:Nnode1+Nnode2+Nnode3); %time 1

save1(round(t/h)+1,:) = A1(1,:);
save2(round(t/h)+1,:) = A2(1,:);
save3(round(t/h)+1,:) = A3(1,:);
time(round(t/h)+1) = t+h;
end

temp = num2str(xin1(1,round((x2-x1+1)/2,0)));
head = [ 'Scattered field intensity at (' temp ', 0)'];
figure()
plot(time',real(save1(:,round((x2-x1+1)/2,0))));
```

```
axis([0 Tfinal min(min(real([save1,save2,save3]))).*.
     max(max(real([save1,save2,save3])))])
grid on
title(head)
xlabel('Time (LM)')
ylabel('Intensity')

temp = num2str(xin2(1,round((x4-x3+1)/2,0)));
head = [ 'Scattered field intensity at (' temp ', 0)'];
figure()
plot(time',real(save2(:,round((x4-x3+1)/2,0))));
axis([0 Tfinal min(min(real([save1,save2,save3]))).*.
     max(max(real([save1,save2,save3])))])
grid on
title(head)
xlabel('Time (LM)')
ylabel('Intensity')
hold off

temp = num2str(xin3(1,round((x6-x5+1)/2,0)));
head = [ 'Scattered field intensity at (' temp ', 0)'];
figure()
plot(time',real(save3(:,round((x6-x5+1)/2,0))));
axis([0 Tfinal min(min(real([save1,save2,save3]))).*.
     max(max(real([save1,save2,save3])))])
grid on
title(head)
xlabel('Time (LM)')
ylabel('Intensity')
hold off

B = max(EXT,[],2);
```

```
figure()
polar(extpoints(:,3),10*log10(real(B)+ones(size(B))))
%output to save file
temp = ['sep' num2str(100*sep1) num2str(100*sep2) 'onoff' num2str(onoff(1)) ...
    num2str(onoff(2)) num2str(onoff(3)) 'depth' num2str(100*d1) num2str(100*d2) ...
    num2str(100*d3) 'epsr' num2str(EPS(1)) num2str(EPS(2)) num2str(EPS(3))];
file = [ 'I:\My Documents\TestRuns_3cavDeep\Test_NEW' temp '.xlsx'];
filename = file;
sheet = 1;
xlswrite(filename, save1, sheet)
sheet = 2;
xlswrite(filename, save2, sheet)
sheet = 3;
xlswrite(filename, save3, sheet)
sheet = 4;
xlswrite(filename, EXT, sheet)
sheet = 5;
xlswrite(filename, extpoints, sheet)
```

B.2 Construct Matrix G

The matrix G is used for computing the approximated scattered fields.

```
function G = MakeG(xx,yy, alpha, r)
%returns matrix G to multiply utilde by for integral approximation
%this function creates a distance matrix vector Nx times Ny X 1.
npts = ceil(20/alpha/r);
[ L1, L2 ] = size(xx);  % remove ground plane nodes -- their value is zero.
xvec = zeros( L1*L2, 1) ;
yvec = xvec;
xvec(:) = xx(:); yvec(:) = yy(:);
```

```
G = zeros (L1*L2);
 g0=1/2/pi*gridK(r,alpha,0,2500)/2;
 %/2 for evaluation over half grid square

 % every L1+1st term is y = 0.
RectA = zeros(size(xx));
LongA = zeros( (2*L2-1)*L1, 1) ;

  for i = 1: L1 %for points in y from zero to max y
      % Partial Green's function relative to first x point and y(i,1).
      A = r^2*1/2/pi*besselk(0,alpha*(sqrt((xvec-xvec(1)).^2 +...
          (yvec-yvec(i)).^2)));
        if i == 1
            %halve the grid near the ground plane
            A(1:L1:L1*L2) = 1/2*A(1:L1:L1*L2);
            A(i) = g0;
             A(npts*L1+1:end) = 0; %%added 2/4
            %A(i+1) =A(i+1)+1/4* g0;
        else
           % if i == L1
        A(i) = 2*g0;
        end

        RectA(:) = A(:);
        RevA = fliplr(RectA); %creates mirror image of A.
        LongA(:) = [RevA(:); A(L1+1:end)]';

     for j = 1:L2
        G( (j-1)*L1+i,:) = LongA(L1*(L2-j)+1:L1*(L2-j)+L1*L2);
     end
  end
```

```
% To replace the diagonal with another value, use A(1:L1*L2+1:end) = value %%
% To apply a function to the matrix, GREEN = 1/pi( besselk(0,A) ) ...%%
```

B.3 Compute Scattered Field

This function directly computes the aperture integral portion of the scattered field equation for the exterior computatoinal region.

```
function A = scatfield3(U,Apnode,x1,x2,x3,xout,yout,alpha)
%This function will calculate the scattered field from internal cavity
%field U with Aperture nodes in Apnode, to outer mesh xout, yout.

N1=length(x1)-1;
N2=length(x2)-1;
N3=length(x3)-1;
L1 = abs(x1(2:end)-x1(1:end-1));
L2 = abs(x2(2:end)-x2(1:end-1));
L3 = abs(x3(2:end)-x3(1:end-1));

A = zeros(size(xout));
for i = 1:N1
    A(2:end, :) =A(2:end, :)+L1(i)*alpha/2/pi *(U(Apnode(i))*yout(2:end,:)./...
        (( (x1(i)-xout(2:end,:)).^2+yout(2:end,:).^2).^(.5)).*...
        besselk(1,alpha*( (x1(i)-xout(2:end,:)).^2+yout(2:end,:).^2).^(.5))...
                +U(Apnode(i+1))*yout(2:end,:)./(( (x1(i+1)-xout(2:end,:)).^2...
        +yout(2:end,:).^2).^(.5)).*besselk(1,alpha*( (x1(i+1)-xout(2:end,:)).^2...
        +yout(2:end,:).^2).^(.5)));
end

for i = 1:N2
        A(2:end, :) =A(2:end, :)+L2(i)*alpha/2/pi*( U(Apnode(N1+1+i)).*...
```

```
        yout(2:end,:)./(( (x2(i)-xout(2:end,:)).^2+yout(2:end,:).^2).^(.5)).*...
        besselk(1,alpha*( (x2(i)-xout(2:end,:)).^2+yout(2:end,:).^2).^(.5))...
            +U(Apnode(N1+i+2)).*yout(2:end,:)./(( (x2(i+1)-xout(2:end,:)).^2...
        +yout(2:end,:).^2).^(.5)).*besselk(1,alpha*( (x2(i+1)-xout(2:end,:)).^2...
        +yout(2:end,:).^2).^(.5)));
end

for i = 1:N3
        A(2:end, :) =A(2:end, :)+L3(i)*alpha/2/pi*( U(Apnode(N1+N2+2+i)).*...
        yout(2:end,:)./(( (x3(i)-xout(2:end,:)).^2+yout(2:end,:).^2).^(.5)).*...
        besselk(1,alpha*( (x3(i)-xout(2:end,:)).^2+yout(2:end,:).^2).^(.5))...
            +U(Apnode(N1+N2+i+3)).*yout(2:end,:)./(( (x3(i+1)-xout(2:end,:)).^2...
        +yout(2:end,:).^2).^(.5)).*besselk(1,alpha*( (x3(i+1)-xout(2:end,:)).^2...
        +yout(2:end,:).^2).^(.5)));
end

end
```

B.4 Compute Matrix T

The operator T was a critical component used to enforce the coupling between cavities. The output from this function is used in the matrix P.

```
function T = ThreeCavT(x1,x2,x3,alpha)
%this function will return one matrix T for a given set of points
%x1, x2 and x3 and scale factor alpha.
N1=length(x1)-1;
N2=length(x2)-1;
N3=length(x3)-1;
L1 = abs(x1(2:end)-x1(1:end-1));
L2 = abs(x2(2:end)-x2(1:end-1));
```

```
L3 = abs(x3(2:end)-x3(1:end-1));
Xi1 = .5*(x1(2:end)+x1(1:end-1));
Xi2 = .5*(x2(2:end)+x2(1:end-1));
Xi3 = .5*(x3(2:end)+x3(1:end-1));
T = zeros(N1+N2+N3,N1+N2+N3);

for i = 1:N1
    for j = 1:N1
        if i == j
           T(i,j) = (-4- alpha^2*L1(i))/...
                (2*alpha*pi)*besselsing(alpha*L1(i)/2);
        else
          T(i,j)=(-4 - alpha^2*L1(j)*L1(i))/...
               (4*pi)*besselk(0,alpha*abs(Xi1(i)-Xi1(j)));
        end
    end
        for k = 1:N2  %k points in cav 2, i points in cav 1. sign = +1
          T(i,N1+k)=(-4 - alpha^2*L2(k)*L1(i))/...
               (4*pi)*besselk(0,alpha*abs(Xi1(i)-Xi2(k)));
        end
        for k = 1:N3  %k points in cav 3, i points in cav 1. sign = +1
          T(i,N1+N2+k)=(-4 - alpha^2*L3(k)*L1(i))/...
               (4*pi)*besselk(0,alpha*abs(Xi1(i)-Xi3(k)));
        end
end

for i = 1:N2
    for j = 1:N2
        if i == j
            T(i+N1,j+N1) = (-4- alpha^2*L2(i))/...
                (2*alpha*pi)*besselsing(alpha*L2(i)/2);
        else
```

```
            T(N1+i,N1+j)= (-4 - alpha^2*L2(j)*L2(i))/...
                (4*pi)*besselk(0,alpha*abs(Xi2(i)-Xi2(j)));
        end
    end
        for k = 1:N1   % k points in cav 1, i points in cav 2. sign = -1
        T(i+N1,k)=(-4 - alpha^2*L1(k)*L2(i))/...
            (4*pi)*besselk(0,alpha*abs(Xi2(i)-Xi1(k)));
        end
        for k = 1:N3   % k points in cav 3, i points in cav 2. sign = -1
        T(i+N1,N1+N2+k)=(-4 - alpha^2*L3(k)*L2(i))/...
            (4*pi)*besselk(0,alpha*abs(Xi2(i)-Xi3(k)));
        end
end

for i = 1:N3
    for j = 1:N3
        if i == j
            T(i+N1+N2,j+N1+N2) = (-4- alpha^2*L3(i))/...
                (2*alpha*pi)*besselsing(alpha*L3(i)/2);
        else
            T(N1+N2+i,N1+N2+j)= (-4 - alpha^2*L3(j)*L3(i))/...
                (4*pi)*besselk(0,alpha*abs(Xi3(i)-Xi3(j)));
        end
    end
        for k = 1:N1   % k points in cav 1, i points in cav 3. sign = -1
        T(i+N1+N2,k)=(-4 - alpha^2*L1(k)*L3(i))/...
            (4*pi)*besselk(0,alpha*abs(Xi3(i)-Xi1(k)));
        end
        for k = 1:N2   % k points in cav 2, i points in cav 3. sign = -1
        T(i+N1+N2,N1+k)=(-4 - alpha^2*L2(k)*L3(i))/...
            (4*pi)*besselk(0,alpha*abs(Xi3(i)-Xi2(k)));
        end
```

```
end

end
```

B.4.1 Singular Bessel Integral.

```
function A=besselsing(x)
%this function returns the approximation of the besselK function integral
%from zero to x -- Error good to about x = 5 or so
gam = 0.5772156649;
lim = 20 ;
T1 =0;
T2 =0;
T3 =0;
part = 0;
k = 0;
    T1 = T1+ (x/2)^(2*k)/(factorial(k)^2*(2*k+1));
    T2 = T2+ (x/2)^(2*k)/(factorial(k)^2*(2*k+1)^2);
    for k = 1:lim  %-1
        T1 = T1+ (x/2)^(2*k)/(factorial(k)^2*(2*k+1));
        T2 = T2+ (x/2)^(2*k)/(factorial(k)^2*(2*k+1)^2);
        part = part + 1/k ;
        T3 = T3+ (x/2)^(2*k)/(factorial(k)^2*(2*k+1))*part;
    end
A= -(gam +log(x/2))*x*T1+x*T2+x*T3;
% fprintf('Error < %g',A-A1)
end
```

B.5 Compute Matrix H

The operator H is important in coupling the time-delayed scattered fields from multiple cavities. The matrix H computed with this function is used to fill vector b.

```
function H = MakeH(xx,yy, apidx, alpha, r)
%returns matrix H to multiply utilde by for integral approximation
%apidx is a reference vector of points on the aperture. This may be
% [x1:x2, x3:x4], and will be related to points in the xout, yout vectors
% by xvec( LY*(apidx(i) - 1)+1 )= xout(1, apidx(i))

[ L1, L2 ] = size(xx);
xvec = zeros( L1*L2, 1) ;
yvec = xvec;
xvec(:) = xx(:); yvec(:) = yy(:);

H = zeros (length(apidx), L1*L2);
      f = @(x) besselk(0,alpha*sqrt(x.^2 + (r/2).^2));
       f0 = @(x) besselk(0,alpha*sqrt(x.^2 ));
h0 =2* alpha^2 / pi *( integral(f0, 0,r/2) -integral(f, 0,r/2));

A = r* alpha^2/pi*(besselk(0,alpha*sqrt( (xvec -  xvec( 1) ).^2+...
    (yvec - r/2).^2 )) - besselk(0,alpha*sqrt( (xvec -  xvec( 1 ) ).^2 +...
    (yvec + r/2).^2 )));
A( 1  :  L1)  = r* alpha^2/pi*(besselk(0,alpha*sqrt( (r/4 ).^2 +...
    (yvec( 1  :  L1) - r/2).^2 )) - besselk(0,alpha*sqrt( (r/4).^2 +...
    (yvec( 1  :  L1) + r/2).^2 )));

A(1:L1:L1*L2) = r*alpha^2/pi/2 *(besselk(0,alpha*sqrt(...
    (xvec(1:L1:L1*L2)-r/4 -  xvec( 1)  ).^2 )) -...
    besselk(0,alpha*sqrt( (xvec(1:L1:L1*L2)-r/4 -  xvec( 1)  ).^2 +...
    ( r/2).^2 ))+besselk(0,alpha*sqrt( (xvec(1:L1:L1*L2)+...
    r/4 -  xvec( 1)  ).^2 )) - besselk(0,alpha*sqrt( (xvec(1:L1:L1*L2)+...
    r/4 -  xvec( 1)  ).^2 + ( r/2).^2 )) );

A(1) = h0;
```

```
RectA = zeros(size(xx));
RectA(:) = A(:);
FlipA = fliplr(RectA);

LongA = zeros(L1*(2*L2-1),1);
LongA(:) = [FlipA(:); A(L1+1:end)]';
for i = 1:length(apidx)
    H(i,:) = LongA(L1*L2+1-(L1*(apidx(i))):2*L1*L2-(L1*(apidx(i))));
end
```

Bibliography

[1] Abramowitz, M. and I. Stegun. *Handbook of Mathematical Functions with Formulas, Graphs, and Mathematical Tables*. U.S. Department of Commerce, Washington D.C., 1964.

[2] Ammari, H., B. Bao, and A. W. Wood. "Analysis of the Electromagnetic Scattering from a Cavity". *Japan J. Indust. Appl. Math*, 19:301–310, 2002.

[3] Anastassiu, H. T. "A Review of Electromagnetic Scattering Analysis for Inlets, Cavities, and Open Ducts". *IEEE Antennas and Propagation Magazine*, 45(6):27–40, 2003.

[4] Balanis, C. A. *Advanced Engineering Electromagnetics*. Wiley & Sons, Hoboken, NJ, 2012, 1989.

[5] Bao, Gang, Kihyun Yun, and Zhengfang Zhou. "Stability of the scattering from a large electromagnetic cavity in two dimensions". *SIAM J. Math. Anal.*, 44(1):383–404, 2012.

[6] Baskin, Dean, Euan Spence, and Jared Wunsch. "Sharp high-frequency estimates from the Helmholtz equation and applications to boundary integral equations". *SIAM J. Math. Anal.*, 48(1):229–267, 2016.

[7] Callihan, R. S. *Analysis of Transient Electromagnetic Scattering From an Overfilled Cavity Embedded in an Impedance Ground Plane*. Ph.D. thesis, Air Force Inst. Tech., 2011.

[8] Chilton, R. A. and R. Lee. "The discrete origin of FETD-Newmark late time instability, and a correction scheme". *Journal of Computational Physics*, 224:1293–1306, 2007.

[9] Du, Kui, Buyang Li, and Weiwei Sun. "A numerical study on the stability of a class of Helmholtz problems". *J. Comput. Phys.*, 287:46–59, 2015.

[10] Durán, M., I. Muga, and J.-C. Nédélec. "The Helmholtz equation in a locally perturbed half-plane with passive boundary". *IMA Journal of Applied Mathematics*, 71(6):853–876, 2006.

[11] Elliott, R. S. "The History of Electromagnetics as Hertz Would Have Known It". *IEEE Transactions of Microwave Theory and Techniques*, 36(5):806–823, 1988.

[12] Eom, Hyo J. *Wave Scattering Theory - A Series Approach Based on the Fourier Transformation*. Springer, Berlin, Germany, 2001.

[13] Garg, Ramesh. *Analytical and Computational Methods in Electromagnetics*. Artech House, Norwood, MA, 2008.

[14] Gedney, S. D. and U. Navsariwala. "An Unconditionally Stable Finite Element Time-Domain Solution of the Vector Wave Equation". *IEEE Microwave and Guided Wave Letters*, 5:332–334, 1995.

[15] Gradshteyn, I.S. and I.M. Ryzhik. *Table of Integrals, Series, and Products*. Academic Press, San Diego, CA, 6th edition, 2000.

[16] Grote, M. and C. Kirsch. "Dirichlet-to-Neumann boundary conditions for multiple scattering problems". *Journal of Computational Physics*, 201:630–650, 2004.

[17] He, Gan H, Q. and D. Jiao. "Explicit Time-Domain Finite-Element Method Stabilized for an Arbitrarily Large Time Step". *IEEE Trans. Antennas and Propag.*, 60(11):5240–5250, 2012.

[18] Hoffman, K. and R. Kunze. *Linear Algebra*. Prentice Hall, Upper Saddle River, NJ, 2nd edition, 1971.

[19] Huang, J. and A. W. Wood. "Numerical Simulation of Electromagnetic Scattering Induced by an Overfilled Cavity in the Ground Plane". *IEEE Antennas and Wireless Propagation Letters*, 4:224–228, 2005.

[20] Huang, J. and A. W. Wood. "Analysis and Numerical Solution of Transient Electromagnetic Scattering from Overfilled Cavities". *Communications in Computational Physics*, 1(6):1043–1054, 2006.

[21] Huang, J., A. W. Wood, and M. J. Havrilla. "A Hybrid Finite Element-Laplace Transform Method for the Analysis of Transient Electromagnetic Scattering by an Overfilled Cavity in the Ground Plane". *Commun. Comput. Phys.*, 5(1):126–141, 2009.

[22] Jiao, Dan and Jian-Ming Jin. "A General Approach for the Stability Analysis of the Time-Domain Finite-Element Method for Electromagnetic Simulations". *IEEE Trans. Antennas and Propag.*, 50(11):1624–1632, 2002.

[23] Jin, J. M. *The Finite Element Method in Electromagnetics*. Wiley & Sons, Hoboken, NJ, 3rd edition, 2014.

[24] Knott, Eugene F., John F. Shaeffer, and Michael T. Tulley. *Radar Cross Section*. Artech House, Norwood, MA, 2nd edition, 1993.

[25] Li, P. and A. W. Wood. "A Two-Dimensional Helmholtz Equation Solution for the Multiple Cavity Scattering Problem". *Journal of Computational Physics*, 240:100–120, 2013.

[26] Li, P. and A. W. Wood. "Electromagnetic Scattering by Multiple Cavities Embedded in the Infinite 2D Ground Plane". *ACES Journal*, 29(7):505–514, 2014.

[27] Li, Peijun, Li-Lian Wang, and Aihua Wood. "Analysis of electromagnetic scattering from a three-dimensional open cavity". *SIAM J. Appl. Math.*, 75(4):1675–1699, 2015.

[28] Newmark, Nathan M. "A Method of Computation for Structural Dynamics". *ASCE*, 85(EM3):67–94, 1959.

[29] O'Neil, M., L. Greengard, and A. Pataki. "On the efficient representation of the half-space impedence Green's function for the Helmholtz equation." *Wave Motion*, 53(1):1–13, 2014.

[30] Pérez-Arancibia, Carlos and Oscar P. Bruno. "High-order integral equation methods for problems of scattering by bumps and cavities on half-planes". *J. Opt. Soc. Am. A*, 31(8):1738–1746, 2014.

[31] Pernischová, Nicole. *A Finite Element Approach to Model Electromagnetic Fields Scattered by a Buried Cavity*. Master's thesis, Duquesne University, McAnulty College and Graduate School of Liberal Arts, 2009.

[32] Renardy, M. and R. C. Rogers. *An Introduction to Partial Differential Equations*. Springer, New York, NY, 2nd edition, 2004.

[33] Senior, Thomas B. A. and John L. Volakis. "Scattering by Gaps and Cracks". *IEEE Trans. Antennas Propag.*, 37(6):744–750, 1989.

[34] Simpson, George R. *Electromagnetic Scattering From a Gap in a Magneto-Dielectric Coating on an Infinite Ground Plane*. Ph.D. thesis, Air Force Inst. Tech., 2002.

[35] Stakgold, I. and M. Holst. *Green's Functions and Boundary Value Problems*. Wiley & Sons, Hoboken, NJ, 3rd edition, 2011.

[36] Van, T. and A. W. Wood. "A Time-Domain Finite Element Method for Helmholtz Equations". *Journal of Computational Physics*, 183:486–507, 2002.

[37] Van, Tri and Aihua Wood. "Finite Element Analysis of Transient Electromagnetic Scattering from 2D Cavities". *Methods Appl. Anal.*, 11(2):221–236, 2004.

[38] Van Genechten, B., B. Bergen, D. Vandepitte, and W. Desmet. "A Trefftz-based numerical modelling framework for Helmholtz problems with complex multiple-scatterer configurations". *Journal of Computational Physics*, 229:6623–6643, 2010.

[39] Wang, Yingxi, Kui Du, and Weiwei Sun. "A Second-Order Method for the Electromagnetic Scattering from a Large Cavity". *Numer. Math. Theor. Meth. Appl.*, 1(4):357–382, 2008.

[40] Wolfram Research, Inc. "BesselK". 2008. URL http://functions.wolfram.com/Bessel-TypeFunctions/BesselK.

[41] Wu, Jiming, Yingxi Wang, Wen Li, and Weiwei Sun. "Toeplitz-type approximations to the Hadamard integral operator and their applications to electromagnetic cavity problems". *Applied Numerical Mathematics*, 58:101–121, 2008.

[42] Zhao, Meiling, Zhonghua Qiao, and Tao Tang. "A fast high order method for electromagnetic scattering by large open cavities". *J. Comput. Math.*, 29(3):287–304, 2011.

Vita

Captain Richard Uber graduated from Humboldt High School in Saint Paul, Minnesota in 1996. He started his undergraduate studies at the University of Minnesota, and prior to graduation, enlisted as an Airborne Cryptologic Language Operator in 2001. Through career-focused training and development, he earned his Associate of Arts degree in Mandarin Chinese from the Defense Language Institute Foreign Language Center and Associate of Applied Science degree in Communications Applications Technology from the Community College of the Air Force. Additionally, he earned a Bachelor of General Studies degree in Mathematics from the University of Nebraska Omaha in 2006 and a Master of Science degree in Mathematics from Texas A&M University in 2010. He was commissioned through Officer Training School in 2010, where he was recognized as the Top Distinguished Graduate.

His first assignment as a commissioned officer was at Randolph AFB as an Operations Research Analyst from December 2010 to July 2013. While stationed at Randolph, he completed the Operations Research Systems Analyst - Military Applications Course, where he was recognized as the Distinguished Graduate. He entered graduate studies at the Air Force Institute of Technology in the fall of 2013. Following completion of his Ph.D. he will join the faculty of the Department of Mathematics and Statistics.

REPORT DOCUMENTATION PAGE

Form Approved
OMB No. 0704–0188

1. REPORT DATE *(DD–MM–YYYY)*	2. REPORT TYPE	3. DATES COVERED *(From — To)*
15–09–2016	Dissertation	October 2013–September 2016

4. TITLE AND SUBTITLE

Time Domain Analysis of Electromagnetic Scattering From Multiple Cavities Embedded in a Ground Plane

5a. CONTRACT NUMBER

5b. GRANT NUMBER

5c. PROGRAM ELEMENT NUMBER

6. AUTHOR(S)

Uber, Richard P., Captain, USAF

5d. PROJECT NUMBER

5e. TASK NUMBER

5f. WORK UNIT NUMBER

7. PERFORMING ORGANIZATION NAME(S) AND ADDRESS(ES)

Air Force Institute of Technology
Graduate School of Engineering and Management (AFIT/EN)
2950 Hobson Way
Wright-Patterson AFB, OH 45433-7765

8. PERFORMING ORGANIZATION REPORT NUMBER

AFIT-ENC-DS-16-S-004

9. SPONSORING / MONITORING AGENCY NAME(S) AND ADDRESS(ES)

10. SPONSOR/MONITOR'S ACRONYM(S)

11. SPONSOR/MONITOR'S REPORT NUMBER(S)

12. DISTRIBUTION / AVAILABILITY STATEMENT

DISTRIBUTION STATEMENT A. APPROVED FOR PUBLIC RELEASE;
DISTRIBUTION UNLIMITED.

13. SUPPLEMENTARY NOTES

14. ABSTRACT

This work examines the scattered fields produced when a transient wave is reflected from an infinite PEC ground plane with multiple embedded cavities. Incident and reflected waves will be decomposed into TM^z and TE^z polarizations, with primary focus given to the TM^z. Cavities may be unfilled, partially filled, or fully filled with non-magnetic dielectric material and no assumptions are made regarding similarity, regularity, or periodicity. The Newmark method is used to discretize time and a variational formulation is presented for each time step. The principle outcome is to show that the variational formulation of the scalar problem is well posed.

Additionally, the variational formulation is applied in a stable numerical model using the FE-BI method. Interior fields are approximated using the FEM for each time step, then the boundary integral is applied using the appropriate Green's function to approximate exterior scattered fields. The exterior fields for one time step provide the boundary conditions for the interior problem at the next time step. In this way, the numerical model marches through time.

Various numerical experiments are run to examine the effect of coupling on aperture and external fields. Of particular interest are the differences between single-cavity and multiple-cavity solutions.

15. SUBJECT TERMS

Electromagnetics, Scattering, PEC, DtN Operator, Cavity

16. SECURITY CLASSIFICATION OF:			17. LIMITATION OF ABSTRACT	18. NUMBER OF PAGES	19a. NAME OF RESPONSIBLE PERSON
a. REPORT	b. ABSTRACT	c. THIS PAGE			Dr. Aihua Wood (ENC)
U	U	U	UU	146	19b. TELEPHONE NUMBER *(include area code)* (937) 255-3636x4272 Aihua.Wood@afit.edu